Development of Laboratory to Field Shift Factors for Hot-Mix Asphalt Resilient Modulus

by

Samer W. Katicha

Thesis submitted to the Faculty of the
Virginia Polytechnic Institute and State University
In partial fulfillment of the requirements for the degree of

Masters Of Science

in

Civil Engineering

Imad L. Al-Qadi, Chair
Gerardo Flintsch
Amara Loulizi

November 2003

Blacksburg, Virginia

Keywords: resilient modulus, hot-mix asphalt, temperature, compaction

Development of Laboratory to Field Shift Factors for Hot-Mix Asphalt Resilient Modulus

Samer W. Katicha

Virginia Polytechnic Institute and State University

Advisor: Imad L. Al-Qadi

Abstract

Resilient moduli of different surface mixes placed at the Virginia Smart Road were determined. Testing was performed on Field cores (F/F) and laboratory-compacted plant mixed (F/L), laboratory mixed and compacted per field design (L/L), and laboratory designed, mixed, and compacted (D/L) specimens. The applied load was chosen to induce a strain ranging between 150 and 500 microstrains. Two sizes of laboratory compacted specimens (100-mm in diameter and 62.5-mm-thick and 150-mm in diameter and 76.5-mm-thick) were tested to investigate the effect of specimen size on the resilient modulus. At 5^{o}C, the measured resilient moduli for both specimen sizes were similar. However, the specimen size has an effect on the measured resilient modulus at 25 and 40^{o}C, with larger specimens having lower resilient modulus. At 5^{o}C, HMA behaves as an elastic material; correcting for the specimen size using Roque and Buttlar's correction factors is applicable. However, at higher temperatures, HMA behavior becomes relatively more viscous. Hence, erroneous resilient modulus values could result when elastic analysis is used. In addition, due to difference in relative thickness between the 100- and 150-mm diameter specimens, the viscous flow at high temperature may be different. In general, both specimen sizes showed the same variation in measurements. Resilient modulus results obtained from F/L specimens were consistently higher than those obtained from F/F specimens. This could be due to the difference in the

volumetric properties of both mixes; where F/F specimens had greater air voids content than F/L specimens. A compaction shift factor of 1.45 to 1.50 between the F/F and F/L specimens was introduced. The load was found to have no effect on resilient modulus under the conditions investigated. However, the resilient modulus was affected by the load pulse duration. The testing was performed at a 0.1s and 0.03s load pulses. The resilient modulus increased with the decrease of the load pulse duration at temperatures of 25^{o}C and 40^{o}C, while it increased at 5^{o}C. This could be due to the difference in specimen conditioning performed at the two different load pulses. Finally, a model to predict HMA resilient modulus from HMA volumetric properties was developed. The model was tested for its fitting as well as predicting capabilities. The average variability between the measured and predicted resilient moduli was comparable to the average variability within the measured resilient moduli.

To my father,
Wehbe Katicha,
my mother,
Nelly Katicha,
and my sister and brother
Nathalie and Nabil

Acknowledgments

First I would like to thank my advisor, Dr. Imad L. Al-Qadi, for his help and patience throughout my graduate studies. His guidance and support made my working and learning experience, a very special one. In addition, I would like to thank Dr. Gerardo Flintsch and Dr. Amara Loulizi for their support and help as members of my advisory committee.

Also, I would like to thank my colleagues Alex Appea, Moustafa Elseifi, Samer Lahour, Stacey Reubush, Edgar De Leon Izeppi, Kevin Siegel, and Alan Christoe at the Roadway Infrastructure Group at the Virginia Smart Road. The good discussions we had, whether related to pavements or football games, made my learning experience much more enjoyable. Last but not least, I would like to extend my thanks to William (Billy) Hobbs, better known as “The Man”, for preparing the samples and fixing the MTS whenever I break it.

Samer W. Katicha

Table of Content

List of Figures

List of Tables

Chapter 1 Introduction

In this chapter an overview of the pavement material characterization is discussed. Hot mix asphalt (HMA) mixtures were tested to determine the creep compliance, fatigue resistance, and resilient modulus of the different mixes which are key input parameters in pavement design and rehabilitation. The characterization of HMA depends on the way the material is obtained. This will lead to the formulation of the problem statement, which will be followed by the research objectives. A summary of the research scope is briefly presented at the end of the chapter.

1.1 Introduction

The Mechanistic-Empirical design of flexible pavements is based on limiting the distresses in the pavement structure. Pavement distresses are caused by the different types of loadings mainly structural and environmental loadings. Environmental loadings are mainly addressed in the selection of the asphalt binder. The structural loading distresses are mainly fatigue cracking and permanent deformation (rutting). Although these two distresses are caused by the structural loading (vehicular loading on the pavement structure), they are also affected by the environmental conditions. The mechanistic-empirical pavement design method requires limiting the cracking and rutting in the pavement structure. Many factors affect the ability of the HMA to meet these structural requirements. These are the different components (aggregates and binders) of the HMA, their interaction, the mix design, and the method of preparation. Great efforts have been made to better understand HMA behavior. However, with the increasing use of new technologies (e.g. modifiers in the binder, and reinforcement of the pavement) and establishment of new design specifications, much work still needs to be done to characterize HMA mixtures. Hot-mix asphalt mixes are primarily designed to resist permanent deformation and cracking. The ability of the HMA to meet those requirements depends on the following:

- The binder characteristics;
- Aggregate characteristics and gradation;
- Modifiers;
- Temperature;
- Moisture;

- Loading (load level, rate, and the loading rest time);
- Aging characteristics;
- State of stress (tension vs. compression, uniaxial, biaxial or Triaxial);
- Compaction method.

1.2 Background

1.2.1 Flexible Pavements

Flexible pavements are designed to provide a smooth surface and reduce the stresses on the natural subgrade. Good quality materials are used at the top of the layered pavement system to reduce the vehicular induced stresses with depth. Inferior materials are used at the bottom where the stresses are low. This design approach allows for the use of cheaper materials. Figure 1-1 shows a typical cross-section of a flexible pavement. Typical flexible pavements are composed of the following:

- The surface course (wearing surface) is the top course in flexible pavement. It is usually constructed by dense graded HMA. Large aggregates account for the carrying capacity of the layer, whereas smaller aggregates account for the skid-resistance and smoothness. The wearing surface thickness varies between 25 and 50 mm.
- Since HMA is too thick to be compacted in one layer, the binder course is placed under the surface course. It is composed of larger size aggregates than that used in the wearing surface. Hence, the quantity of asphalt binder used in the binder course is less than in the surface course due to the reduction in the aggregate surface area. This will allow more cost savings without compromising the structural capacity since the stresses in the binder course are lower. Asphalt base course thickness usually varies between 50 and 100 mm.
- The base course is a layer of aggregates constructed under the binder course. It is usually composed of crushed stones that can be untreated or stabilized with small quantities of cement or asphalt binder. The base course thickness varies between 100 and 300 mm.
- The subbase is a layer of lower quality aggregates placed beneath the base course. The reason for using different materials is for economy. The subbase thickness varies between 100 and 300 mm.

- The subgrade is the bottom layer of compacted in-situ soil or selected material. The subgrade should be compacted at the optimum moisture content to get a high density.

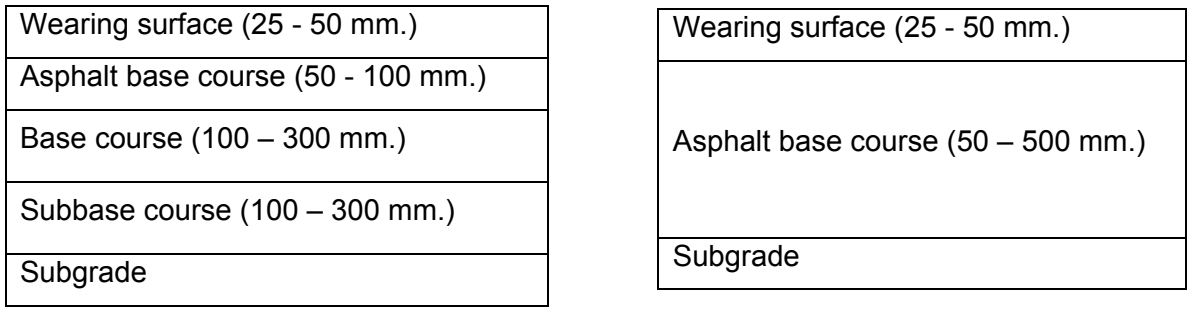

(a) Regular pavement (b) Full depth pavement

Figure 1-1 Flexible pavement cross-section.

It should be noted that the use of the various layers is based on either the necessity (vehicular and environmental loading) or economy (materials cost and availability, and construction constraints). Therefore, the number of layers in a pavement system could vary. In some cases, full depth pavement shown in Figure 1-1 (b) may be considered.

1.2.2 Flexible Pavement Design

Pavement response to loading and performance require the proper characterization of paving materials. Hot mix asphalt is a viscoelastic material, which means that its stress-stain relationship is time and temperature-dependent. Pavements have been analyzed using different theories such as the elastic, the viscoelastic, and the viscoplastic theory. It has become of practice that different pavement responses are predicted using different theories. For example, viscoelastic theory is used to predict thermal stresses and strains as well as permanent deformation. In this case the time and temperature dependant stiffness is used as a material characteristic input. On the other hand, load-induced stresses and strains can be accurately predicted by linear elastic layer theory at temperatures below about 30^{o}C (Roque and Buttlar, 1992). Material characterization in elastic theory requires the determination of two parameters which are the elastic modulus and Poisson's ratio.

The elastic modulus has been traditionally determined in the field using deflection obtained from non destructive tests such as the Falling Weight Deflectometer (FWD). However, moduli determined through back calculation are for a specific temperature at which the test was performed. Although generalized relationships between HMA elastic modulus and temperature have been developed, their use can lead to considerable error since these relationships can vary between one asphalt mix and another. Moreover, it has been shown that near surface layer moduli determined using deflection basins from FWD testing are not accurate. These problems can be overcome in the laboratory where materials from each layer can be tested at a controlled temperature. Material properties determined in the laboratory can vary considerably from one test setup to another. Proper material properties are obtained when the laboratory setup induces stress states that are similar to the ones experienced in the filed.

Testing in the lab can be performed on field specimens or laboratory-produced specimens. Differences have been shown to exist between field and laboratory-produced specimens using different methods of compaction. Gyratory compaction has been proven to better correlate with field compaction than other methods (Button et al., 1994). The gyratory compaction is the one used in the Superpave design protocol, and will be used in the following research.

1.2.3 Failure Criteria in Flexible Pavements

Fatigue Cracking:

Fatigue cracking of flexible pavements is thought to be based on the horizontal tensile strain at the bottom of the HMA layer. The failure criterion relates the allowable number of load repetitions to the tensile strain. The cracking initiates at the bottom of the HMA where the tensile strain is highest under the wheel load. The cracks propagate initially as one or more longitudinal parallel cracks. After repeated heavy traffic loading, the cracks connect in a way resembling the skin of an alligator. Laboratory fatigue tests are performed on small HMA beam specimens. Due to the difference in geometric and loading conditions; especially rest period between the laboratory and the field, the allowable number of repetitions for actual pavements is greater than that obtained from laboratory tests. Therefore, the failure criterion may require incorporating a shift factor to account for the difference.

Rutting:

Rutting is indicated by the permanent deformation along the wheelpath. Rutting can occurs in any of the pavement layers or the subgrade, usually caused by the consolidation or the lateral movement of the materials due to traffic loads. Rutting in the HMA layer is controlled by the creep compliance of the mix. Rutting occurring in the subgrade is caused by the vertical compressive strain at the top of the subgrade layer. To control rutting occurring in the subgrade, the vertical compressive strain at the top of the subgrade is limited to a certain value.

It is noticed that fatigue cracking and rutting depend on the level of strain; tensile strain at the bottom of the HMA layer for fatigue cracking, and compressive strain at the top of the subgrade layer for rutting. Therefore, to be able to predict the fatigue as well as the rutting lives of the pavement structure, the aforementioned strains must be determined. Load induced stresses and strains in pavements are determined using the elastic layered theory. This requires the determination of the moduli of the different layers in the pavement structure. Moduli are usually determined in the field by performing the FWD test. However, near surface moduli (modulus of the wearing surface) are difficult to obtain using FWD results. Moreover, for the design of the pavement, layers moduli must be determined prior to the pavement is construction.

1.3 Material Characterization

Hot mix asphalt can be characterized as either a viscoelastic or an elastic material. Viscoelastic characterization involves measuring the dynamic complex modulus and the creep compliance. Elastic characterization involves measuring the resilient modulus. Since HMA's properties are functions of time and temperature, its characterization should reflect this fact.

1.3.1 Dynamic Complex Modulus

The dynamic complex modulus has been used for the design of pavements (Shook, 1969). The complex modulus test performed in the laboratory by applying a sinusoidal or haversine loading with no rest period. This testing approach is one of many methods for describing the stress-strain relationship of viscoelastic materials. The dynamic complex modulus is composed of two parts: the real part, which represents the elastic stiffness and the imaginary part, which represents the internal damping due to the

viscoelastic properties of the material. The absolute value of the complex modulus is referred to as the dynamic modulus of HMA. The axial strains are measured using two strain gauges. The ratio between the axial stress and the recoverable strain is the dynamic elastic modulus. The dynamic complex modulus is determined from the dynamic modulus and the phase angle. The phase angle being the lag between the stress and strain maximum values.

The dynamic complex modulus test, ASTM D3497-79 (ASTM, 2003), is usually conducted on cylindrical specimens subjected to a compressive haversine loading varying with the loading frequency. The testing mode selected will have an effect on the design if the design is based on the viscoelastic theory; in such a case the loading and frequency should be selected such that it best simulates the traffic loading. Most of the dynamic modulus tests use a compressive load applied to the specimen. However, other tests have also been used such as the tension and tension-compression tests. A haversine load is applied to the specimen for a minimum of 30s not exceeding 45s at temperatures of 5, 25, and 40^{o}C and a load frequency of 1, 4, and 16 Hz for each temperature.

The test is affected by the setup and the effect becomes more prominent at higher temperatures. Therefore if a design is based on elastic theory with a given dynamic modulus for HMA, the three different testing temperature results may be used.

1.3.2 Resilient Modulus

The resilient modulus is the elastic modulus used in the layered elastic theory for pavement design. Hot mix asphalt is known to be a viscoelstic material and, therefore, experiences permanent deformation after each application of the load. However, if the load is small compared to the strength of the material and after a relatively large number of repetitions (100 to 200 load repetitions), the deformation after the load application is almost completely recovered. The deformation is proportional to the applied load and since it is nearly completely recovered it can be considered as elastic.

The resilient modulus is based on the recoverable strain under repeated loading and is determined as follows:

$$M_r = \frac{\sigma_d}{\varepsilon_r}$$

where σ_d is the deviator stress and ε_r is the recoverable (resilient strain). Because the applied load is usually small compared to the strength of the specimen, the same specimen may be used for the same test under different loading and temperatures.

The resilient modulus is evaluated from repeated load tests. Different types of repeated load tests have been used to evaluate the resilient modulus of HMA. The most commonly used setups are the uniaxial tension, the uniaxial compression, the beam flexure, the triaxial compression, and the indirect diametral tension (IDT). The IDT setup has a main advantage in its ability to simulate the stress states that exist at the bottom of the HMA layer underneath the applied wheel load, which are of concern in pavement design. The state of stress in an IDT specimen is rather complex, however extensive research has been performed to address this subject, and data analysis methods are available to accurately predict stresses and strains (Roque and Buttlar, 1992; Kim, et al., 2002).

The resilient modulus can be performed on laboratory prepared specimens or field cores. For consistency in design, results obtained from laboratory prepared specimens should match with results obtained from field cores.

1.3.3 Creep Compliance

The creep test is used to characterize linear viscoelastic materials. Viscoelastic materials such as hot mix asphalt experience an increase in total deformation as the applied load is sustained. This phenomenon is time and temperature dependent. The creep compliance is defined as the ratio of the instantaneous strain over the applied stress. Creep testing is used to characterize permanent deformation. Test setups that have been used are uniaxial (Van de Loo, 1978) and more recently indirect tension (Roque and Buttlar, 1992; Buttlar and Roque, 1994; Wen and Kim, 2002; Kim, et al., 2002). The advantages and disadvantages of the IDT setup for creep testing are the same as for resilient modulus testing.

Specimen compaction is an important parameter that affects the dynamic modulus, resilient modulus, and creep compliance laboratory results.

1.4 Problem Statement and Research Objective

Gyratory compaction was introduced by the Strategic Highway Research Program (SHRP) as the compaction method that best replicates compaction performed

in the field. However, correlation between laboratory compacted HMA specimens properties and field compacted HMA properties are not well established. Discrepancies between laboratory prepared specimens and field cores are not solely due to compaction; differences between the designed and as built mixes system can be quiet significant. Specimens in the laboratory can be prepared to conform to the designed or the as built pavement. Therefore, the development of correction factors between laboratory-prepared specimens and specimens obtained from the field will provide valuable information for adjusting design procedures. Hence, better prediction of pavement performance can be achieved.

The main objective of this research was to develop shift factors to correlate laboratory-determined resilient moduli of field cores to those of laboratory-prepared specimens. These factors could be dependent on compaction method, specimen size, temperature, mix production, and loading.

1.5 Scope

This research attempted to quantify the variations in resilient modulus results due to different parameters. These parameters are specimen size, load pulse duration, temperature, and method of production and compaction. The most important task was to develop shift factors to relate resilient modulus of laboratory-prepared specimens to resilient modulus of field cores. Chapter 1 is an introduction to the subject. Chapter 2 presents an overview of the present stage of knowledge regarding resilient modulus testing and the parameters affecting its values. The resilient modulus results depend on the analysis method used. The analysis method used should be the one that gives the best representation of the state of stress in the specimen. The different analysis methods available are discussed in chapter 2. In Chapter 3 the research approach is outlined and details on specimen preparation, testing, and analysis of the results are presented. The material used were obtained either directly from the Virginia Smart Road, in form of road cores or loose-bagged mixture samples collected during construction, or were produced in the laboratory from raw materials to meet design specifications. The research results and interpretation are presented in Chapter 4. Finally, the conclusions and recommendations are presented in Chapter 5. The research determin specimen size shift factors (100- and 150-mm samples), Load duration shift factors, and the relationship between the resilient modulus and the HMA properties.

Chapter 2 Present State of Knowledge

This chapter considers the present state of knowledge regarding flexible pavements, materials characterization, factors affecting resilient modulus results, and methods of analysis.

2.1 Flexible Pavement and Their Main Design Factors

By their very nature, pavement structures must be relied upon to perform successfully and simultaneously serve several functions, among them carrying capacity, riding comfort, safety, skid resistance, and surface drainage. While loads applied on top of the pavement cause stresses throughout its layers, they are particularly higher at the top than at the bottom. Therefore, in the most sensible and cost effective pavement designs, stronger and more expensive material is placed on the top to receive the brunt of stresses while weaker, less expensive material is placed at the bottom, where stresses are lower. The resulting flexible pavement structure generally consists of the following:

- Surface course or wearing surface
- Binder course
- Base and subbase course
- Subgrade

The wearing surface is the top layer of pavement, which must be strong enough to resist stresses applied on it but at the same time provide a smooth ride. The general mix design for wearing surfaces is a dense graded HMA. Additionally, such a layer must minimize infiltration of water which can also achieved by providing a drainage layer.

The binder course or second layer is similar in nature to the wearing surface in that it is a HMA. The difference between the binder and surface mixes is that in order to reduce cost, larger aggregates and less asphalt binder are used in the former. The larger aggregate size also provides greater strength. A base HMA may also be used.

The base course is a layer beneath the HMA layer. It is composed of crushed material, sometimes stabilized by either Portland cement or asphalt. The subbase, a layer of lower quality, cost-efficient material placed under the base course, often serves as a filter between the base and subgrade.

The subgrade is a prepared *in situ* soil. It is usually compacted near the optimum moisture content.

2.1.1 Input Design Parameters

Successful pavement designs recognize three major parameters: traffic and loading, material properties, and environment.

Traffic and Loading:

The *traffic and loading* design involves axle loads, number of repetitions, tire contact areas, and vehicle speed.

The most common axle configurations are *single axle with single tires*, *single axle with dual tires, tandem axles with dual tires*, and *tridem axles with dual tires*. Because analyzing multiple axles proves difficult, the Equivalent Single Axle Loads (ESALs) method, which involves a standard 80-kN (18-kip) single-axle load, is used. Design of the pavement is based on the number of ESAL repetitions that can take place before pavement failure occurs in the form of either cracking or rutting. The applied truck load is distributed over the tire contact area. The tire contact area is calculated by dividing the applied load by the tire contact pressure. For simplicity the tire contact pressure is usually taken to be equal to the tire pressure.

Finally, due to the viscoelastic nature of HMA, vehicle speed also is important to loading. When a load is applied, viscoelastic materials, like HMA, exhibit deformations that are time dependent. The duration of the applied truck load in the HMA layer depends on the truck speed. In the elastic theory of pavement design and analysis, the resilient modulus selected for each pavement layer should reflect the vehicle speed; in other words, in calculating the resilient modulus of the HMA layer—whether in the field or in the laboratory—the duration of the load pulse is function of the vehicle speed. Higher speeds result in lower loading times and, therefore, smaller strains and larger resilient modulus. Therefore, to accurately determine the resilient modulus of HMA, the loading time that is achieved in the filed, under highway speed, should be used in the test.

Material Properties:

In the linear elastic theory, the elastic modulus and Poisson's ratio are used to characterize each layer. Because the elastic modulus of HMA varies with the time of

loading (due to the viscoelastic nature of HMA), the resilient modulus is selected in the analysis.

In the viscoelastic theory, creep compliance is measured by the time-temperature shift factor, which accounts for differences between test temperature and that of the actual pavement.

Environment:

Three major environmental factors affect pavement design: temperature, moisture level, and frost penetration. The HMA resilient modulus is affected most by temperature; the subgrade resilient modulus, by moisture content. Frost penetration on the other hand affects the entire pavement system.

At high temperatures, the HMA layer becomes viscous in nature, while at low temperatures, it becomes elastic. In flexible pavements, low temperatures cause cracking, while high temperatures cause permanent deformation. Frost penetration results in a stronger subgrade during winter and a weaker subgrade during spring. The spring reduction in subgrade strength occurs when ice that has formed during colder weather melts and leaves the subgrade saturated with water. The moisture level will affect the strength of the subgrade. Moisture content above optimum will result in a lower subgrade modulus.

Pavement Distresses:

Before 2002, the AASHTO pavement design method was based on the Present Serviceability Index (PSI). However, the mechanistic-empirical (ME) pavement design has gained enough recognition as an acceptable alternative that it has become part of the 2002 AASHTO guide. In the M-E pavement design method, failure criteria are established using specific types of distresses: fatigue cracking, rutting, and low temperature cracking.

Fatigue cracking results from the repeated application of a heavy load on the pavement structure. Such repeated application creates tensile strain at the bottom of the HMA layer, which ultimately causes cracks to develop. The failure criterion is based on a laboratory fatigue test to relate the allowable number of load repetitions to the tensile strain.

Rutting is characterized by a surface depression along the wheel path. It is associated primarily with vertical compressive strain on top of the subgrade; however, it

can also occur as a result of weakness in other pavement layers one of which is the HMA layer. The failure criterion relates the allowable number of load repetitions to the compressive strain at the top of the subgrade.

Low temperature cracking results in transverse cracking. These are mainly caused by the shrinkage of HMA and daily temperature cycling, which result in cyclic stress and strain.

2.2 Material Characterization

In the overall design of pavement systems, the HMA layer plays an important role. As the upper most layer, it experiences the highest stresses. Therefore, understanding its properties, including its resilient modulus, are crucial to the design process. Stresses induced by a wheel load on a typical HMA layer can be described or categorized by the following four general cases:

1. Triaxial compression on the surface underneath the wheel load.
2. Longitudinal and transverse tension combined with vertical compression at the bottom of the HMA layer underneath the wheel load.
3. Longitudinal or transverse tension at the surface of the HMA layer at some distance from the wheel load.
4. Longitudinal or transverse tension at the bottom of the HMA layer at some distance from the wheel load.

The critical location of load-induced cracking is generally found at the bottom of the HMA layer, immediately underneath the load, where the stress state consists of longitudinal and transverse tension combined with vertical compression. With the exception that it induces tension in one direction instead of two, the indirect tension (IDT) setup best simulates this state of stress; therefore, it was chosen in this research to evaluate the resilient modulus of HMA. Other advantages of the IDT setup, beyond its relative ease of use, involve the facts that failure is not seriously affected by surface conditions and that a specimen can be tested across various diameters. Moreover, the setup can be used to provide valuable information on a number of HMA characteristics, including tensile strength, Poisson's ratio, and fatigue and creep levels. When

characterizing the material used in flexible pavements, one must consider the resilient modulus as well as results of the indirect tension test.

2.2.1 Resilient Modulus

A material's resilient modulus is analogous to Young's modulus of elasticity for linear elastic materials. By their nature, paving materials are not elastic, which means that they inevitably experience some permanent deformation after each load cycle. The strain in viscoelastic materials can be divided into the *elastic strain*, also called the resilient strain, and the *viscous strain*. Only the resilient strain is recovered after a load is removed.

In the field, the resilient modulus of the pavement materials can be determined through nondestructive testing such as falling weight deflectometer (FWD) testing. In the laboratory, the resilient modulus of HMA can be measured using different test setups. These include triaxial, uniaxial, and indirect tension. Laboratory tests can be performed on field cores or on specimens produced in the laboratory. Differences have been shown to exist between such diversely-produced specimens using different methods of compaction (Al-Sanad, 1984, Consuegra et al., 1989, Button et al., 1994, Brown et al., 1996, Khan et al., 1998). Although they are more easily controlled, material properties determined in the laboratory can vary considerably from one test setup to another and each test has its advantages and disadvantages. Therefore, proper material properties can be obtained when the laboratory setup induces stress states similar to those experienced in the field. In addition to the test setup used, the method by which the data is analyzed can greatly affect the measured resilient modulus.

The moduli used in elastic layer theory are the resilient moduli (Mr) of each layer. As a result of air voids being filled during the initial stages of specimen loading, HMA experiences an accumulation of plastic strain during repeated loading. However, the accumulated strain is greatest during the first few cycles and becomes negligible after around 100 to 200 cycles at which stage the resilient modulus is calculated. The laboratory-determined resilient modulus of the HMA depends on the following parameters:

- Resilient modulus test setup used,
- Method of compaction (gyratory compaction vs. Marshall compaction),
- Level of compaction (number of gyration when using gyratory compaction),

- Temperature,
- Load level, duration, and rest period,
- Specimen size and geometry, and
- Data analysis procedure.

The IDT possesses several advantages over other setups as indicated later: the IDT has the ability to simulate the stress states that exist at the bottom of the HMA layer beneath the applied wheel load, which are of concern in pavement design. Although the triaxial setup induces stresses similar to the ones in the field, the failure in a triaxial specimen does not result from tension stresses as it is the case in the field. Therefore, the IDT setup was selected in this study.

2.2.2 Indirect Tension Test

The indirect tension (IDT) test is conducted by repeated application of compressive loads along the vertical diameter of a cylindrical specimen. This loading configuration develops relatively uniform compressive stresses along the direction of the applied load, as well as perpendicular to the direction of the applied load. Moreover, the values obtained from the diametral resilient modulus test would depend on the magnitude of the applied load (Almudaiheem and Al-Sugair, 1991; Brown and Foo, 1991).

Originally the IDT test was used to measure rupture strain in concrete (Blakey and Beresford, 1955), it was thereafter adapted to determine the elastic properties (E and ν) of concrete (Wright, 1955; Hondros, 1959). Kennedy and Hudson (1968) first suggested the use of the test for stabilized materials, while Schmidt (1972) used the test to determine the resilient modulus of HMA. Since then, IDT has become the main setup selected by most engineers for evaluation of HMA resilient modulus (Brown, and Foo, 1991). Significant research has been done over the past three decades. For example, based on extensive work, Mamlouk and Sarofim (1988) concluded that among the common methods of measurement of elastic properties of HMA, the resilient modulus is more appropriate for use in multilayer elastic theories. Baladi and Harichandran (1988) further indicated that, in terms of repeatability, resilient modulus measurement by the indirect tensile test is the most promising. Roque and Ruth (1987) showed that when the moduli were used in elastic layer analysis, values obtained using the IDT setup resulted in excellent predictions of strains and deflection measured on full-scale pavements at low in-service temperatures (less 30^{o}C). The main advantage of the IDT

is that the failure plane is known, which makes direct measurements possible. The test offers many advantages over other methods (Lytton et al., 1993):

- It is relatively simple to perform;
- It is readily adaptable to measuring several properties such as tensile strength, Poisson's ratio, fatigue characteristics, and permanent deformation characteristics;
- Failure is not significantly affected by specimen surface conditions;
- Failure is initiated in a region of relatively uniform tensile stress;
- Test variation is acceptable; and
- Specimens may be tested across various diameters to evaluate homogeneity.

However, several problems are associated with the test: stress distribution within the specimen is non-uniform and must be determined theoretically; stress concentrations around the loading platens make vertical diametral measurements unfeasible; and specimen rotation during loading can result in incorrect horizontal deformation measurements (Lytton et al., 1993).

Despite its drawbacks, the test was adopted by the American Society of Testing and Materials (ASTM) as a standard method of measuring the resillient modulus of HMA (ASTM D 4123). Also, in 1992, the Strategic Highway Research Program (SHRP) Protocol P07 laid out a step-by-step method for resilient modulus testing using the indirect tension method. The haversine load utilized in the protocol has a period of 0.1s, followed by an appropriate rest period. The initial form of the protocol required testing the replicates at three temperatures (5°, 25°, and 40°C), during three rest periods (0.9, 1.9, and 2.9s), and at two load orientations (0° and 45°). The magnitude of the applied load causes tensile stress levels within the specimen equivalent to 30, 15, and 5% of the tensile strength at 25^{o}C, at 5^{o}C, 25^{o}C, and 40^{o}C respectively; and the seating load is 3, 1.5, and 0.5 percent (10 percent of the applied load) of the specimen tensile strength measured at 25^{o}C, at each of the three test temperature, respectively. The tensile strength of each replicated set is determined prior to testing by performing an indirect tensile test on a companion specimen.

Additional evaluation of the SHRP P07 Protocol resulted in several changes designed to increase testing efficiency (Hadley and Groeger, 1992b). Since the load orientation and rest period were not statistically significant, it was therefore discovered that the resilient modulus could be determined from testing one orientation with a load sequence having only one rest period, 0.9s. Additionally, the requirements were

changed such that only duplicate, rather than triplicate, specimens were necessary. As they were found to be statistically significant, the three test temperatures were kept by the protocol.

Four different analysis methods were presented in the litterature: ASTM Analysis, Elastic Analysis, SHRP P07 Analysis, and Roque and Buttlar's Analysis (the analysis will be presented in section 2.4). However, no particular analytical method was favored for calculating the resilient modulus and Poisson's ratio; in fact, the choice of method is highly dependent upon the equipment used. In all cases, however, resilient modulus results are affected by rest period, which becomes negligible when the ratio of rest period over load duration exceeds 8, temperature, sample size, including diameter and thickness, and, most importantly, Poisson's ratio (Kim et al., 1992; Lim et al., 1995). If accurate measurements of Poisson's ratio were obtained from the test, then an accurate estimation of the resilient modulus can occur (Heinicke and Vinson, 1988; Kim et al., 1992; Roque and Buttlar, 1992). On the other hand, load duration also is thought to have significant effects on test results. The IDT test is now performed according to ASTM D 4123 or SHRP P07 using a load pulse duration of 0.1s and a rest period of 0.9s. However, based upon stress pulse measurements induced in the HMA layer of the Virginia Smart Road by a moving truck and FWD testing, Loulizi et al. (2002) recently suggested reducing the pulse duration to 0.03s.

2.3 Factors Affecting Resilient Modulus Results

Several factors affect the results of resilient modulus testing, including the mix components, loading, Poisson's ratio, and testing axis. Specimen size and measuring methods must also be considered.

2.3.1 Mix Components Effect

The mix components of an HMA include the binder, and the aggregates. A detailed laboratory investigation undertaken by Gemayel and Mamlouk (1988) showed that in laboratory-prepared specimens, the asphalt content and aggregate gradation considerably influenced density, air voids, Marshall stability, instantaneous and total resilient moduli, and coefficient of permeability. The same study determined significant differences between the predicted performance of open-graded and dense-graded HMA, a fact that can be attributed to aggregate gradation and the percentage of air voids. The

resilient modulus test was performed at the three temperatures: 5°C, 25°C, and 40°C, according to ASTM D4123. The difference between laboratory prepared specimens and field cores was also evaluated. They concluded that field cores densities are much lower than those of laboratory prepared specimens; the average resilient modulus of field core is lower than that of laboratory prepared specimens. Their results are based on specimen tested at 5°C and 25°C.

Baladi et al. (1988) performed regression analyses to evaluate the relationship between the measured resilient modulus and mix parameters such as air voids, aggregate angularity, binder kinematic viscosity, and gradation. In their study, they reported that the modulus was affected by air voids, aggregate angularity, and binder kinematic viscosity with air voids exerting the greatest influence. It was also seen that increasing aggregate angularity and higher binder viscosities increased the magnitude of the resilient modulus. For evaluating the resilient modulus, the study also questioned the repeatability and accuracy of the procedure found in ASTM D4123.

2.3.2 Loading Effect

Values of the resilient modulus can be used in two ways: to evaluate the relative quality of materials and as an input value for pavement design, evaluation, and analysis. As recommended by ASTM D4123, the load magnitude should range from 10 to 50% of the indirect tensile strength of the specimen. Almudaiheem and Al-Sugair (1991) suggest that a larger load should be used in the test because it yields a smaller resilient modulus value, which in turn results in a more conservative design. The loads they used ranged from 10 to 30% of the indirect tensile strength of the specimen. They found that the difference in resilient modulus values at loads of 1000 and 2700 N was as great as 4% for specimens with an asphalt content of 4%. The difference in values decreased as the content of asphalt increased. On the other hand, some researchers have suggested that the effect of stress level on the measured resilient modulus is inconsistent (Schmidt, 1972, Howeedy and Herrin, 1972, Adedare and Kennedy, 1976).

In general, the resilient modulus decreases with increasing load intensity and loading duration (Bourdeau et al. 1992), and the extent of resilient modulus change due to load duration depends on the test temperature. Stroup and Newcomb (1997) conducted an extensive study on load duration effect on the resilient modulus. The ranges investigated were 0.1 and 1.0s at the temperatures of -18, 1, 25, and 40°C. As the loading duration increased, the resilient modulus decreased for all temperatures

except at -18°C; at this temperature, the resilient modulus was found to have slightly increased. At higher temperatures, the loading duration obviously had a greater effect. Fairhurst et al. (1990) reported that the resilient modulus increases with increasing cycle frequency. They suggested that this increase occurred because the decreased recovery time caused by increased test frequencies resulted in an accumulation of strain in the specimen.

2.3.3 Effect of Poisson's Ratio

The Poisson's ratio of a perfectly elastic material is the ratio of the deformation due to an applied load in the unloaded axis to the deformation in the loaded axis of a cubical element. A value of Poisson's ratio greater than 0.5 would result in an expansion or reduction in the volume when the cube is either compressed or put into tension, respectively. However, HMA is a viscoelastic material and the Poisson's ratio determined from the IDT is not based on a cubical element. Values higher than 0.5 of Poisson's ratio determined from vertical and horizontal deformation measurements have been obtained in the laboratory. These values are more frequent at high temperatures where the HMA behaves more as a viscous material than as an elastic one.

The indirect tension test measures horizontal deflection and applied stress. The determination of the resilient modulus, however, requires that the Poisson's ratio be known *a priori* or determined during the test. Determination of Poisson's ratio requires taking both vertical and horizontal deflection measurements. Ultimately, the effect of Poisson's ratio on the resilient modulus values can be quite significant.

Baladi and Harichandran (1989) found that using an assumed value of 0.35 for Poisson's ratio resulted in values of the resilient modulus 1.5 to 2 times higher than those obtained using a Poisson's ratio calculated from measured horizontal and vertical deformations. Also, Kim et al. (1992) reported that resilient modulus values obtained using assumed values for Poisson's ratio were as much as five times greater than those obtained from calculated ones. On the other hand, Vinson (1989) concluded from a theoretical finite element study that an increase in Poisson's ratio from 0.15 to 0.45 did not greatly affect the calculated resilient modulus. He suggested that for a resilient modulus test performed under typical loading conditions, because of induced shear stresses in the specimen, the modulus obtained using an assumed Poisson's ratio is more accurate than that obtained using a calculated one. Conversely, McGee (1989) concluded from an experimental study that resilient modulus values obtained using an

assumed Poisson's ratio value of 0.35 showed more scatter in the results. In all cases, Poisson's ratio of HMA increases as the temperature rises, which contributes to a decrease in the resilient modulus (Fairhurst et al., 1990). The literature agrees that the resilient modulus values obtained using assumed values of Poisson's ratio differ from those obtained using calculated ones. However, opinions differ regarding the extent to which resilient modulus results differ when assumed values of Poisson's ratio are used. It appears that the effect of Poisson's ratio on the resilient modulus values depend on how data is analyzed. In determining the resilient modulus, HMA is considered an elastic homogeneous isotropic material, which is far from being true. As a result of this assumption, deflection measurements obtained from the IDT would lead to errors in calculating the resilient modulus, as well as Poisson's ratio. Moreover, there are different analytical procedures available for determining the resilient modulus and Poisson's ratio, most of which are based on empirical data and can often lead to erroneous values of the latter (negative values of Poisson's ratio; or Poisson's ratio greater than 0.5).

2.3.4 Effect of Testing Axis

It is important to perform the IDT along the same axis at all the test temperatures. Kim et al. (1992) showed that resilient modulus values were slightly higher along the diametral axis tested first. The axis dependency became more significant when values were determined from Poisson's ratio calculated from vertical and horizontal deformations. Fairhurst et al. (1990) used laboratory-compacted specimens to study the change in resilient modulus values based on calculated Poisson's ratio at different specimen rotations. Resilient modulus values at the initial axis position, called the 0-degree specimen position, were larger than those at the 90-degrees specimen position. The 90-degrees position is taken with respect to the initial 0-degrees position. Since the 90-degree position was always tested after the initial 0-degree position, findings suggested that the decrease in values could result from internal damage to the specimen during initial position testing. Another interesting finding indicated that Poisson's ratio at the 90-degree position was slightly higher than that at 0-degrees. This could be due to a redistribution of the applied load into the region outside the center (as a result of the "weakened" central zone), which causes greater overall horizontal deformation, hence a higher Poisson's ratio. From these observations, Poisson's ratio could be used to indicate excessive damage in the specimen during testing.

2.3.5 Specimen Size Effect

In the indirect tension test setup, the resilient modulus depends on the specimen size as well as on the maximum-stone-size-to-specific-diameter ratio (Lim et al., 1995). Since they are less affected by a single aggregate than smaller specimens, those having larger diameters seem to result in more realistic resilient modulus values. Moreover, a high diameter to maximum aggregate size ratio would better represent the overall mix behavior. Within the same mix, resilient modulus values decrease as specimen diameter increases. This trend was also evident in the indirect tension strength of the specimen (Lim et al.,1995).

2.3.6 Effect of Measuring Devices

In an indirect tension tested specimen, highly variable stresses exist. Therefore, the moduli obtained from measurements taken on the specimen's exterior are average. Moreover, damage occurring near the steel loading heads may significantly effect the vertical and horizontal measurements obtained on the specimen's exterior (Sousa et al., 1991). Sousa concluded that strains obtained from exterior measurements do not represent what occurs in the failure plane. Also, externally mounted sensors record not only the deformation of a specimen, but also any rotation resulting from misalignment or irregularities.

Along the diameter, the vertical and horizontal stress distribution in an indirect tension specimen is non-uniform (Figure 2.1-according to Hondros, 1959). Stresses and strains near the center at the face of the indirect tensile specimen are fairly uniform and are unaffected by end effects caused by the loading plates. Therefore, accurate deflection measurements can be taken in this zone of uniform stress, which will enable accurate estimations of the resilient modulus and Poisson's ratio.

In indirect tension tests, the failure plane is located along the vertical centerline. Measurements can be obtained on the failure plane by placing a horizontal sensor at the specimen's center (Ruth and Maxfield, 1977; Hussain, 1990). Interior strain measurements can be obtained using strain gauges or linear variable deflection transducers (LVDTs), each of which has its advantages and disadvantages. Strain gauges provide superior precision and accuracy; however, they are time consuming to mount and cannot be reused. LVDTs are easily used, reasonably inexpensive, and provide decent accuracy; however, they are affected by specimen bulging (Roque and Buttlar, 1992).

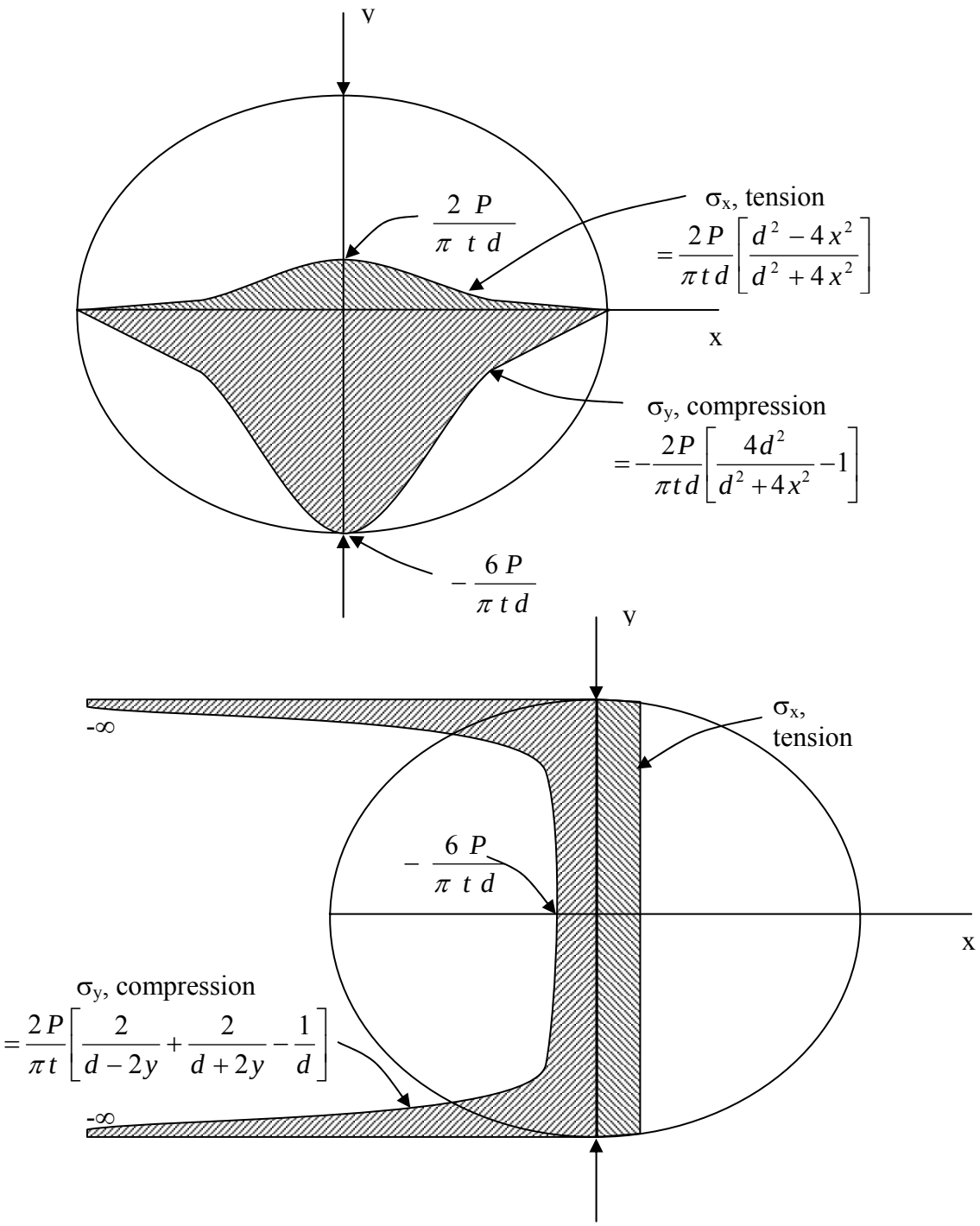

Figure 2-1 Elastic stress distribution in indirect tension specimen.

2.3.7 Effect of Moisture

Additionally, environmental effect such as moisture susceptibility can have a significant effect on the resilient modulus. Heincke and Vinson (1988) investigated the effect of moisture on the resilient modulus. Specimens were conditioned in three sets. The control set was left dry, one test set was subject to vacuum saturation, and one set was exposed to vacuum saturation followed by one freeze thaw cycle. This conditioning requirement is the same one used in determining the tensile strength ratio (Lottman, 1978). The index of retained resilient modulus (IRM_r) is offered as a predictor of pavement moisture susceptibility. The IRM_r is determined as:

$$IRM_r = \frac{M_r \ of \ conditioned \ specimen}{M_r \ of \ control \ specimen}$$

Where, M_R is the resilient modulus. The authors refer to work by Hicks et al. (1985), which establishes the criteria for IRM_R evaluation:

$IRM_R > 0.70$ Mixture passes as designed; and
$IRM_R < 0.07$ Mixture fails and must be redesigned.

In conclusion, the mix components and the compaction method used have a significant effect on the resilient modulus results. The variation between laboratory compacted specimens and field cores resilient moduli is an important parameter to be investigated. In addition, the loading used to perform the IDT test should simulate the field loading. To make any sense of IDT test results, the loading magnitude and duration should be reported along with the resilient modulus values. Traditionally only vertical deflection measurements used to be taken in the IDT and a value of Poisson's ratio was assumed to determine the resilient modulus. However, it has been shown that the resilient modulus determined from assumed Poisson's ratio values can significantly be in error.

Different data analysis methods have been developed to determine the resilient modulus from the IDT test. These data analysis methods are developed for specific deflection measuring devices and are sometimes applicable to any specimen size.

2.4 Resilient Modulus Data Analysis Methods

There are several methods for analyzing the resilient modulus testing of HMA. In this section, a summary of these methods is presented. Special interest is given to Hondro's 2-D plane stress solution as it is a basis for all the developed methods (Hondros, 1959), Roque and Buttlar's indirect tension specimen analysis (Roque and Buttlar, 1992), and Kim et al.'s 3-D solution (Kim et al., 2002).

2.4.1 Hondros' 2-D Plane Stress Solution

The theoretical elastic stress distribution in an indirect tension specimen is shown in **Error! Reference source not found.** after Hondros (1959). This distribution is derived from the plane stress solution. As indicated by Hondros (1959), the elastic stresses along the horizontal and vertical diameters are expressed by the following:

$$\sigma_x(x) = \frac{2P}{\pi a d}\left[\frac{\frac{1-x^2}{R^2}\sin 2\alpha}{\frac{1+2x^2}{R^2\cos 2\alpha}+\frac{x^4}{R^4}} - \arctan\left(\frac{\frac{1-x^2}{R^2}}{\frac{1+x^2}{R^2}}\tan\alpha\right)\right] \tag{2.1}$$

$$\sigma_y(x) = -\frac{2P}{\pi a d}\left[\frac{\frac{1-x^2}{R^2}\sin 2\alpha}{\frac{1+2x^2}{R^2\cos 2\alpha}+\frac{x^4}{R^4}} + \arctan\left(\frac{\frac{1-x^2}{R^2}}{\frac{1+x^2}{R^2}}\tan\alpha\right)\right] \tag{2.2}$$

$$\sigma_x(y) = \frac{2P}{\pi a d}\left[\frac{\frac{1-y^2}{R^2}\sin 2\alpha}{\frac{1+2y^2}{R^2\cos 2\alpha}+\frac{y^4}{R^4}} - \arctan\left(\frac{\frac{1+y^2}{R^2}}{\frac{1-y^2}{R^2}}\tan\alpha\right)\right] \tag{2.3}$$

$$\sigma_y(y) = -\frac{2P}{\pi a d}\left[\frac{\frac{1-y^2}{R^2}\sin 2\alpha}{\frac{1+2y^2}{R^2\cos 2\alpha}+\frac{y^4}{R^4}} + \arctan\left(\frac{\frac{1+y^2}{R^2}}{\frac{1-y^2}{R^2}}\tan\alpha\right)\right] \tag{2.4}$$

where,

σ = stress along the vertical or horizontal diameter;

P = applied load;

a = loading strip width;

d = specimen thickness;

R = specimen radius; and

α = radial angle subtended by the loading strip.

By introducing a specimen mounted extensometer system that measures deformations across the center of the specimen, one can overcome the difficulties of obtaining horizontal and vertical deformation measurements (Lytton et al., 1993). In general, the main problem associated with the test is its failure to completely simulate the stress conditions of in-situ pavements. Hadley et al. (1970) first developed a direct method of estimating the modulus of HMA based on the equations for the indirect tensile test developed by Hondros (1959). Their work is a base for the equation used in ASTM D4123.

To calculate the resilient modulus of HMA, Schmidt (1972) adapted the Hondros solution:

$$M_r = \frac{P(\nu + 0.2732)}{t\Delta} \tag{2.5}$$

where,

M_r = modulus of elasticity, assumed to be equal to the resilient modulus;

ν = Poisson's ratio;

t = specimen thickness; and

Δ = total horizontal deformation.

The equation proposed by Schmidt (1972) assumed that Poisson's ratio is known. He suggested that a value of 0.35 is used. Cragg and Pell (1971) reported Poisson's ratio values ranging between 0.35 and 0.45. Since HMA is a viscoelastic material, Equation 2.5 can be used for loading times of short durations (Schmidt, 1972).

He suggested that load duration of 0.1sec, followed by a rest period of 3sec, would be adequate.

Comparing the theoretical and actual values of the modulus, Hadley and Vahida (1983) used finite element analysis to evaluate the use of the indirect tensile test in determining the resilient modulus. As a result of the study, modified equations were developed to determine the measured resilient modulus for 100-mm and 150-mm diameter specimens; and presented in equations 2.6 through 2.9 and 2.10 through 2.13 respectively;

$$\nu = \frac{0.0800R - 0.8590}{0.0403 - 0.2851R} \tag{2.6}$$

$$M_r = \frac{P\,D}{x\,t} \cdot \left(0.0800 + 0.2970\,\nu + 0.425\,\nu^2\right) \tag{2.7}$$

$$\sigma_T = \frac{P}{t} \cdot \left(0.1777 + 0.0223\,\nu\right) \tag{2.8}$$

$$\varepsilon_T = \left(0.3696 + 0.6354\,\nu\right) \cdot x \tag{2.9}$$

$$\nu = \frac{0.0619R - 0.7515}{0.0257 - 0.2182R} \tag{2.10}$$

$$M_r = \frac{P\,D}{x\,t} \cdot \left(0.0646 + 0.2357\,\nu + 0.0290\,\nu^2\right) \tag{2.11}$$

$$\sigma_T = \frac{P}{t} \cdot \left(0.1400 + 0.0112\,\nu\right) \tag{2.12}$$

$$\varepsilon_T = \left(0.3696 + 0.6354\,\nu\right) \cdot x \tag{2.13}$$

where,

R	=	ratio of y to x;
x	=	horizontal deformations resulting from applied load P;
y	=	vertical deformations resulting from applied load P;
σ_T	=	tensile stress; and
ε_T	=	tensile strain.

In an attempt to improve repeatability and accuracy of results, Baladi et al. (1988) developed another configuration for the indirect tensile test. Assumptions for the test were that plane-stress conditions exist in the specimen, that there is no friction between the loading plate and the specimen, and that the material behaves as homogenous isotropic linear elastic. Calculations of the resilient modulus and Poisson's ratio are based on the fixture and specimen geometry, as well as the response. The suggested equations for Poisson's ratio and the resilient modulus follow:

$$\nu = \frac{3.58791 - 0.26985 \cdot DR}{0.062745 + DR} \tag{2.14}$$

$$M_r = \frac{P\left(3.58791 - 0.062745 \cdot U\right)}{L \cdot V} \tag{2.15}$$

$$M_r = \frac{0.319145 \cdot P \cdot U}{L} \tag{2.16}$$

$$INCS = \frac{0.475386 \cdot P}{t} \tag{2.17}$$

$$INTS = \frac{0.156241 \cdot P}{t} \tag{2.18}$$

such that

$$DR = \frac{DV}{DH} \tag{2.19}$$

where,

DR = deformation ratio;
V = resilient deformation of the specimen along the vertical diameter;
H = resilient deformation of the specimen along the horizontal diameter;
L = radial deformation along the longitudinal axis (thickness) of the specimen;
INCS = indirect compressive strength at the center of the specimen; and

INTS = indirect tensile strength at the center of the specimen.

Heinicke and Vinson (1988) also developed equations for calculating the resilient modulus and Poisson's ratio for an indirect tension specimen. This equation is the one used by SHRP. They used the plane stress elastic theory assuming homogeneous and isotropic conditions. The resilient modulus and Poisson's ratio are calculated as follows:

$$M_r = \frac{P}{H \cdot t}(\nu + 0.27) \tag{2.20}$$

$$\nu = \frac{-3.59 - 0.27\left(\frac{V}{H}\right)}{-0.063 + \left(\frac{V}{H}\right)} \tag{2.21}$$

The tensile strain at the center of the specimen is calculated as follows:

$$\varepsilon_t = \left(\frac{0.16 + 0.48\nu}{0.27 + \nu}\right) H \tag{2.22}$$

where, ε_t is the tensile strain at the center of the specimen.

These equations are only valid for 100-mm diameter specimens. The validity of the plane stress and load configuration assumptions were verified by finite element analysis. Two two-dimensional and two three-dimensional models were considered. Results indicated that the resilient modulus test is adequately represented by elastic theory and the specimen's assumption of plane stress response. In this case, assuming the value of Poisson's ratio had little effect on the accuracy of the resilient modulus. Results also suggested that the resilient modulus is strain-dependent and that the dependency increases as test temperatures rises; that is, its viscoelastic behavior becomes more pronounced as the temperature of the test increases.

Equations 2.23 and 2.24 are the ones given by ASTM D4123. These two equations may be manipulated by substituting for ν in equation 2.23 to remove the horizontal deformation for calculating the resilient modulus as presented in equation 2.25 (Fairhurst et al., 1990).

$$M_r = \frac{P}{\Delta H_t \cdot t}(0.27 + \nu) \tag{2.23}$$

$$\nu = 3.59\frac{\Delta H_t}{\Delta V_t} - 0.27 \tag{2.24}$$

$$M_R = \frac{3.59 \cdot P}{t \cdot \Delta V_t} \tag{2.25}$$

This equation requires that Poisson's ratio be assumed. ASTM D4123 suggests a value of 0.35; however, Fairhurst et al. (1990) and others have shown that values of Poisson's ratio vary with temperature and loading; hence the assumption of the ratio is not recommended. Poisson's ratio was found to increase as temperature rises, so a value of 0.35 could be reasonably assumed for 25°C testing.

The equations developed for the SHRP P07 Protocol are reported to produce resilient modulus values 20 to 25% greater than those evaluated using the ASTM D4123 equations (Hadley and Groeger, 1992a). The equations introduced in the SHRP P07 Protocol for resilient modulus calculation follow:

$$E_{RI} = \frac{P\,D\,\left(0.080 + 0.297\,\nu + 0.0425\,\nu^2\right)}{H_I \cdot t} \tag{2.27}$$

$$E_{RT} = \frac{P\,D\left(0.080 + 0.297\,\nu + 0.0425\,\nu^2\right)}{H_T \cdot t} \tag{2.28}$$

where

E_{RI} = instantaneous resilient modulus of elasticity;

E_{RT} = total resilient modulus of elasticity;

The values for Poisson's ratio are calculated as follows:

$$\nu_{RI} = \frac{0.859 - 0.08\,R_I}{0.285\,R_I - 0.040} \tag{2.29}$$

$$\nu_{RT} = \frac{0.859 - 0.08\,R_T}{0.285\,R_T - 0.040} \tag{2.30}$$

$$R_I = \frac{V_I}{H_I} \tag{2.31}$$

$$R_T = \frac{V_T}{H_T} \tag{2.32}$$

where

V_I = instantaneous recoverable vertical deformation; and

V_T = total recoverable vertical deformation.

Another research effort, by Fairhurst *et al*. (1990), evaluated the MTS test system for the determination of resilient modulus. Results indicated that the M_R decreases and Poisson's ratio increases as the testing temperature rises. In addition, the resilient modulus was found to increase with cycle frequency. Possibly, this increase occurred because the decreased recovery times caused by increased test frequencies resulted in an accumulation of strain in the specimen. It was found that after a 90° rotation of the specimen, the resilient modulus was lower and Poisson's ratio slightly higher that the results in the 0° position. This could have occurred due to slight internal damage during testing in the 0° position. The increase in Poisson's ratio may be caused by a redistribution of stresses around the damaged area, which results in greater specimen deformations during testing at the 90° position.

2.4.2 Roque and Buttlar's Indirect Tension Specimen Analysis

Roque and Buttlar's indirect tension specimen analysis is based on the conception that plane stress conditions from the IDT test traditionally assumed to determine moduli do not actually apply for standard size specimens (Mamlouk and Sarofim, 1988). Therefore, moduli determined using measured vertical deformation can be significantly erroneous (Heinicke and Vinson, 1988). Using three-dimensional finite element (FE) analysis, Roque and Buttlar (1992) showed that the horizontal stress along the specimen thickness is not uniform. They found that the plane stress assumption is valid only for specimen thicknesses less than 25-mm. For thicknesses of 60-mm and more, non-uniformity in the stress, measured along the specimen thickness, will cause irregular bulging on the x and y axes and will, therefore, affect measurements obtained from the surface mounted sensors, causing them to rotate (Figure 2-2, after Roque and Buttlar, 1992).

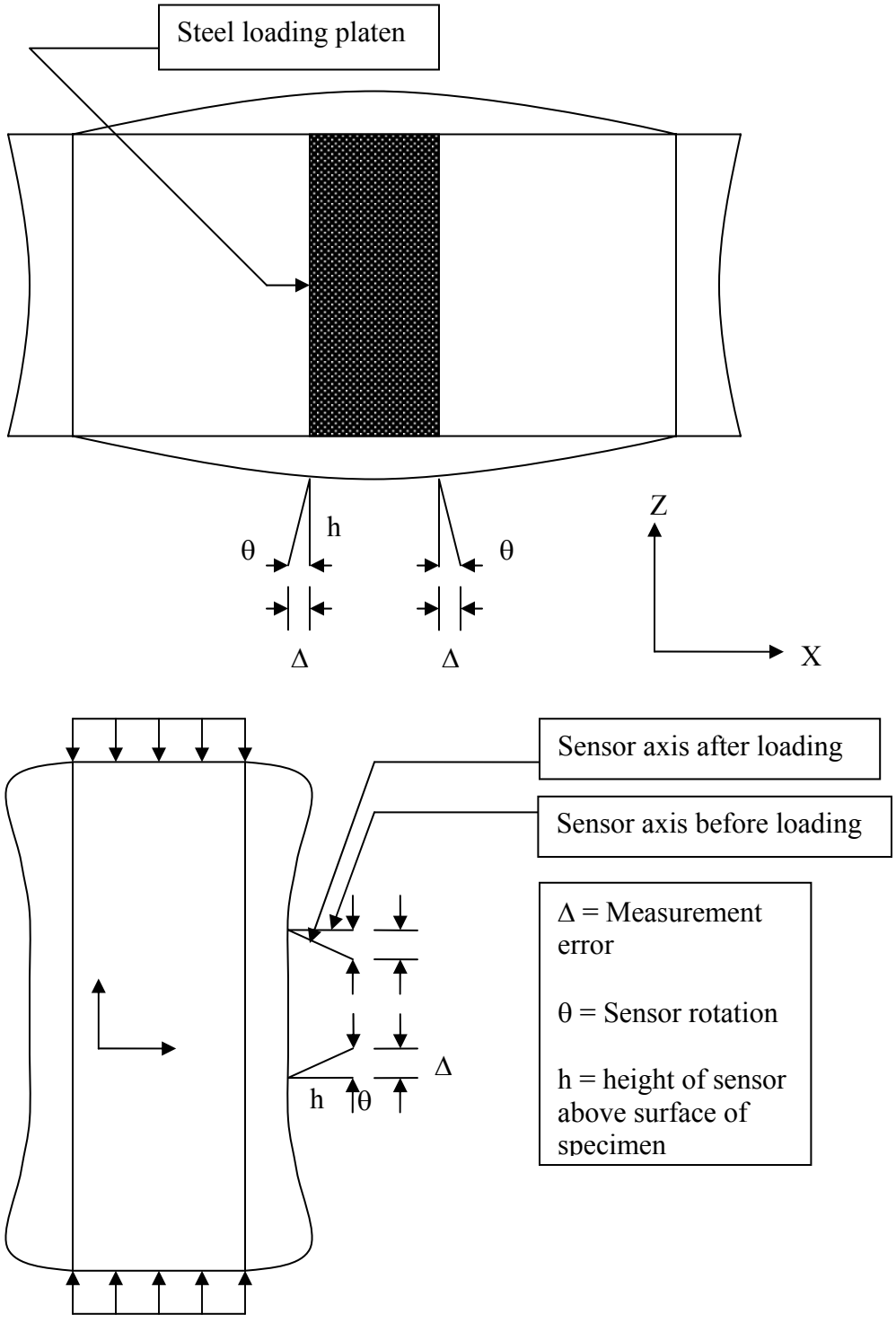

Figure 2-2 Illustration of Bulging Effects

The extent of bulging in the specimen was found to depend upon Poisson's ratio. Analyses were performed assuming a modulus of 1,380 MPa and three values of Poisson's ratio: 0.20, 0.35, and 0.45. For specimen bulging effect, correction factors, based on the specimens' diameter to thickness ratio, obtained from the three-dimensional FE solution were developed to adjust for the measured deformations along both axes. These correction factors permit researchers to approach the three-dimensional problem using two-dimensional analysis. Since the extent of bulging depends on Poisson's ratio, which is not known *a priori*, the analysis involves an iterative procedure, which should be valid for both 100- and 150-mm diameter specimens.

The analysis applies only for a gauge-length-to-diameter ratio of 1:4 and when the height of the extensiometers is 6.25-mm from the specimen surface. Tensile deformation is considered to be positive; compressive deformation is negative. The Roque and Buttlar data analysis was used in this research for the following reasons:

- The deflection measurement devices used in the research are similar to the ones the method was developed for,
- The method takes into account the deviation from the plane stress assumptions,
- The method allows the calculation of Poisson's ratio from deflection measurements, and,
- The method is valid for any specimen size, which is the case in this research where 100- and 150-mm diameter specimens were tested.

2.4.3 Three Dimensional Solution for the Indirect Tensile Test

The following three-dimensional solution for the indirect tensile test is based on the two-dimensional plane stress solution presented by Wijk (1978), wherein the latter is a "special case" of the three-dimensional one with stresses σ_z, τ_{xz}, and τ_{yz} approaching zero.

If the potential stress function of the two-dimensional problem is $\varphi(x, y)$, then the normal stresses are $\sigma_x(x, y)$ and $\sigma_y(x, y)$ in the following format (Wijk 1978):

$$\sigma_x = \frac{\partial^2 \varphi(x, y)}{\partial y^2} \tag{2.33}$$

$$\sigma_y = \frac{\partial^2 \varphi(x,y)}{\partial x^2} \tag{2.34}$$

Three-dimensional solutions may be obtained for the IDT with the following observations:

$$\sigma_z(x, y, z) = \tau_{zx}(x, y, z) = \tau_{zy}(x, y, z) = 0 \tag{2.35}$$

Based on this observation, Wijk (1978) derived the following equations for stresses:

$$\sigma_x(x,y,z) = \sigma_x(x,y) + \frac{\partial^2 \Delta\varphi(x,y,z)}{\partial y^2} \tag{2.36}$$

$$\sigma_y(x,y,z) = \sigma_y(x,y) + \frac{\partial^2 \Delta\varphi(x,y,z)}{\partial x^2} \tag{2.37}$$

$$\Delta\varphi(x,y,z) = -\frac{z^2}{2(1/\nu+1)}\left\{\frac{\partial^2}{\partial x^2} + \frac{\partial^2}{\partial y^2}\right\}\varphi(x,y) \tag{2.38}$$

where ν is Poisson's ratio.

Input equation (2.38) into equations (2.36) and (2.37) result in the following:

$$\sigma_x(x,y,z) = \sigma_x(x,y) - \frac{z^2}{2(1/\nu+1)}\left\{\frac{\partial^2}{\partial x^2 \partial y^2} + \frac{\partial^2}{\partial y^4}\right\}\varphi(x,y) \tag{2.39}$$

$$\sigma_y(x,y,z) = \sigma_y(x,y) - \frac{z^2}{2(1/\nu+1)}\left\{\frac{\partial^2}{\partial x^4} + \frac{\partial^2}{\partial x^2 \partial y^2}\right\}\varphi(x,y) \tag{2.40}$$

The normal and shear stresses at the faces of an indirect tensile specimen are zero for both the two-dimensional and three-dimensional cases. The stress-strain relationship in a three-dimensional problem is therefore the same as that in a two-dimensional one:

$$\varepsilon_x = (\sigma_x - \nu\sigma_y)/E \tag{2.41}$$

$$\varepsilon_y = (\sigma_y - \nu\sigma_x)/E \tag{2.42}$$

where E is Young's modulus.

The three-dimensional stresses σ_x and σ_y from Equations (2.39) and (2.40) are input into Equations (2.41) and (2.42), thus obtaining the following general expressions of three-dimensional strain distribution:

$$\begin{aligned}\varepsilon_x = \Big\langle\ \sigma_x(x,y) - \frac{z^2}{2(1/\nu+1)}\left\{\frac{\partial^2}{\partial x^2\partial y^2}+\frac{\partial^2}{\partial y^4}\right\}\varphi(x,y) - \\ \nu[\sigma_y(x,y) - \frac{z^2}{2(1/\nu+1)}\left\{\frac{\partial^2}{\partial x^4}+\frac{\partial^2}{\partial x^2\partial y^2}\right\}\varphi(x,y)]\ \Big\rangle/E\end{aligned} \tag{2.43}$$

$$\begin{aligned}\varepsilon_y = \Big\langle\ \sigma_y(x,y) - \frac{z^2}{2(1/\nu+1)}\left\{\frac{\partial^2}{\partial x^4}+\frac{\partial^2}{\partial x^2\partial y^2}\right\}\varphi(x,y) - \\ \nu[\sigma_x(x,y) - \frac{z^2}{2(1/\nu+1)}\left\{\frac{\partial^2}{\partial x^2\partial y^2}+\frac{\partial^2}{\partial y^4}\right\}\varphi(x,y)]\ \Big\rangle/E\end{aligned} \tag{2.44}$$

Horizontal and vertical displacements are obtained by integrating the strains along the gauge length. The solutions for the vertical and horizontal displacements are functions of the specimen diameter, and the gauge length as follows:

$$U = \frac{P(C_1 + C_2\nu + C_3\nu^2 + C_4\nu^2 d^2)}{Et(1+\nu)} \tag{2.45}$$

$$V = \frac{P(C_5 + C_6\nu + C_7\nu^2 + C_8\nu^2 d^2)}{Et(1+\nu)} \tag{2.46}$$

2.5 Summary

Pavement design requires the characterization of the paving materials. Hot mix asphalt resilient modulus is an important material property that needs to be determined for pavement design. The IDT test has become the most widely used laboratory test to determine the resilient modulus of HMA. However the resilient modulus depends on many parameters. In addition, data analysis of the IDT test is somewhat complicated. Significant effort has been directed towards determining the state of stress in the IDT specimen (Roque and Buttlar, 1992; Kim et al., 2002). The Roque and Buttlar data analysis was developed for a testing system similar to the one used in this research and seems very promising since it takes into account three dimensional effects. The next chapter presents the research approach undertaken in this study.

Chapter 3 Research Approach

This chapter discusses the research approach. The topics it focuses on are specimen production, specimen testing, and data analysis.

3.1 Introduction

As indicated in chapter 2, the resilient modulus of HMA depends on the test setup, mix preparation and properties, sample size, test temperature, and the data analysis procedure. The IDT test was chosen in this study due to its ability to closely simulate the state of stress the HMA layer experiences in the field under traffic loading. In addition, it allows obtaining horizontal and vertical deflection measurements necessary for calculating the Poisson's ratio. The main objective of this research was to develop shift factors between the measured resilient modulus of laboratory prepared specimens and field cores. In the process of achieving this objective, the different mixes used for the construction of the Virginia Smart Road were tested. The resilient modulus of HMA can be determined in the laboratory using 100- or 150-mm specimen size diameters. Due to the relatively thin wearing surface at the Virginia Smart Road, only 100-mm cores could be tested. However, 100- and 150-mm diameter specimens were prepared to evaluate the effect of specimen size. The effect of load pulse duration, temperature, and volumetric properties were also investigated. Finally two data analysis procedures to determine the resilient modulus, were investigated; Roque and Buttlar's procedure (Roque and Buttlar, 1992) and Kim et al.'s procedure (Kim et al., 2002). In order to accomplish the objective of this study, a research plan that utilized the materials used at the Virginia Smart Road and testing facility was developed.

3.2 Virginia Smart Road

The Virginia Smart Road is a research facility built in southwest Virginia. Upon completion, the Virginia Smart Road will be a 9.2 km connector highway between Blacksburg and I-81, with the first 2.5 km designated as a controlled test facility. Different sensors (measuring stresses, strains, and climatic parameters) have been installed in the pavement layers to monitor the health of the pavement and its performance. Pavement response to loading was monitored under different loading

conditions, truck tire pressure, temperature, and driving speed. The vertical compressive stress pulse induced by a moving truck and by FWD testing was determined at different locations. The average pulse width of the moving truck was determined at 8, 24, 40, and 72 km/h.

The flexible pavement part of the Virginia Smart Road test facility includes 12 heavily instrumented flexible pavement sections. Section length varies between 76 and 117 m. Seven of the 12 sections are located on a fill, while the remaining five sections are located on a cut. Different layers are used in each section (all designations and HMA designs are in accordance with the Virginia Department of Transportation Specifications). The different pavement layers are as follows:

- Wearing surface: Seven types of HMA wearing surface are used (SM-9.5A, SM-9.5A with high laboratory compaction, SM-9.5D, SM-9.5E, SM-12.5D, and an open-graded friction course [OGFC]). Five of these seven mixes are Superpave™. All of the mixes, with the exception of the OGFC, were constructed at 38-mm-thick. The OGFC was constructed at 19-mm-thick.
- Intermediate HMA layer: BM-25.0 at different thicknesses ranging from 100 to 244 mm.
- Three sections have the Superpave™ SM9.5A fine mix placed under the BM-25.0 to examine the benefits of such a design on reducing fatigue cracking.
- Open-graded drainage layer [OGDL]: Out of the 12 sections, three sections were built without the OGDL. Seven sections are treated with asphalt cement and two are treated with Portland cement. The thickness of this layer was kept constant at 75 mm throughout the project.
- Cement stabilized subbase: 21-A cement-stabilized layer used in 10 sections at a thickness of 150 mm.
- Subbase layer: 21-B aggregate layer was placed over the subgrade at different thickness with and without a geosynthetic.

The structural configuration of the Virginia Smart Road is presented in figure 3.1. The laboratory-measured resilient moduli can be used to calculate stresses and strains in using the layered elastic theory and then compare the obtained values to field measurements obtained from truck testing. Mix properties other than the resilient modulus that are being determined at the Virginia Smart Road are creep and fatigue characteristics.

Material	Section / Thickness (mm)								
	A - D	E	F	G	H	I	J	K	L
OGFC* HMA Wearing Surface	-	-	-	-	-	-	-	19	-
HMA Wearing Surface	38	38	38	38	38	38	38	19	38
HMA Base	150	225	150	100	100	100	225	244	150
HMA Surface (placed as base)	-	-	-	50	50	50	-	-	-
Asphalt Stabilized OGDL**	75	-	-	-	75	75	75	-	-
Cement Stabilized OGDL	-	-	-	-	-	-	-	75	75
Cement Stabilized Aggregate Base	150	150	150	150	150	150	-	-	150
21B Aggregate Base	175	75	150	150	75	75	75	150	75

* OGFC - Open Graded Friction Course
** OGDL - Open Graded Drainage Layer

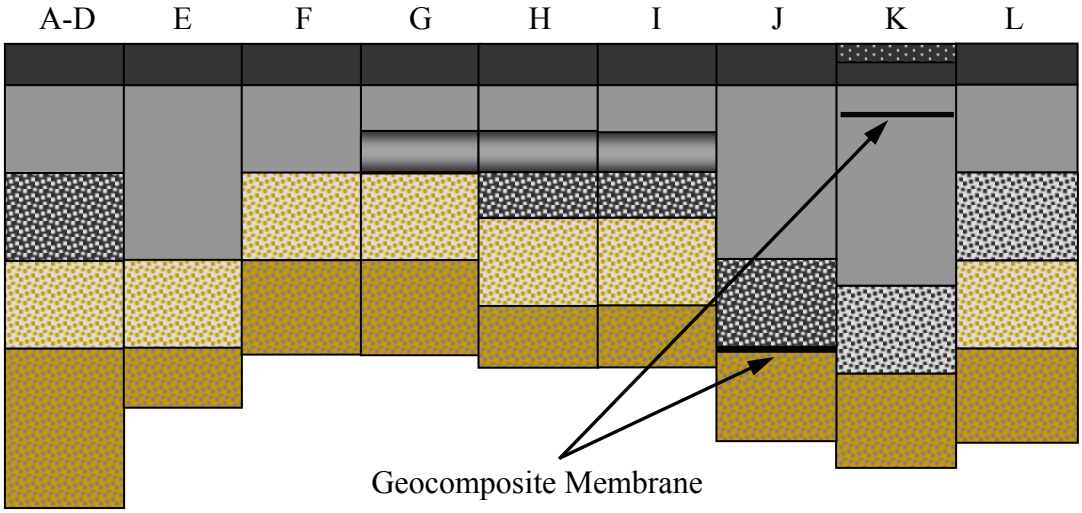

Figure 3-1 Structural configuration of Virginia Smart Road.

3.3 Hot Mix Asphalt Preparation

The seven different mixes that were placed at the Virginia Smart Road are presented in Table 3.1. Materials for this study were provided either directly from the

Virginia Smart Road, in the form of road cores or loose bagged mixture samples collected during construction, or were produced from raw materials to meet either volumetric criteria determined from road cores or to meet design specifications. All raw materials used for production of specimens were obtained from the source utilized during construction. Practices recommended by the Virginia Department of Transportation and in accordance with Superpave protocol were implemented in specimen preparation.

Table 3-1 Mixture characteristics at the Virginia Smart Road

Section	HMA Wearing Surface	Characteristics
A	SM-12.5D	12.5mm nominal maximum aggregate size PG 70-22 binder
B, E – H, J	SM-9.5D	9.5mm nominal maximum aggregate size PG 70-22 binder
C	SM-9.5E	9.5mm nominal maximum aggregate size PG 76-22 binder
D, I	SM-9.5A	9.5mm nominal maximum aggregate size PG 64-22 binder Section I designed with high lab compaction
K	OGFC	12.5mm nominal maximum aggregate size PG 76-22 binder
L	SMA-12.5	12.5mm nominal maximum aggregate size PG 76-22 binder

3.3.1 Specimen Designation and Characteristics

Three specimen types were produced in two different sizes; 100-mm diameter specimens and 63.5-mm thick and 150-mm diameter specimens and 76.2-mm thick. A fourth specimen type was obtained from the Virginia Smart Road in form of 100-mm diameter field cores. The thickness of the field cores was controlled by the thickness of the constructed HMA layer. The four specimen types are divided into the following categories:

- Field/field (F/F): field cores from the Virginia Smart Road, only available in 100-mm diameter. Field core thickness is controlled by the wearing thickness at the Virginia Smart Road and varied between 37 and 50 mm;
- Field/lab (F/L): specimens compacted in the laboratory from loose mixtures samples obtained from the field at the time of construction;
- Lab/lab (L/L): specimens produced and compacted in the laboratory using volumetric results from field specimens; and
- Design/lab (D/L): specimens produced and compacted in the laboratory according to design specifications.

The analysis of volumetric properties was performed for all mixtures. It included specimen bulk specific gravity and compaction densification curves, mixture maximum theoretical specific gravity (Rice), aggregate gradation, and asphalt content measurements for the four different types of mixes. The results are presented in Appendices A and B. The Summary of the tests specimens for resilient modulus evaluation is presented in Table 3-2.

Table 3-2 Number of Tested Specimens

Section	Mixture	F/F	F/L		L/L		D/L*	
		a	a	b	a	b	a	b
A	SM12.5D	2	3	2	3	2	6	2
B	SM-9.5D	2	3	2	3	2	6	2
C	SM-9.5E	2	3	2	3	2	6	2
D	SM-9.5A	2	3	2	3	2	6	2
E	SM-9.5D	2	3	2	3	2	Same as B	
F	SM-9.5D	2	3	2	Same as E			
G	SM-9.5D	2	3	2				
H	SM-9.5D	2	3	2				
I	SM-9.5A*	2	3	2	3	2	6	2
J	SM-9.5D	2	3	2	3	2	Same as B	
K	OGFC	Not tested						
L	SM-12.5	2	3	2	3	2	6	2

D/L* 3 specimens tested at 0.1 sec load pulse and 3 specimens tested at 0.03 sec load pulse

a 100-mm diameter specimens with 63-mm thickness

b 150-mm diameter specimens with 75-mm thickness

3.3.2 Specimen Preparation

Field/Field Specimens

F/F specimens consist of cores obtained from the Virginia Smart Road wearing surface. After core extraction, the wearing surface was separated from the base mix (BM). The extracted samples' surfaces had to be treated so that they are smooth enough to mount the extensiometers. The specimen thickness was recorded as the average of three measurements taken at 120^{o} intervals.

Field/Lab Specimens

Field/Lab mixes were collected during the construction of the Virginia Smart Road. Samples were heated to be brought up to compaction temperature. This procedure was performed in less than an hour to prevent specimen aging. The specimens were then compacted using a troxler gyratory compactor. The compaction temperature ranged between 135 and 144^{o}C. The specimens volumetric properties were then taken before they were cut to the specified thickness (63.5- and 76.2-mm for 100- and 150-mm specimens respectively) to be tested.

Lab/Lab Specimens

Lab/Lab mixes were produced in the laboratory to replicate F/L mixes. Aggregate gradation and asphalt content were determined by from F/L mixes, using the ignition oven for asphalt content determination. Lab/Lab gradations were designed to replicate as closely as possible F/L gradations by mixing the proper amount of the different aggregate types used for the construction of the Virginia Smart Road. The proper amount of asphalt binder was then added to the aggregate for mixing. The mixing temperature ranged between 135 and 170^{o}C. The procedure for compaction and final sample preparation was the same as for F/L specimens.

Design/Lab Specimens

The procedure for preparing D/L specimens was the same as the one for L/L specimens except that the aggregate gradation and asphalt content are determined from the design sheets.

3.3.3 Laboratory Compaction

The effect of mix preparation and construction practices can be minimized with better quality control. The effect of compaction can only be controlled when the compaction method used in the laboratory simulates field compaction. However, this could be difficult to achieve due to the difference between pavement construction and laboratory prepared specimens. Laboratory compacted specimens are designated as F/L, L/L, and D/L. In this case, only differences in mix preparation between the laboratory and the mixing plant were considered. Gyratory compaction has been shown to be the method of compaction that most accurately replicates field compaction. The gyratory compactor used is the Troxler compactor, in accordance with AASHTO TP-4 (Table 3-2).

Figure 3-2 Troxler Gyratory Compactor.

The compaction pressure used is 600 KPa at an angle of 1.25^{o}. The number of gyrations is as specified in Table 3-3. The specimens were compacted at N Design.

Table 3-3 Number of Gyrations for each Mix

Section	HMA Wearing Surface	Number of Gyrations		
		N Design	N Initial	N max
A	SM-12.5D	75	7	115
B, E – H, J	SM-9.5D	75	7	115
C	SM-9.5E	75	7	115
D, I	SM-9.5A	65	7	100
K	OGFC	Not Tested		
L	SMA-12.5			

Prior to compaction, the HMA and the mold were heated to the specified compaction temperature. When compaction was completed, the specimens were allowed to cool down before being extracted from the mold, which would reduce the possibility of inducing residual stresses on the specimen sides. The volumetric properties were then measured before cutting the samples to the specified thickness for testing.

3.4 Specimen Testing

As indicated in chapter 2, the IDT setup was chosen in this research mainly due to its relative simplicity in comparison to the triaxial setup and its ability to simulate the state of stress that is present in the field.

AASHTO TP9-96 provides the standard test method for IDT test. The test procedure is based on ASTM D4123. One difference between the AASHTO setup and the one used in this study is the loading frame which consists of four columns in AASHTO TP9-96 whereas this study uses a two columns loading frame. Another difference is that AASHTO TP9-96 uses mounted LVDTs for deflection measurements whereas in this study spring mounted extensiometers were used as shown in Figure 3.3. Bracket mounts are glued on both specimen faces as shown in Figure 3.3a. The distance between the mounts is 25.4- and 38.1-mm for 100- and 150-mm specimens, respectively. Then the brackets are fixed on the mounts as shown in Figure 3.3b. Two sets of brackets were used; one for 100-mm specimens and another for 150-mm specimens. Two sets were required since the same set of extensiometers is used for both diameter sizes while the gauge length is different. Finally, the exstensiometers are

mounted on the brackets (Figure 3.3c). The specimen diameter to gauge length ratio is the same for both specimen sizes. The gauge length is set at 25.4-mm for 100-mm diameter specimens as specified in AASHTO TP9-96. The gauge length for the 150-mm diameter specimens is 38.1-mm. The gauge length chosen is important to minimize the possibility of placing the gauge in a zone primarily influenced by a single aggregate. A minimum of 25.4 mm gauge length is, therefore, required for 100-mm diameter specimens and was used by Roque and Buttlar (1992), Ruth and Maxfield (1977), Anderson and Hussein (1990), and Hugo and Nachenius (1989). Also, a gauge of 25.4-mm for 100-mm specimens and 38.1-mm for 150mm specimens will ensure that deflections are measured over an area of relatively uniform stress distribution as suggested by Roque and Buttlar (1992).

a) Glued mount

b) Brackets

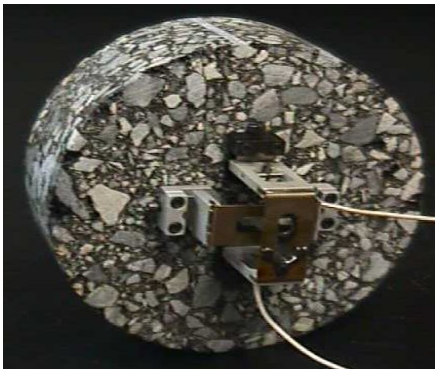

c) Extensiometers

Figure 3-3 Extensiometer Mounting

The IDT test was performed using an MTS servo-hydraulic closed-loop testing machine. An environmental chamber was used to control the temperature of the specimens. Specimens were conditioned for 24hrs for 5 and 25°C and at least 3 to 6hrs for 40°C testing. Applied loads were measured by the MTS load cell calibrated for 8900N, 22200N, and 89000N. The 8900N calibration was used for resilient modulus testing at 25°C and 40°C, while the 22000N calibration was used for resilient modulus testing at 5°C. The 89000N calibration was used for the indirect tensile strength test (IDTST). Deflection measurements were taken at both specimen surfaces to evaluate the within specimen variation. The test configuration of the IDT test is shown in Figure 3-4.

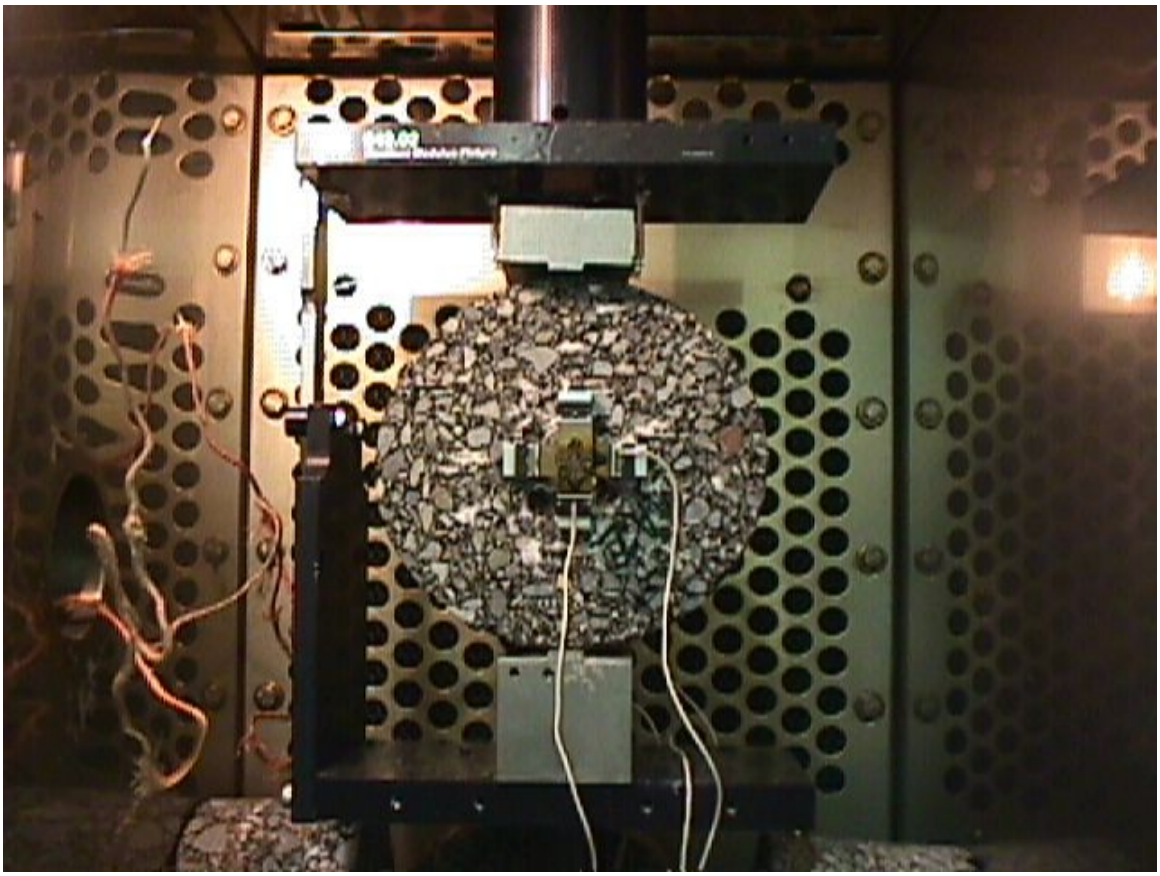

Figure 3-4 Test configuration of the Indirect Tension Test

3.4.1 Loading

The applied load was selected in a way to limit the strain between 150 and 500 microstrain. The upper limit of 500 microstrain was set to prevent specimen damage as recommended by Roque and Buttlar (1994), whereas the lower limit of 150 microstrain is set to obtain measurements much higher than the LVDTs' sensitivity. In this study, the 150 microstrain criterion was used after it was found that the signal to noise ratio of the extensiometers, at this range of strains, was very high. Hence, the applied load varied between mixes design and specimen sizes. The load used is a haversine load of 0.1 sec pulse duration and 0.9 sec rest period for all the specimens. A second set of D/L specimens was tested at a load of 0.03 sec pulse duration and 0.97 rest period as suggested by Loulizi et al. (2002). Since the load was not known a priori, many tests were performed on the first specimen of each section to define the appropriate loading. The initial applied load was relatively small to prevent damaging the specimen. The specimen was allowed to recover for a period of 30mins before it was tested again under a different loading. The load at which the measured horizontal and vertical deformations fell in the range of 150 and 500 microstrain was the load used to test the rest of the specimens. This same procedure was repeated for each mix at the three different temperatures (5, 25, and 40^{o}C). The final loads used for testing are presented in Chapter 4.

3.4.2 Testing and Data Collection

The IDT test for the resilient modulus was conducted at 100 cycles for all testing temperatures. After 100 cycles, the accumulated plastic strain per cycle becomes negligible. The 100 conditioning cycles simulate the consolidation that occurs in pavements when it is opened for traffic. Deflection and load readings were recorded for the last 5 cycles of the test at 0.0048828 sec intervals. The readings were averaged to determine the resilient modulus and Poisson's ratio. The calculated resilient modulus variation in any two loading cycles has to be lower than 5% for test results acceptance. Two resilient modulus and Poisson's ratio values were determined for every specimen; one at each specimen's surface. An example of the collected data is presented in figure 3.5.

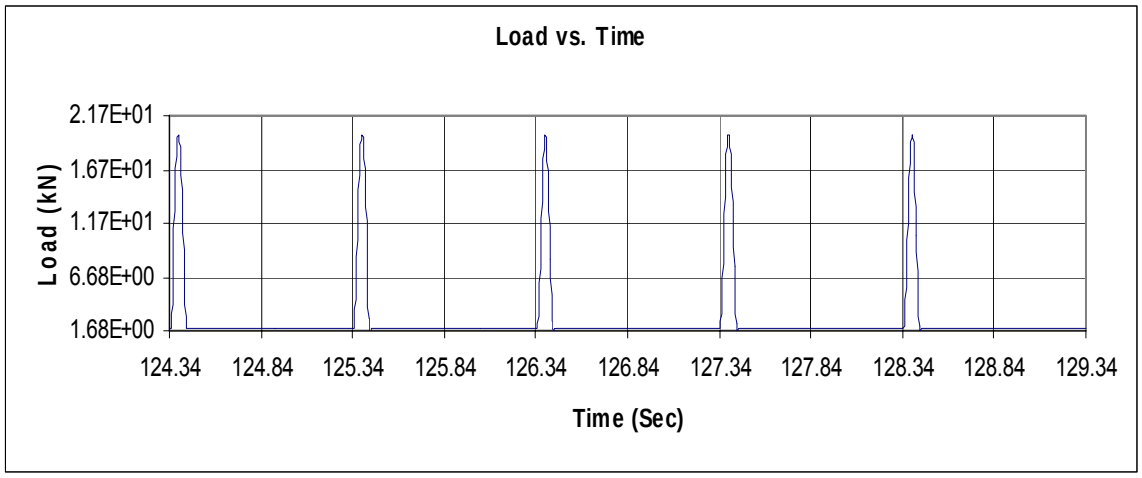

(a) Applied Load

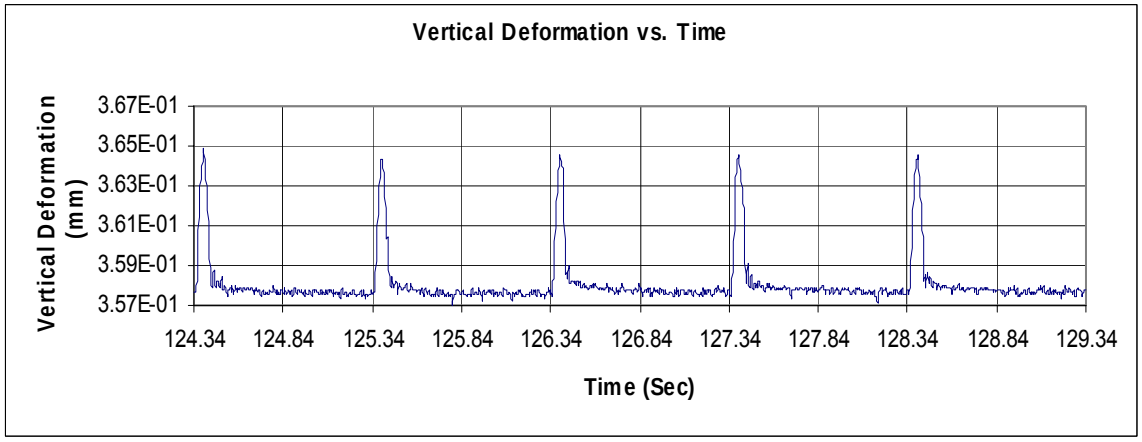

(b) Measured Vertical Deformation

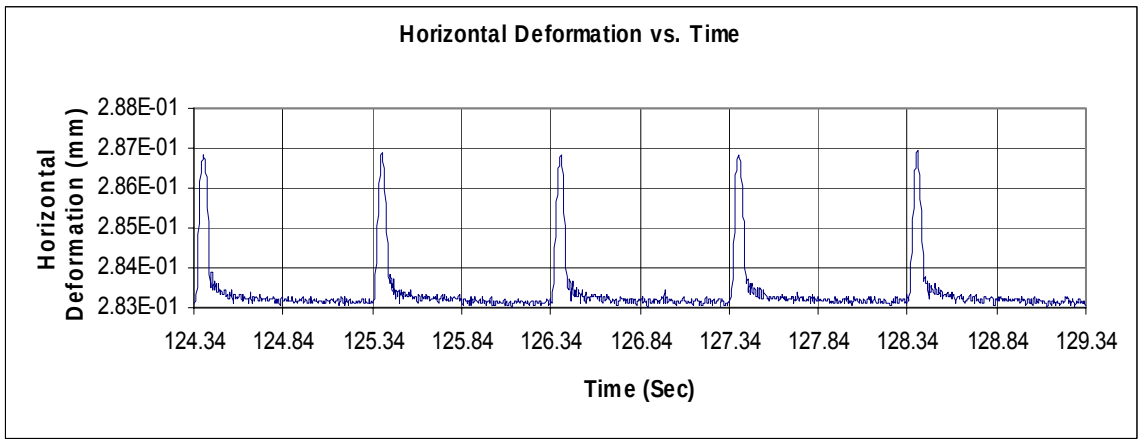

(c) Measured Horizontal Deformation

Figure 3-5 Collected Data for Resilient Modulus Testing

The IDT test for resilient modulus is run in such a way that 10% of the maximum applied load is maintained during the rest period. This is done to ensure contact between the loading plates and the specimen throughout the test which will reduce the risk of specimen movement during loading and unloading. The horizontal and vertical deformations are taken as the difference between the maximum and the minimum readings of each of the vertical and horizontal extensiometers, respectively.

3.4.3 Indirect Tensile Strength Test

After the resilient modulus test was performed at the three different temperatures of 5, 25, and 40^{o}C, specimens were allowed to recover for a period of 24 hrs before they were tested for their indirect tensile strength. The indirect tensile strength test was performed at a temperature of 25^{o}C. The test was performed to compare the applied load for resilient modulus testing to the indirect tensile strength, since this is the procedure suggested by ASTM D 4123. A load was applied to the specimen at a constant crosshead rate; it is desirable to have a constant strain rate input. However, since the strain is calculated from extensiometer measurements and in order to prevent damaging them, the extensiometers had to be removed from the specimen surfaces, and a constant crosshead rate of 50.1 mm/min was used. Failure is detected when the applied load drops to 75% of the maximum applied load. Since the extensiometers are removed, it is not possible to calculate Poisson's ratio during testing. Hence, the stress in the specimen is calculated using Hondro's plane stress solution. The indirect tensile strength results are presented in Appendix C.

3.5 Resilient Modulus Calculations

As presented in Chapter 2, many methods were developed by different researchers to calculate the resilient modulus from indirect tensile testing. The Roque and Buttlar (1992) method and Kim et al. method (2002) were used in this research for the following reasons:

- The analyses take into account three-dimensional effects
- The analyses allows for determining Poisson's ratio instead of assuming one
- The analyses take into account the specimen dimensions (thickness and diameter)
- The Roque and Buttlar analysis was verified by finite element analysis

3.5.1 Roque and Buttlar's Procedure for Resilient Modulus Calculation

The Roque and Buttlar's procedure account for the effect of specimen bulging. Specimen bulging would cause the externally mounted extensiometers to rotate and, therefore, affect the vertical and horizontal deflection readings. The extent of bulging is dependent on the Poisson's ratio (Roque and Buttlar, 1992). Since Poisson's ratio is not known a priori, the analysis involves an iterative procedure. The determination of the resilient modulus and Poisson's ratio for an IDT test specimen based on the Roque and Buttlar data analysis is as follows (Roque and Buttlar, 1992):

1. Assume Poisson's ratio

2. Correct for horizontal deformation to account for bulging effect as follows:

$$C_{B_x} = \left\{1.01 - 0.12\nu - 0.05\left(\frac{t}{t_{std}}\right)\right\} \quad (3.1)$$

where,

C_{B_x} = correction factor applied for the measured horizontal deformation to correct for specimen bulging = H/H_M,
H = corrected horizontal deformation,
H_M = measured horizontal deformation,
t = measured specimen thickness,
t_{std} = standard specimen thickness (62.5mm for 100mm specimens),
H_M = measured horizontal deformation, and
ν = Poisson's ratio.

3. Correct vertical deformation to account for bulging effect as follows:

$$C_{B_y} = \left(0.994 - 0.128\nu\right) \quad (3.2)$$

where,

C_{B_y} = correction factor applied to the measured vertical deformation to correct for specimen bulging = Y/Y_M ;

Y = corrected vertical deformation; and

Y_M = measured vertical deformation.

4. Convert the average strains measured by the gages to point strains. The relationship between average and point strain is independent of Poisson's ratio. The horizontal and vertical strains are then calculated as follows:

$$\varepsilon_{CTR_x} = 1.07 \frac{H}{GL} \times C_{B_x} \text{ (horizontal strain)} \quad (3.3)$$

$$\varepsilon_{CTR_y} = 0.98 \frac{Y}{GL} \times C_{B_y} \text{ (vertical strain)} \quad (3.4)$$

where,

GL = gage length, mm;

H = horizontal deformation, mm; and

Y = vertical deformation, mm.

5. Correct for horizontal and vertical point stress at the center of the specimen:

$$\sigma_{x_{CORR}} = \frac{2P}{\pi \times t_{std} d} C_{TxCTR} \quad (3.5)$$

$$\sigma_{y_{CORR}} = \frac{6P}{\pi \times t_{std} d} C_{TyCTR} \quad (3.6)$$

where,

$\sigma_{x_{CORR}}$ = corrected horizontal point stress;

$\sigma_{y_{CORR}}$ = corrected vertical point stress;

C_{TxCTR} = correction factor applied to the horizontal point stress; and

C_{TyCTR} = correction factor applied to the vertical point stress;

The correction factor for both the horizontal and the vertical stress are given in Table 3-4.

Table 3-4 Correction Factors for Horizontal and Vertical Stress

		Diameter to Thickness Ratio				
D=100 or 150-mm	ν	0.167	0.333	0.500	0.625	0.750
C_{TxCTR}	0.20	0.9471	0.9773	1.0251	1.0696	1.1040
	0.35	0.9561	1.0007	1.0871	1.1682	1.2321
	0.45	0.9597	1.0087	1.1213	1.2307	1.3171
C_{TyCTR}	0.20	-0.9648	-0.9754	-0.9743	-0.9693	-0.9611
	0.35	-0.9732	-0.9888	-0.9844	-0.9710	-0.9538
	0.45	-0.9788	-0.9971	-0.9864	-0.9646	-0.9395

6. Determine Poisson's ratio as follows:

$$\nu = \frac{\sigma_{x_{CORR}} - \left(\frac{\varepsilon_{CTR_x}}{\varepsilon_{CTR_y}}\right)\sigma_{y_{CORR}}}{\sigma_{y_{CORR}} - \left(\frac{\varepsilon_{CTR_x}}{\varepsilon_{CTR_y}}\right)\sigma_{x_{CORR}}} \tag{3.7}$$

If Poisson's ratio calculated using equation (3.7) differs by more than 0.01 with assumed Poisson's ratio in step 1 then replace the new value in step 1 and repeat step 2 to 6, otherwise continue to step 7

7. The HMA resilient modulus is determined as follows:

$$M_R = \frac{1}{\varepsilon_{CTR_x}}\left(\sigma_{x_{CORR}} - \nu\sigma_{y_{CORR}}\right) \tag{3.8}$$

3.5.2 Three-Dimensional Solution

Wijk (1978) suggested constructing the solution of a three-dimensional problem using the solution to a two-dimensional problem. A three-dimensional solution to the indirect tensile test can therefore be constructed based on the two-dimensional plane stress solution where the stresses σ_z, τ_{xz}, and τ_{yz} vanish.

The final solution to calculate the three-dimensional strains is given by (Kim et al., 2002):

$$\varepsilon_x = \Big\langle\ \sigma_x(x,y) - \frac{z^2}{2(1/\nu+1)}\left\{\frac{\partial^2}{\partial x^2\partial y^2}+\frac{\partial^2}{\partial y^4}\right\}\varphi(x,y) - \nu[\sigma_y(x,y) - \frac{z^2}{2(1/\nu+1)}\left\{\frac{\partial^2}{\partial x^4}+\frac{\partial^2}{\partial x^2\partial y^2}\right\}\varphi(x,y)]\ \Big\rangle / E \tag{3.9}$$

$$\varepsilon_y = \Big\langle\ \sigma_y(x,y) - \frac{z^2}{2(1/\nu+1)}\left\{\frac{\partial^2}{\partial x^4}+\frac{\partial^2}{\partial x^2\partial y^2}\right\}\varphi(x,y) - \nu[\sigma_x(x,y) - \frac{z^2}{2(1/\nu+1)}\left\{\frac{\partial^2}{\partial x^2\partial y^2}+\frac{\partial^2}{\partial y^4}\right\}\varphi(x,y)]\ \Big\rangle / E \tag{3.10}$$

The horizontal and vertical displacements under a certain loading are obtained by integrating the strain function along the gauge length. The linear three-dimensional solution for the vertical and horizontal displacements across a 25.4 mm gauge length and on a 100.8 mm diameter specimen are calculated as follows:

$$U = \frac{P(0.23+\nu+0.78\nu^2+80.6\nu^2d^2)}{Ed(1+\nu)} \tag{3.11}$$

$$V = \frac{P(0.3+1.38\nu+0.78\nu^2+222\nu^2d^2)}{Ed(1+\nu)} \tag{3.12}$$

where,

U, V = horizontal and vertical displacements, respectively;
P = load;
ν = Poisson's ratio;
d = thickness of specimen; and
E = Young's modulus.

For a specimen of 150-mm diameter, the vertical and horizontal displacements across a 38.1-mm gauge lengths are as follows:

$$U = \frac{P(0.18 + 0.773\nu + 0.588\nu^2 + 30.81\nu^2 d^2)}{Ed(1+\nu)} \tag{3.13}$$

$$V = \frac{P(0.21 + 0.89\nu + 0.68\nu^2 + 48.5\nu^2 d^2)}{Ed(1+\nu)} \tag{3.14}$$

The two unknwons that need to be determined are Poisson's ratio and the resilient modulus. In the case of a 100-mm diameter specimen, equations 3.11 and 3.12 can be rewritten as follows:

$$E = \frac{P(0.23 + \nu + 0.78\nu^2 + 80.6\nu^2 d^2)}{Ud(1+\nu)} \tag{3.15}$$

$$E = \frac{P(0.3 + 1.38\nu + 0.78\nu^2 + 222\nu^2 d^2)}{Vd(1+\nu)} \tag{3.16}$$

Similarly for the case of a 150-mm diameter specimen equations 3.13 and 3.14 are rewritten as follows:

$$E = \frac{P(0.18 + 0.773\nu + 0.588\nu^2 + 30.81\nu^2 d^2)}{Ud(1+\nu)} \tag{3.17}$$

$$E = \frac{P(0.21 + 0.89\nu + 0.68\nu^2 + 48.5\nu^2 d^2)}{Vd(1+\nu)} \tag{3.18}$$

Combining equations 3.15 through 3.18, an expression to calculate Poisson's ratio results in the following:

$$\frac{(0.23 + \nu + 0.78\nu^2 + 80.6\nu^2 d^2)}{(0.23 + \nu + 0.78\nu^2 + 80.6\nu^2 d^2)} = \frac{V}{U} \tag{3.19}$$

$$\frac{(0.21+0.89\nu+0.68\nu^2+48.5\nu^2d^2)}{(0.18+0.773\nu+0.588\nu^2+30.81\nu^2d^2)}=\frac{V}{U} \quad (3.20)$$

After calculating Poisson's ratio, the resilient modulus can be easily determined from equations 3.15 to 3.18.

The two data analysis methods presented earlier are tools used to determine resilient modulus values of the different HMA tested. The parameters investigated in this research are the effect of compaction method, mainly field compaction and laboratory gyratory compaction, as well as specimen size, load duration, and specimen volumetric properties on the laboratory measured resilient modulus using the IDT test setup.

3.6 Research Methodology

Differences in the resilient moduli are due to test variability as well as compaction method, mix preparation, specimen size, and loading time duration. Therefore, before analyzing the difference due to compaction, mix preparation, specimen size and loading time duration, it is essential to quantify the variability in the IDT itself.

3.6.1 Test Variability

The resilient modulus is determined using Roque and Buttlar's and Kim et al.'s approaches. Variations in the calculated resilient modulus will be evaluated and include:

- Within specimen variation; variation between the resilient modulus calculated from each face of the specimen. This variation is due to non-homogeneity across the specimen, the fact that the specimen is not centered on the loading plates, and error from the displacement measuring devices. It should be noted that error from the displacement measuring devices can be in such a way that both of them are wrong. However, the extensiometers were calibrated before the testing program had started.
- Variation between specimens of the same mix and section due to non-homogeneity. Variation due to non-homogeneity is also found within the same specimen. However, it cannot easily be separated from variation due to specimen miss-centering.

3.6.2 Shift Factors

Shift factors are developed for the method of compaction, the specimen size, and the loading time duration. The compaction shift factor reflects the difference in the measured resilient modulus from F/F and F/L specimens. Since these specimens differ only in the way they were compacted, any difference in the measured resilient moduli will be due to difference in compaction. To validate the effect of compaction on the measured resilient moduli, two volumetric properties are investigated: sample specific gravity and air void content.

The state of stress in the IDT specimen as well as deflection measurements taken at the specimens' surfaces should result in the same resilient modulus for either 100- or 150-mm diameter specimens. This is not the case for Hondro's plane stress solution. Roque and Buttlar (1992) developed correction factors for stress and strain in the IDT specimen. These correction factors are applied to Hondro's solution and are independent of the specimen size. The ability for these correction factors to be able to take into account the specimen size and therefore, result in the same resilient modulus results for 100- and 150-mm diameter specimens is evaluated. A specimen size shift factor is developed to take into account any variation between the 100- and 150-mm diameter specimens.

Hot-mix asphalt being a viscoelastic material, its response to loading depends on the time the load is applied. Two different loading time durations were tested. A shift factor is developed to take into account the loading time duration. This shift factor depends on the loading time durations used in testing and the test temperature. The loading times used are 0.1 and 0.03 sec pulse duration. The temperatures investigated are 5, 25, and 40^{o}C.

3.6.3 Resilient Modulus Prediction from Volumetric Properties

The resilient moduli of F/L, L/L, and D/L specimens will vary due to the different volumetric properties. The model developed assumes that the resilient modulus varies as a function of temperature in an exponential form: $Mr = \alpha e^{-\beta T}$. α and β depend on the HMA volumetric properties. A statistical analysis is performed to identify the volumetric properties that affect the measured resilient modulus. The procedure involves fitting the model to the available data and evaluating the model prediction capabilities. This is performed by using linear regression and the PRESS method. The model is developed

for the 100-mm specimens for the following reasons: three specimens were tested per section while only two were tested for 150 mm specimens, and the developed model can be used to calculate resilient modulus and compare it to the measured resilient modulus for field cores. Based on the model performance for F/L, L/L, and D/L samples, it can be concluded whether the difference between F/L and F/F resilient moduli is solely due to the difference in volumetric properties or whether, even after correcting for the difference in volumetric properties, there still is a difference between field compaction and laboratory gyratory compaction.

Chapter 4 Results and Analysis

4.1 Introduction

Under this research program the different parameters affecting the resilient modulus calculation of HMA—parameters related to the mix properties and the selected data analysis method—were determined. Before determining the parameters affecting the resilient modulus, the variability in the IDT test was evaluated. Since horizontal and vertical deformations are taken from both of the specimen faces, variation within the same specimen was evaluated. The variation between the specimens of the same mix was determined. Then, variation between specimens of the same mix and section is evaluated. Shift factors are developed between, laboratory and field compaction, different loading pulse durations (mainly 0.1 s and 0.03 s), and different specimen sizes (100- and 150-mm diameter specimens). It is already known that two factors will greatly affect the resilient modulus: the temperature at which the test is being conducted and the volumetric properties of the mix. A model is, therefore, developed relating the resilient modulus to the test temperature and the volumetric properties. The model was developed using the data taken from testing 100-mm diameter F/L, L/L, and D/L specimens. In order to develop and validate the model, the PRESS-statistic was used.

Before presenting the testing results, the chosen applied load and the procedure followed to determine the applied load to be used for testing is presented. Since each specimen was tested at three different temperatures, one major concern in determining the load to be applied was to prevent inducing damage to the specimens at any given temperature. Therefore, the load intensity was changed with temperature, with lower loads used for higher test temperature.

4.2 Load Determination

The resilient modulus is reported at a given temperature and load level. Since the resilient modulus of HMA is used as an input parameter for material properties in the elastic layered theory, and since its value depends on the load intensity, laboratory testing ideally should be performed at a load that will induce stress levels comparable to those experienced in the field. However, researchers have suggested using a load level that will induce stresses in the range of 10-50% of the indirect tensile strength of HMA at

25°C, with lower loads being used at higher temperatures. The load thus determined falls within a wide range, and while it is limited by the indirect tensile strength of HMA, it cannot guarantee prevention of damage to the specimen.

In a study that evaluated the measurement and analysis systems for indirect tensile testing, Buttlar and Roque (1994) suggested using a load level that would induce strains of between 150 and 500 microstrains, based on the reading accuracy of the measuring devices and on the necessity of preventing damage to the specimen. The strain level that induced damage was found to be 2000 microstrains, however, the authors suggested limiting the maximum strain less than 500 microstrains to ensure that the strain is well under the range where damage is induced. This criterion was developed for 1000s duration creep testing, at temperatures below 0°C, using the indirect tensile setup. As a result, it was used in this study for resilient modulus testing using the indirect tensile setup. Although the resilient modulus test is performed at higher temperatures (5, 25, and 40°C), it was assumed that, for the load duration for which the load is applied, typically 0.1s and 0.03s, the stress-strain material response is linear, which was to be true in the range of the applied load (Almudaiheem and Al-Sugair, 1991; Bourdeau et al., 1992). As a result of limiting the strain between 150 and 500 microstrains, the applied load at 25°C was about 20% of the indirect tensile strength measured at the same temperature.

During the early stages of testing to determine the appropriate load application, the resilient modulus was found to be load-independent at 5°C and 25°C (Table 4-1). Data relevant to load-dependency of the resilient modulus at 40°C could not be obtained since the tested range of applied load is very small (between 1000 and 3500 N). This observation contradicts findings reported in the literature in which it is suggested that the resilient modulus of HMA depends on load intensity. However, the dependence of the resilient modulus on loading can be attributed to non-linearity, which is caused by two factors: non-linearity in the elastic response and/or non-linearity due to viscous effects. The data presented in Table 4-1 was obtained using Roque and Buttlar's Data Analysis, which is a linear elastic data analysis approach.

In the resilient modulus calculation, only the recoverable strain is used; therefore, at a given temperature the viscous behavior is ignored. The viscous response of an HMA can be linked to the fact that the resilient modulus is calculated at three different temperatures; therefore, non-linearity due to the viscous part of HMA—which will lead to different moduli at different load levels—is not measured in the test. As for the non-

linearity in the elastic response, the range of applied load level used is small compared to the specimen indirect tension strength at a given temperature. The resilient modulus tests performed at 25°C can be used to verify that. As can be seen in Table 4-1, the applied load for specimen L3-6in-FL was between 2000 and 4500 N, which is 9 to 20% of the indirect tensile strength of the specimen at 25°C (22214 N). This small range of applied load is not sufficient to detect non-linearity. Although the indirect tension strength test was not performed at 5°C, it is expected that the strength at this temperature be much higher than that at 25°C, and the applied load range (4000 to 18000N) is presumably very small compared to the specimen strength.

Table 4-1 Resilient Modulus Variation with Loading

Specimen	temperature (°C)	Load (N)	Poisson's ratio	Mr (MPa)
C1-6in-FL	5	4000	0.08	12776
		7000	0.08	13555
		10000	0.05	12886
		15000	0.05	13459
		18000	0.05	13562
L3-6in-FL	25	2000	0.19	4185
		2500	0.18	4130
		3500	0.2	4406
		4000	0.21	4392
		4500	0.2	4268

Although the resilient modulus calculated according to the Roque and Buttlar method was found to be independent of the applied load in the tested load range, a 150 to 500 microstrains limiting criteria was set for the following reason: the research did not focus on whether the load intensity affected the resilient modulus values; therefore, the amount and range of data collected is not enough to totally ignore the effect of loading on the resilient modulus. Additionally, the strain limiting range is set to ensure that deflection measurements are well above the reading sensitivity of the strain gauge, which results in negligible error in the gauges and to reduce the risk of specimen damage. The applied loads used in the testing program as a function of temperature are summarized in Table 4-2. The induced strain as a function of temperature are

summarized in Table 4-3.The applied loads were different for 100-mm and 150-mm specimens and varied according to mix (F/F, F/L, L/L, and D/L).

Table 4-2 Applied Load as Function of Temperature, Mix, and Specimen Size

5°C	**Applied Load (N)**							
Section	**F/F**	**F/L**		**L/L**		**D/L**		**D/L-0.03**
	a*	a*	b*	a*	b*	a*	b*	a*
A	7000	12000	18000	14000	18000	12000	18000	12000
B	7000	13000	18000	13000	18000	12000	18000	13000
C	6000	14000	18000	14000	18000	12000	18000	12000
D	6000	14000	18000	13000	18000	12000	18000	12000
E	NA	12000	18000	12000	18000	Same as B		Same as B
F		12000	18000	Same as E				
G		14000	19000					
H	7000	13000	19000					
I	7500	15000	20000	14000	20000	14000	20000	14000
J	NA	13000	18000	12000	18000	Same as B		Same as B
L		10000	15000	10000	15000	10000	15000	10000
25°C	**Applied Load (N)**							
Section	**F/F**	**F/L**		**L/L**		**D/L**		**D/L-0.03**
	a*	a*	b*	a*	b*	a*	b*	a*
A	2500	4000	6300	5000	6000	4000	5000	5500
B	2500	4500	6000	4500	6000	4000	5000	5500
C	2250	4500	6300	4000	6000	4000	5000	5500
D	2500	4500	6000	4000	6000	4000	5000	5500
E	NA	4000	4500	4000	6000	Same as B		Same as B
F		4500	4500	Same as E				
G		5500	5000					
H	2500	4500	6000					
I	3000	5500	7000	5000	7000	5000	6000	6500
J	NA	4500	6300	4000	6000	Same as B		Same as B
L		3250	4500	2500	3500	2500	2500	4000
40°C	**Applied Load (N)**							
Section	**F/F**	**F/L**		**L/L**		**D/L**		**D/L-0.03**
	a*	a*	b*	a*	b*	a*	b*	a*
A	1000	2000	2000	2500	2000	2000	2000	2500
B	1000	2000	2000	2000	2500	2000	2000	2500
C	1000	2000	2000	2000	2000	2000	2000	2500
D	1000	2000	2000	2000	2000	2000	2000	2500
E	NA	2000	2500	1500	2500	Same as B		Same as B
F		2000	2500	Same as E				
G		2500	2500					
H	1000	2000	2800					
I	1250	2750	3500	2500	2500	2500	2000	2500
J	NA	2500	2000	2000	2500	Same as B		Same as B
L		1500	2000	1250	1500	1250	1250	2500

a* 100-mm diameter specimens with 63-mm thickness

b* 150-mm diameter specimens with 75-mm thickness

The applied load was chosen to induce strains ranging between 150 and 500 microstrains. The actual induced strains are presented in Table 4-3. In general the induced strain for 150-mm diameter specimens was higher than the one for 100-mm diameter specimens. This suggests that the resulting induced strain rate is higher for 150-mm diameter specimens since the load pulse duration is the same for both specimen sizes. The effect of having a different strain rate is discussed in section 4.5.2.

Table 4-3 Induced Vertical Strain as Function of Temperature, Mix, and Specimen Size

5°C	**Induced Strain (microstrain)**							
Section	**F/F**	**F/L**		**L/L**		**D/L**		**D/L-0.03**
	a*	a*	b*	a*	b*	a*	b*	a*
A	-303	-275	-303	-295	-293	-286	-381	-272
B	-347	-305	-315	-264	-288	-273	-391	-255
C	-326	-300	-288	-278	-325	-278	-356	-283
D	-334	-274	-362	-261	-311	-263	-363	-267
E	NA	-255	-265	-302	-312	Same as B		Same as B
F		-287	-285	Same as E				
G		-304	-299					
H	-399	-298	-314					
I	-328	-312	-326	-285	-321	-267	-381	-289
J	NA	-262	-283	-273	-391	Same as B		
L		-3.55	-396	-299	-379	-314	-497	-301

25°C	**Induced Strain (microstrain)**							
Section	**F/F**	**F/L**		**L/L**		**D/L**		**D/L-0.03**
	a*	A*	b*	a*	b*	a*	b*	a*
A	-358	-295	-285	-291	-287	-233	-302	-241
B	-327	-245	-275	-275	-289	-296	-381	-244
C	-396	-268	-302	-248	-275	-250	-293	-291
D	-298	-263	-287	-301	-319	-240	-289	-222
E	NA	-242	-299	-268	-297	Same as B		Same as B
F		-271	-254	Same as E				
G		-264	-288					
H	-323	-289	-283					
I	-363	-283	-308	-278	-304	-218	-322	-257
J	NA	-304	-278	-264	-255	Same as B		
L		-303	-354	-299	-307	-253	-247	-248

40°C	Induced Strain (microstrain)							
Section	F/F	F/L		L/L		D/L		D/L-0.03
	A*	A*	b*	a*	b*	a*	b*	a*
A	-365	-264	-284	-287	-266	-259	-295	-295
B	-324	-291	-278	-256	-287	-388	-382	-245
C	-402	-274	-299	-279	-304	-266	-285	-268
D	-367	-271	-248	-268	-323	-306	-288	-255
E	NA	-255	-268	-249	-286	Same as B		Same as B
F		-234	-287	Same as E				
G		-241	-258					
H	-345	-269	-304					
I	-356	-278	-269	-294	-278	-284	-271	-234
J	NA	-298	-307	-283	-266	Same as B		
L		-291	-283	-276	-306	-292	-287	-279

a* 100-mm diameter specimens with 63-mm thickness

b* 150-mm diameter specimens with 75-mm thickness

In general the applied load at 5°C, 25°C, and 40°C was about 45, 20, and 10% of the indirect tensile strength measured at 25°C, respectively, which falls within the range suggested in the literature. To verify that specimens are not being damaged during testing, tests were conducted on duplicates. A statistical analysis of the resilient modulus test result showed no significant difference in the measured resilient modulus. Therefore, limiting the strain to a value less than 500 microstrains appears to be appropriate for resilient modulus testing to prevent damaging the specimens.

4.3 Resilient Modulus Results

The resilient modulus results are obtained utilizing the Roque and Buttlar analysis approach. The resilient modulus was also calculated using Kim et al.'s three-dimensional approach (Kim et al., 2002). However, the resilient moduli calculated from the vertical and horizontal deflection measurements failed to produce converging results. Hence, Kim et al.'s approach could not be used. The results can be divided into the following categories:

- Two 150 mm F/L, L/L, and D/L specimens per section tested at 5°C, 25°C, and 40°C. The applied load used is 0.1 sec loading and 0.9 sec rest period.
- Three 100 mm F/L, L/L, and D/L specimens per section and two F/F specimens per section tested at 5°C, 25°C, and 40°C. The applied load used was 0.1s loading and

0.9 sec rest period. Three 100 mm D/L specimens per section tested at 5°C, 25°C, and 40°C with an applied load of 0.03 sec loading and 0.97 sec rest period.

The results for the 100-mm specimens are presented in Table 4-4. In reviewing the results, section I (SM-9.5A*) resulted in the highest resilient modulus. This result is consistent for all test temperatures (5°C, 25°C, and 40°C), and is in accordance with expectations since section I has a high compaction effort. On the other hand, SMA-12.5 (stone mastic asphalt mix) had, by far, the lowest resilient modulus at all three test temperatures. SMA-12.5 has a fiber additive and higher asphalt content and percent fines that may help in resisting fatigue and low temperature cracking.

With regard to the maximum nominal aggregate size of mixes SM-12.5D and SM-9.5D, it was found that SM-12.5D was finer than what would be expected. Therefore, the effect of aggregate size on resilient modulus could not adequately investigated. Results of a comparison between F/L, L/L, and D/L reveal that although the resilient modulus varies between the different sections, this variation is random and no clear shift factor can be identified (within a mix, as well as for the same section between the different mixes). It is clear, however, that there is a difference in resilient modulus between the different mixes. The difference in measured resilient modulus among F/L, L/L, and D/L specimens is believed to be due to the difference in volumetric properties; the effect of volumetric properties on the resilient modulus is investigated in section 4.6.

Each mix's susceptibility to temperature is reflected by the change in resilient modulus as a function of temperature. No conclusion can be made as to which binder performs better in terms of resistance to temperature changes. However, due to its relatively high asphalt content, the SMA-12.5 mix of section L proved to be the most susceptible to temperature changes. As a conclusion, for the binders used in this research, the binder content is thought to have an effect on the resilient modulus.

The effect of binder type is observed at 40°C between the PG 76-22 and the PG 64-22 (sections C and D, respectively). At that temperature, the PG 76-22 had a higher resilient modulus for all the mixes. Differences between the PG 70-22 and the other binder grades are inconsistent. The results of tests performed at 25°C also show an inconsistency as to which binder grade performs better. At 5°C, the measured resilient modulus was practically the same for both binder grades. As a conclusion, the effect of the high temperature grade of the binder was found to be important at high temperatures (40°C).

Table 4-4 Resilient Modulus Results for 100-mm Specimens at the Three Test Temperatures

(a) 5°C

Section	Mix	Resilient Modulus (MPa)				
		F/F	F/L	L/L	D/L	D/L*
A	SM-12.5D	8296	12004	14868	13741	11974
B	SM-9.5D	9154	12700	15819	15145	12604
C	SM-9.5E	8591	15165	15553	14441	12335
D	SM-9.5A	9760	15041	15516	14981	12879
E	SM-9.5D	9862	13740	11317	Same as B	Same as B
F	SM-9.5D	NA	14249	Same as E		
G	SM-9.5D		13943			
H	SM-9.5D	9447	13575			
I	SM-9.5A*	12634	18315	15807	17211	12841
J	SM-9.5D	NA	11512	13807	Same as B	Same as B
L	SMA-12.5	5853	9792	10152	10629	8960

* 0.03s loading duration

(b) 25°C

Section	Mix	Resilient Modulus (MPa)				
		F/F	F/L	L/L	D/L	D/L*
A	SM-12.5D	3883	4760	6460	5841	6898
B	SM-9.5D	3579	5875	6051	4627	6138
C	SM-9.5E	2609	5431	5780	5676	7781
D	SM-9.5A	2356	6540	4884	5754	7196
E	SM-9.5D	3730	6087	5239	Same as B	Same as B
F	SM-9.5D	NA	6232	Same as E		
G	SM-9.5D		5982			
H	SM-9.5D	4100	5670			
I	SM-9.5A*	4479	7591	6106	8017	8469
J	SM-9.5D	NA	5282	5344	Same as B	Same as B
L	SMA-12.5	2193	3485	3582	3141	5216

(c) 40°C

Section	Mix	Resilient Modulus (MPa)				
		F/F	F/L	L/L	D/L	D/L*
A	SM-12.5D	1745	1926	2924	2703	3331
B	SM-9.5D	1834	2517	2450	2116	3220
C	SM-9.5E	1207	3347	2360	2691	3730
D	SM-9.5A	968	2630	1966	2314	3023
E	SM-9.5D	NA	1843	1978	Same as B	Same as B
F	SM-9.5D		2308	Same as E		
G	SM-9.5D		2325			
H	SM-9.5D	1899	2427			
I	SM-9.5A*	1954	3320	2567	3484	5015
J	SM-9.5D	NA	2512	2112	Same as B	Same as B
L	SMA-12.5		1390	1224	1508	2301

*0.03s load duration

The resilient modulus results showed that mix characteristics and preparation, and compaction method (laboratory gyratory compaction vs. field compaction) influence resilient modulus values with the latter being more influential. As it can be seen from Table 4-5, the measured resilient modulus fell in the same range for F/L, L/L, and D/L specimens. However, the resilient modulus of field cores was distinctively lower than that of either F/L, L/L, or D/L. Field/Lab and F/F specimens are obtained from the same mix. The difference is in the way the specimens were compacted. On the other hand, F/L, L/L, and D/L have the same compaction method but different mix characteristics. Apart from sections I and L whose resilient moduli were significantly different, the average resilient modulus at 5, 25, and 40°C are presented in Table 4-5.

Table 4-5. Average Resilient Modulus

Temperature(°C)	F/F		F/L		L/L		D/L	
	M_r (MPa)	Variation (%)	M_r (MPa)	Variation (%)	M_r (MPa)	Variation (%)	M_r (MPa)	Variation (%)
5	9185	6.9	13548	9.3	14480	11.6	14577	4.3
25	3676	21.3	5762	9.4	5626	10.3	5475	10.4
40	1531	27.2	2426	18.0	2298	15.9	2456	11.8

The difference in resilient modulus between F/F specimens and the other specimen types, mainly F/L specimens, is substantial; therefore, a compaction shift

factor is necessary, if resilient modulus values of field cores and laboratory prepared specimens are to be compared. The average resilient modulus for F/L, L/L, and D/L at the three test temperatures is practically the same considering the calculated coefficient of variation (Table 4-5). These three mixes where all compacted in the laboratory. As it will be presented in section 4.6, the difference between the resilient modulus of the different mixes measured for the same section, will be a result of the difference in volumetric properties.

The load duration had also an effect on the resilient modulus. Results of D/L specimens tested at 0.03 sec load duration are presented in Table 4-4. Excluding sections I and L, the average resilient modulus was 12448, 7003, and 3326 MPa with a coefficient of variation of 3.1, 9.8, and 9.0% at 5, 25, and 40^{o}C, respectively, which is considerably different from the results of D/L specimens tested at 0.1 sec load duration. The different resilient modulus results at the two loading durations are analyzed in section 4.5 which consists of the integration of a shift factor that relates 0.1 to 0.03 sec loading duration test results.

The results presented in Table 4-4 are the average of three specimens (two specimens for F/F). Two readings are taken from each specimen making a total of six resilient modulus readings per section per mix (four for F/F specimens). The variability in the readings is a measure of the IDT test repeatability; it can also be used as a measure of homogeneity between the specimens of the same mix. Therefore, the variability in the test results is presented in the following section.

4.4 Variability

The resilient modulus results reported in Section 4.3 represent the average of measured test values. For mixes F/L, L/L, and D/L, the number of specimens used per section for testing was three and two for 100- and 150-mm specimens, respectively. Due to the fact that fewer specimens were available from the Virginia Smart Road, for F/F mixes, only two 100 mm specimens were tested per available section. During testing, readings are taken from the two faces of each specimen; therefore, two resilient modulus values are obtained per specimen. Variation between the two reported values per specimen can be traced to the inherent non-homogeneity of HMA, as well as miscentering of the specimen. Non-homogeneity in HMA also occurs between different specimens and can thus lead to differences in resilient modulus values between the

different specimens. Therefore, variations in resilient modulus can be classified into two categories: *within specimen* variation and *within mix* variation. A discussion of each type follows.

4.4.1 Within Specimen Variation

Variability of the calculated resilient modulus within the same specimen is due to specimen miscentering and to the non-homogeneity of HMA. Since specimen miscentering causes an imbalance in the net applied load between the two faces, stresses within the specimen will, therefore, vary between the front and the back, causing resilient modulus values to be overestimated on one side and underestimated on the other. However, since resilient modulus values are independent of the applied load (within the range of testing), the correct resilient modulus can be calculated by averaging the resilient moduli calculated from each side of the specimen. The effect of specimen miscentering on the stress distribution is presented in Figure 4-1. Variation between the two sides is not due solely to specimen miscentering, but also to inherent inhomogeneity of the mix. However, non-homogeneity can be estimated from the variation between the specimens of the same mix, which is identified as the *within mix variability*.

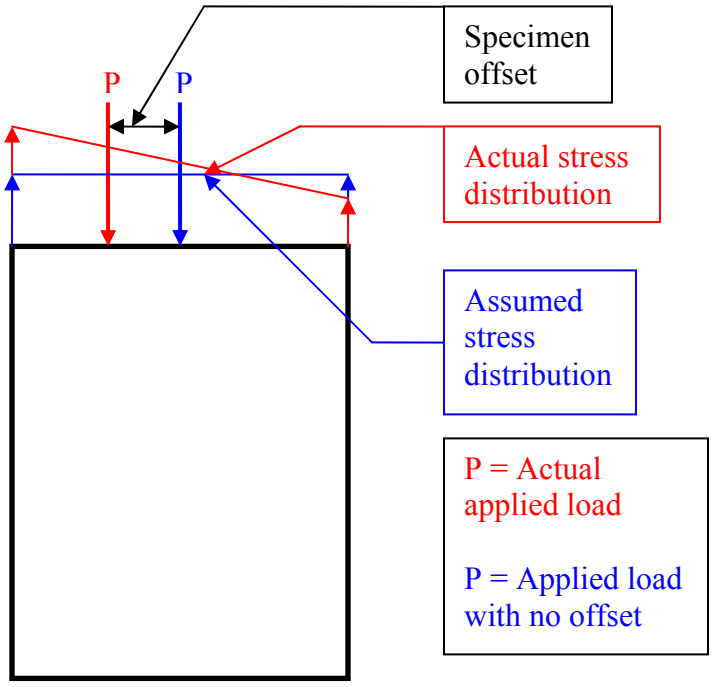

Figure 4-1 Stress Distribution

4.4.2 Within Mix Variation

Within mix variation represents the variation that occurs in the resilient modulus due to inhomogeneity in the mix, which leads to different values of resilient modulus for the different specimens tested. The within mix variation measures the repeatability of the test setup used. In general, within mix variation that is smaller than the within specimen variation indicates a good potential for repeatability. The variability in resilient modulus calculation is summarized in Table 4-6.

Table 4-6 Resilient Modulus Variability

Mix	Type	Variability (in %)		
		Temperature (°C)		
		5	25	40
F/F	Average/specimen	21.8	35.5	26.7
	Average/mix	10.3	8.9	4.3
	Maximum/specimen	103.3		
	Maximum/mix	20.0		
F/L	Average/specimen	7.4	6.7	14.4
	Average/mix	7.8	6.6	13.7
	Maximum/specimen	73.6		
	Maximum/mix	52.7		
L/L	Average/specimen	11.6	17.7	18.9
	Average/mix	6.25	10.5	11.36
	Maximum/specimen	79.5		
	Maximum/mix	42.6		
D/L	Average/specimen	13.5	15.7	17.9
	Average/mix	5.7	9.7	9.8
	Maximum/specimen	48.2		
	Maximum/mix	27.3		
D/L-0.03	Average/specimen	16.3	16.0	13.3
	Average/mix	8.7	12.9	13.9
	Maximum/specimen	60.8		
	Maximum/mix	21.9		

The maximum within specimen variability was 103.3%, 73.6%, 79.5%, 48.2%, and 60.8% for F/F, F/L, L/L, D/L, and D/L-0.03 mixes, respectively; while the maximum mix variability was 20.0%, 52.7%, 42.6%, 27.3%, and 21.9%, respectively. An interesting observation was that results from the F/F specimen exhibited the highest within specimen maximum variability of 103.3%, while at the same time possessing the lowest maximum mix variability (20.0%). Moreover, it was observed from data analysis

that, in general, within specimen variability for F/F specimens was relatively high compared to that of F/L, L/L, and D/L specimens, while the mix variability was roughly equal, if not better. This suggests that homogeneity is more successfully achieved for specimens compacted in the laboratory than for field cores, which can vary depending upon the compaction quality. In addition, field core specimens were thinner than the other specimens and therefore, any specimen offset will have a larger effect on the specimen stress distribution.

The average specimen variability ranged between 6.7% and 35.5%, while the average mix variability ranged between 5.7% and 13.9%. The average mix variability results indicate that the repeatability of the indirect tension test for resilient modulus calculation is good. As mentioned previously, variability within a specimen occurs as a result of inhomogeneity and specimen miscentering. Since the minimum average mix variability is 5.7% and the maximum average mix variability is 13.9%, while the maximum average within specimen variability is 35.5%, an estimate of the maximum average variability due to specimen miscentering would be between 21% and 30%.

4.5 Shift Factors

The main objective of this research was to account for the difference between the resilient moduli of field cores (F/F specimens) and laboratory prepared specimens. For this purpose, three different laboratory compacted mixes were prepared: F/L, L/L, and D/L. Field cores were obtained from the Virginia Smart Road. The resilient modulus results for F/L and F/F mixes showed that there is a discernible difference between the designed and in-situ HMA layer properties. Lab/Lab specimens were prepared to replicate F/L specimens; however, resilient modulus results and volumetric properties revealed a difference between mixes prepared in the laboratory and the ones prepared in the mixing plant. Differences between F/L, L/L, and D/L can be attributed solely to the volumetric properties and are discussed in Section 4.6.

As a result of FWD testing and data of actual truck induced stresses and strains measured at the Virginia Smart Road, loading pulse duration was another parameter that was evaluated in this research. Hot-mix asphalt being a viscoelastic material, its properties are time-dependent. In other words, the resilient modulus is believed to be affected by both the load duration and the rest period. Currently, ASTM D4123-82 recommends the use of a load pulse duration of 0.1 sec and a rest period of 0.9 sec.

Based on FWD testing and actual stress and strain measurements taken from the field at the Virginia Smart Road, Loulizi et al. (2002) suggested that at 0.03s load pulse duration is more representative of actual traffic loading. Therefore, another set of 100-mm specimens were mixed and compacted to be tested a 0.03s load pulse duration. The resilient modulus calculated at 0.03 sec load pulse duration was then compared to the resilient modulus of specimens tested at 0.1 sec load pulse duration and shift factors were developed to account for the effect of load pulse duration. Finally, it was observed that at 5^{o}C, the resilient modulus of 100- and 150-mm specimens is the same. However, at higher temperatures the different specimen sizes gave different resilient modulus results. The discrepancy between the two specimen sizes increased as the test temperature was increased.

The statistical analysis showed that there is a significant difference, which is not attributed to the variation in the resilient modulus test, between the resilient modulus of F/L and F/F specimens. Therefore, incorporating compaction shift factor (laboratory vs. field compaction) is essential if resilient modulus values of field cores and laboratory prepared specimens are to be compared.

4.5.1 Compaction Shift Factor

Different compaction methods are used in the field than in the laboratory. Gyratory compaction is used in the laboratory to replicate field compaction. However, there still are some differences between the two compaction methods. Some of these differences are confinement and direction of compaction. Confinement is higher in the laboratory than in the field. Compaction is performed in all directions in the laboratory, while it is applied in the direction of traffic in the field.

Figure 4.1 shows the ratio of the resilient modulus of the 100 mm F/L specimens to the resilient modulus of the F/F specimens at the three test temperatures. Except for the SM-12.5D mix (section A) at 40^{o}C, the resilient modulus of F/L specimens was clearly higher than that of F/F specimens. For Section D (SM-9.5A), the compaction shift factor increases considerably from 5^{o}C to 25^{o}C and then appears to level out at 40^{o}C. Section C (SM-9.5E) results also show an increasing shift factor with temperature. In general, taking into account the variability in the IDT test, the shift factor appears to remain constant at the three test temperatures. The increase with temperature in the compaction shift factor for sections C and D can be explained by the fact that a higher grade binder is used (section C has PG 76-22 asphalt grade and section D has PG 70-

22 asphalt grade). Indeed, the resilient modulus of both sections dropped dramatically from 5°C to 25°C for the F/F specimens compared to the other sections: 8591 MPa to 2609 MPa for Section C and 11762 MPa to 2356 MPa for Section D. As for the remaining mixes, the compaction shift factor varies between 1.23 and 1.70, with an average of 1.46. A compaction shift factor between 1.45 and 1.50 seems to be applicable to all the mixes, except sections C and D. The average shift factors are 1.45 at 5°C and 1.51 at 25°C (excluding sections C and D) and 1.45 at 40°C (excluding sections A, C, and D). Data for section L (SMA-12.5) is not presented in Figure 4.1 since section L could not be tested at 40°C. However, tests performed at 5 and 25°C resulted in a compaction shift factor of 1.63 and 1.59, respectively, which is slightly higher than the average shift factor of the other sections. Section L has fiber which may affect the shift factor.

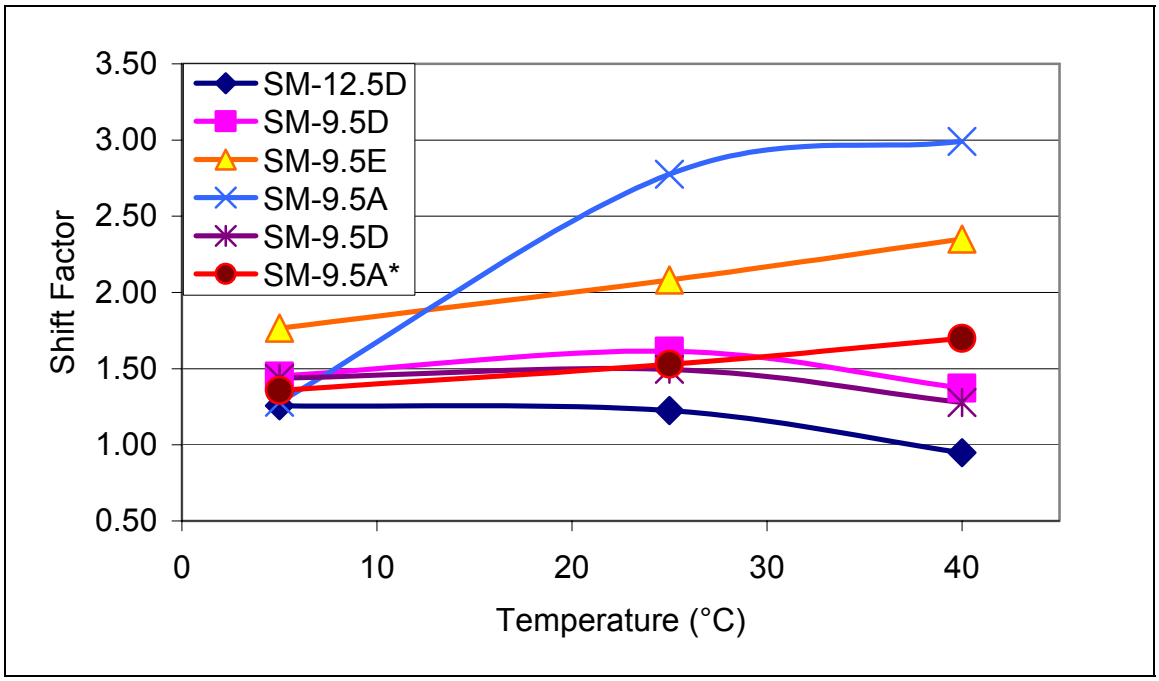

Figure 4-2 Compaction shift factor

Differences in the calculated resilient modulus between F/L and F/F specimens can be attributed to compaction and, therefore, the bulk density and percent of air voids content. The bulk density and percent of air voids content of the different F/L and F/F mixes are summarized in Table 4-7.

Table 4-7 Percent Air Voids and Bulk Specific Gravity of F/L and F/F Specimens

Section	Bulk Specific Gravity			Air Voids (%)		
	Mix		Ratio	Mix		Ratio
	F/L	F/F		F/L	F/F	
A	2.345	2.282	1.028	3.2	5.8	0.552
B	2.362	2.239	1.055	3.6	8.6	0.419
C	2.399	2.309	1.039	2.3	6	0.383
D	2.408	2.393	1.006	1.3	1.9	0.684
E	2.4	2.317	1.036	1.4	4.8	0.292
F	2.412	2.317	1.041	3.6	4.8	0.750
G	2.410	2.317	1.040	3.6	4.8	0.750
H	2.403	2.317	1.037	4.1	4.8	0.854
I	2.429	2.440	0.995	1.5	1.1	1.364
J	2.328	2.252	1.034	7.5	10.6	0.708
L	2.359	2.226	1.060	1.8	7.3	0.247

In general, the measured bulk specific gravity for F/L specimens is higher than that for F/F specimens, which means that a better compaction was achieved in the laboratory and, therefore, a higher resilient modulus value was measured for F/L specimens. The same conclusion can be drawn from air void measurements, in which F/L specimens had a much lower air voids content than F/F ones. The effect of bulk specific gravity and air voids on the resilient modulus is discussed in Section 4.6, where a model for predicting resilient modulus from volumetric properties is developed using F/L, L/L, and D/L 100-mm specimens' data. The F/F data is not used in the model development due to the different compaction method used for F/F specimens. However, the model can be used to verify if the compaction method has an effect which can not be explained by the difference in volumetric properties on the resilient modulus. This task is achieved by calculating the resilient modulus using the developed model, and comparing it to the measured one from testing.

4.5.2 Specimen Size Shift Factor:

The resilient modulus calculation (Roque and Buttlar, 1992) is based on correction factors used to correct the calculated stress, obtained from Hondros' plain stress solutions (Hondros, 1959), and the measured strain. These correction factors are function of the diameter-to-thickness ratio and should be applicable to any specimen diameter or thickness. Therefore, theoretically, after applying the correction factors, the resilient modulus determined from 150-mm specimens should be the same as the one determined from 100-mm specimens, after applying the correction factors. Figure 4.3a is a plot of the resilient modulus ratio of 100- to 150-mm F/L specimens excluding section D. It is evident that 100-mm specimen result in a higher resilient modulus. This ratio varies between 0.81 and 1.41 (Figure 4.3a). The average shift factors between 100- and 150-mm F/L specimens are 0.98, 1.00, and 1.13 at 5°C, 25°C, and 40°C, respectively, with an overall average of 1.04.

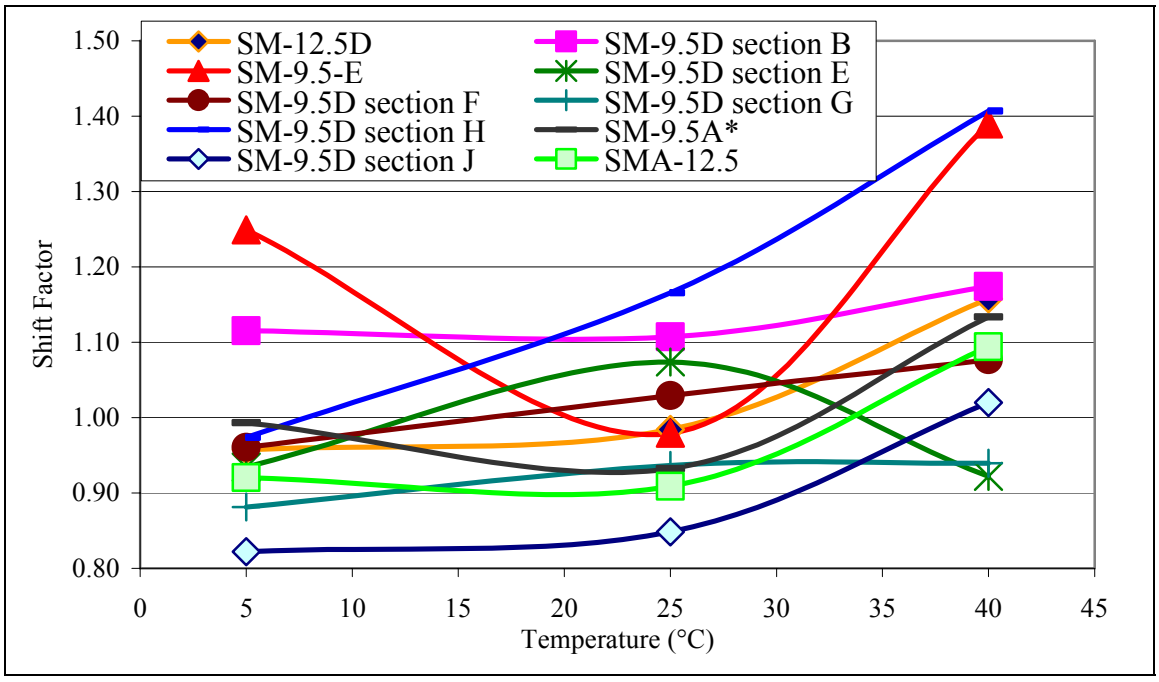

(a)

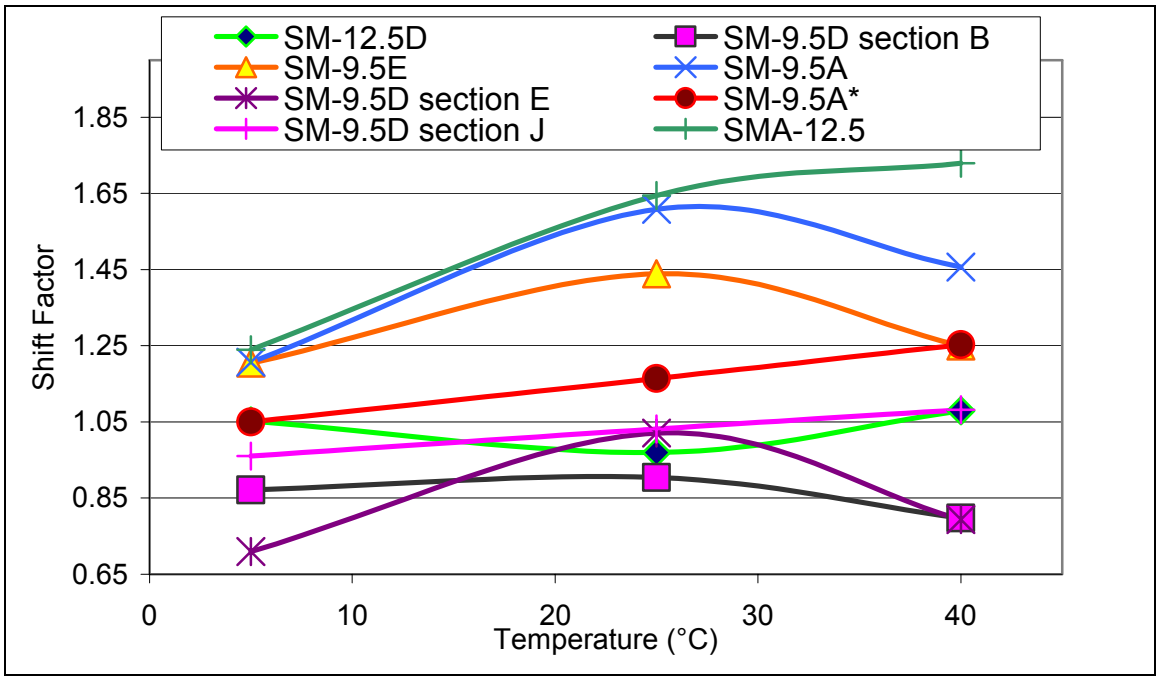

(b)

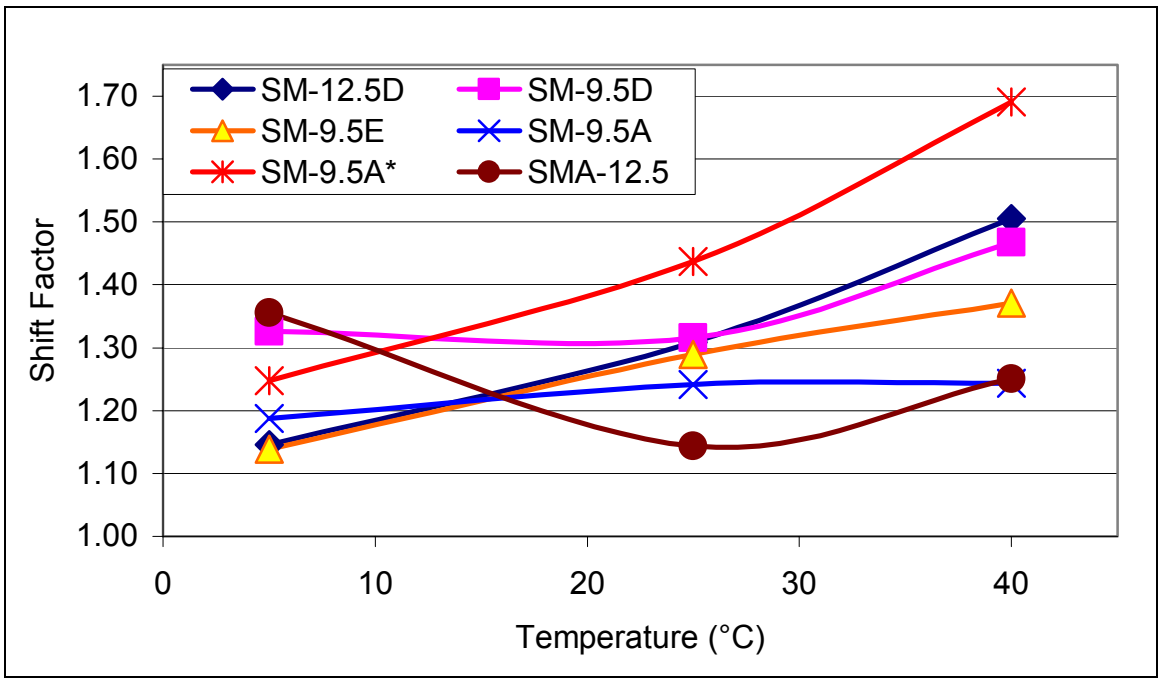

(c)

Figure 4-3 Specimen size shift factor (a) F/L specimens, (b) L/L specimens, and (c) D/L specimens

From F/L results, it seems that the calculated resilient modulus is the same for 100- and 150-mm diameter specimens at all tested temperatures. However, results from L/L and D/L do not support this finding. The average shift factor for L/L specimens was 1.04, 1.22, and 1.18 at 5°C, 25°C, and 40°C, respectively, with an overall shift factor of 1.15 (Figure 4.3b); while the average shift factor for D/L specimens was 1.23, 1.29, and 1.42 at 5°C, 25°C, and 40°C, respectively, with an overall shift factor of 1.31 (Figure 4.3c). It appears that D/L specimens have greater specimen size shift factor than L/L specimens. Sections B, E, and J in D/L have unexpectedly low shift factors. Sections E and J were not produced in D/L since they were identical to sections B. Therefore, excluding these three sections, the specimen size shift factor for L/L specimens becomes 1.15, 1.38, and 1.39 at 5, 25, and 40°C, respectively, which is comparable to the results from D/L specimens. One interesting observation is that, while the specimen size shift factor varies considerably between the three mixes, one general trend can be seen; which is the fact that the specimen size shift factor increases as the temperature increases. At 5°C, the average specimen size shift factor for the three mixes is 1.08. Since the average variability for the three mixes at 5°C is 7.58%, and since the HMA volumetric properties are not affected by the specimen size, this shift factor is most likely due to variation in the resilient modulus test. Therefore, it is suggested that at 5°C the resilient modulus obtained from 100- and 150-mm diameter specimens is comparable. However, at 25°C the average specimen size shift factor increases to 1.17, which is beyond the resilient modulus variation (COV = 10.00%), at that temperature. The specimen size shift factor increases even more to 1.24 when the test temperature is increased to 40°C. The average variability in the resilient modulus is 12.99%, at that temperature.

At 5°C, HMA behaves as an elastic material with minimal viscous behavior. The correction factors developed by Roque and Buttlar were developed for an elastic material. They depend on the thickness to diameter ratio, and, therefore, the resilient modulus obtained from 100- and 150-mm specimens is practically the same. As temperature increases, HMA exhibits more viscous behavior. Therefore, the bulging, which depends on Poisson's ratio for elastic materials, will also be affected by the amount of viscous flow that is exhibited in the material. The tested 150-mm diameter specimens are relatively thinner than the tested 100-mm diameter specimens; the 150-mm diameter specimens have a thickness to diameter ratio around 0.50, while this ratio

is around 0.625 for 100-mm diameter specimens. Hence, the viscous flow could increase as the specimen's thickness to diameter ratio decreases. This limits the application of the correction factor when the materials behave more viscously.

Moreover, the 150-mm diameter specimens are more representative since they are expected to be less affected by aggregate size than 100-mm diameter specimens. However, the resilient modulus variability analysis showed no significant difference between 100- and 150-mm specimens, in that 100-mm specimens are more affected by aggregate size. Therefore, it is suggested that, for mixes with maximum aggregate sizes of 12.5mm and less, the resilient modulus determined from 100-mm specimens is as representative of the overall mix as the one determined from 150-mm specimens.

4.5.3 Loading Duration Shift Factor

The resilient modulus of HMA is measured in the laboratory using a haversine stress pulse. This haversine pulse is thought to replicate what actually occurs in the pavement: While a truck tire is at a considerable distance from a point in the pavement, the stress at that point is zero; when the tire is exactly on the considered point, the stress is maximum. The loading time (duration) of the applied pulse was found to depend on the truck speed and the depth below the pavement surface (Huang, 1993). Since vehicle speed varies significantly and the depth of the material may not be known during design, it was recommended that a haversine load duration of 0.1 sec and a rest period of 0.9 sec be used for the laboratory test (Huang, 1993).

Loulizi et al. (2002) measured the vertical compressive stress pulse induced by a moving truck and by FWD loading at different locations beneath the pavement surface. They found that a haversine or a normalized bell-shape equation well represent the measured normalized vertical compressive stress pulse of a moving vehicle. Haversine duration times varied from 0.02s for a vehicle speed of 70km/h at a depth of 40mm, to 1s for a vehicle speed of 10km/h at a depth of 597mm. For the FWD loading, a haversine with a duration of 0.03s was found to well-approximate the induced stress pulse at any depth below the pavement surface. The researchers recommended reducing the loading time of HMA dynamic tests to 0.03s to better match loading times obtained from moving trucks at average speed and from FWD testing. In light of these findings, this study was conducted to evaluate the effect of reducing the pulse duration from 0.1 sec to 0.03 sec on the laboratory measured resilient modulus.

Because HMA is a viscoelastic material, its stress-strain relationship is time-dependent; that is, for a given stress the calculated strain depends on the duration of time for which the load is sustained. In general, for a given load intensity, the longer the load application duration, the higher the induced stain, which leads to a lower resilient modulus value. Two sets of 100 mm D/L specimens were tested at the same load intensity for two different load durations. The load durations used are 0.1 sec loading with a 0.9 sec rest period and 0.03 sec loading with a 0.97 sec rest period. A load-duration shift factor was calculated as the ratio of the resilient modulus of specimens tested at 0.03 sec load duration to the resilient modulus of specimens tested at 0.1 sec. A statistical analysis of the difference in mean measured resilient modulus between the test performed at 0.1 sec loading and the one performed at 0.03 sec was performed. Since the two tests are independent, the paired t-statistic was performed. The paired t-statistic was used instead of a regular t-test because each measurement from the IDT performed at 0.1 sec loading can be matched to the measurement of the test performed at 0.03 sec for the same mix. The parameter tested is the difference between the means at α = 0.05. The results of the paired t-statistic are presented in Table 4-8. the test shows that there is a significant difference between the resilient modulus measured at 0.1 sec loading pulse and the resilient modulus measured at 0.03 sec loading pulse.

Figure 4-4 presents the shift factor of each section as a function of the test temperature. As expected, the shift factor increases with the increase in test temperature; this is due to the fact that viscoelastic properties of HMA become more predominant as the mix temperature is increased. Theoretically, as the test temperature is decreased, elastic behavior should become more dominant and, therefore, the resilient moduli measured at the two different load durations should converge to the same value.

Table 4-8. t-statistic at: (a) 5°C, (b), 25°C, and (c) 40°C.

(a)

	0.1 sec load	*0.03 sec load*
Mean	14358	11932
Hypothesized Mean Difference	0	
df	5	
P(T<=t) two-tail	**0.001935352**	
t Critical two-tail	2.570577635	

(b)

	0.1 sec load	*0.03 sec load*
Mean	5509.333333	6972.418456
Hypothesized Mean Difference	0	
Df	5	
t Stat	-5.447955832	
P(T<=t) two-tail	**0.002830647**	
t Critical two-tail	2.570577635	

(c)

	Variable 1	*Variable 2*
Mean	2469.333333	3409.373682
Hypothesized Mean Difference	0	
df	5	
t Stat	-6.921965475	
P(T<=t) two-tail	**0.000965239**	
t Critical two-tail	2.570577635	

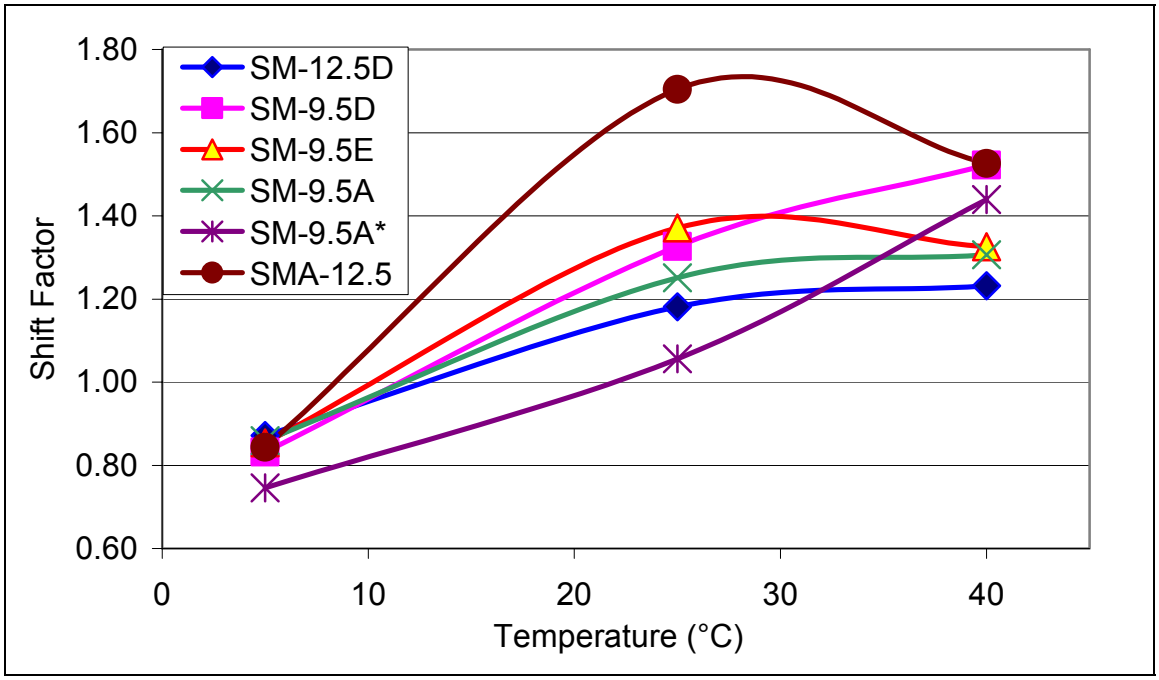

Figure 4-4 Load Duration Shift Factor

However, results of tests performed at 5°C produced a shift factor lower than 1 for all the tested sections, which would indicate that the measured strain induced by a load sustained for a shorter period of time is higher than the one induced by the same load sustained for a longer period of time, which is theoretically and practically impossible. The explanation for a shift factor smaller than unity is related to the IDT test execution. The resilient modulus test is a repetitive loading test. Hot-mix asphalt experiences an accumulation of plastic strain during repetitive loading. However, the accumulated plastic strain decreases with every new loading cycle and eventually becomes negligible. The accumulated plastic strain per cycle is a function of the load duration and increases with longer load durations. The resilient modulus test was run for 100 cycles for both loading durations, which may lead to a higher total accumulated plastic strain for specimens tested for longer load durations. It is, therefore, possible that the accumulated strain per cycle for specimens tested at shorter load durations will still be significant and that those specimens need additional conditioning cycles, which will lead to lower resilient moduli. The load duration shift factors varied between 0.75 and 0.87, 1.06 and 1.70, 1.23 and 1.53 with an average of 0.83, 1.31, and 1.39 at 5°C, 25°C, and 40°C, respectively.

The development of shift factors (compaction, specimen size, and loading duration shift factors) is possible when there is a significant difference in paired data; meaning there is a significant difference in the data of the same section for different mixes and the same pattern can be detected for all sections. These variations between and within mixes are due to changes in volumetric properties and is discussed in the following section.

4.6 Resilient Modulus Prediction from Volumetric and Binder Properties

The shift factor developed between the F/L and F/F specimens is due to the differences in compaction that occur between the field and the laboratory. On the other hand, F/L, L/L, and D/L specimens have all undergone the same laboratory compaction. The calculated resilient modulus for those mixes will depend on other identified parameters.

4.6.1 Factors Affecting Resilient Modulus

As expected, the resilient modulus was found to be highly dependent on the test temperature. Correlation between the resilient modulus and the test temperature— with the resilient modulus decreasing as temperature increases—is found to be highest and best represented in an exponential form as follows (also see Figure 4-5):

$$M_r = \alpha e^{-\beta T} \tag{4.1}$$

where α and β are parameters that are functions of binder and mix properties

Using Equation 4.1, the fitted exponential relationship between the resilient modulus and temperature incorporated two different coefficients, α and β, which varied with the mix type (A through L) and preparation method (F/L, L/L, and D/L). The values of α and β are presented in Table 4-9. The goodness of fit (R-square) for the different sections is presented in Table 4-10. The different values of α and β suggest that, although temperature is a major parameter affecting the HMA resilient modulus, other parameters could also play a role affecting the resilient modulus of HMA. These identified parameters can be mix properties, mainly bulk density, air voids, asphalt binder content, voids in mineral aggregates, voids filled with asphalt, G*/sinδ, and fine to asphalt ratio.

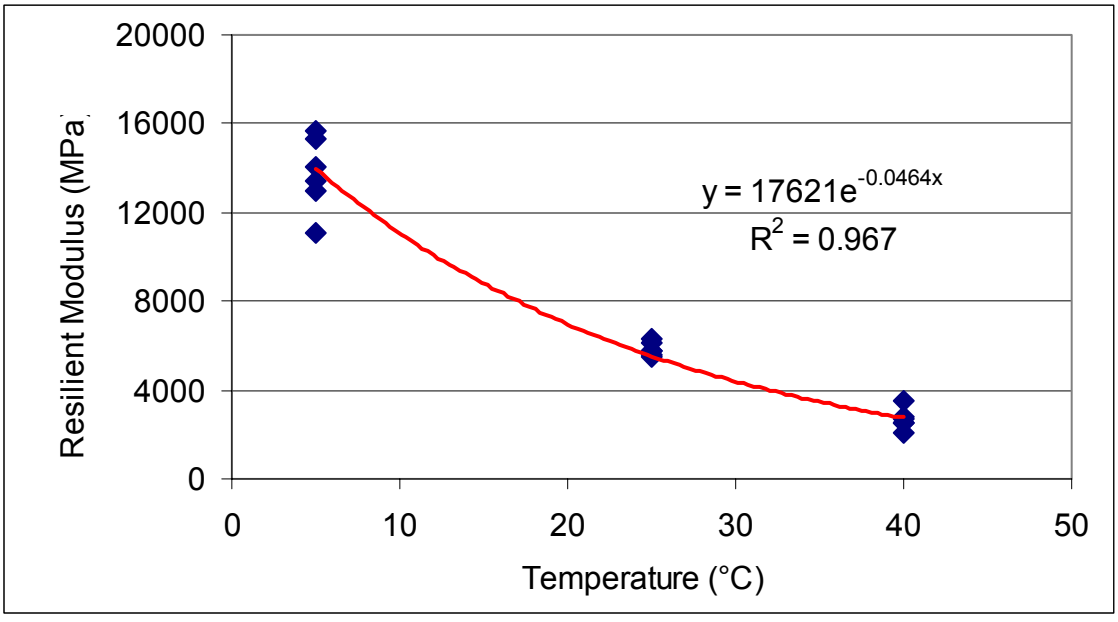

Figure 4-5 Resilient Modulus Variation with Temperature (Specimen A1-4in D/L)

Table 4-9 Values of α and β

Section	α (MPa)							
	F/F	F/L		L/L		D/L		D/L-0.03
	a*	a*	b*	a*	b*	a*	b*	a*
A	11805	16168	12533	19103	12532	17621	10740	14978
B	11327	17348	10201	21020	15624	19533	10201	15603
C	11100	19146	11118	20649	11148	18222	11118	16212
D	13476	19720	16578	20200	11274	19846	11273	17118
E	NA	19279	13089	15791	13575	Same as B		Same as B
F		19578	13200	Same as E				
G		18751	14663					
H	9119	17963	13499					
I	16146	23068	16872	20523	13441	21751	12653	15443
J	NA	14561	12884	17522	12169	Same as B		Same as B
L		13105	10556	13841	7834	13676	6810	11511

a* 100-mm diameter specimens with 63-mm thickness

b* 150-mm diameter specimens with 75-mm thickness

Section	β ($^oC^{-1}$)							
	F/F	F/L		L/L		D/L		D/L-0.03
	a*	a*	b*	a*	b*	a*	b*	a*
A	0.0458	0.052	0.0629	0.046	0.0472	0.0464	0.0541	0.035
B	0.046	0.0471	0.0593	0.0527	0.0517	0.0568	0.0593	0.0401
C	0.0566	0.0492	0.0541	0.0538	0.0561	0.0478	0.0541	0.0348
D	0.0675	0.0472	0.0669	0.0564	0.0637	0.0533	0.0545	0.04
E	NA	0.0538	0.0534	0.051	0.055	Same as B		Same as B
F		0.0512	0.0535	Same as E				
G		0.0501	0.0535					
H	0.0475	0.0489	0.059					
I	0.0486	0.0494	0.0544	0.0492	0.0551	0.0477	0.0538	0.0272
J	NA	0.0431	0.05	0.0481	0.0498	Same as B		Same as B
L		0.0563	0.0598	0.0592	0.0708	0.057	0.0537	0.0365

Table 4-10 R^2 Values for the Different Mixes

Section	R^2							
	F/F	F/L		L/L		D/L		D/L-0.03
	a*	a*	b*	a*	b*	a*	b*	a*
A	0.81	0.99	0.85	0.98	0.96	0.97	0.98	0.83
B	0.95	0.96	0.98	0.95	0.91	0.95	0.98	0.89
C	0.95	0.93	0.95	0.94	0.94	0.96	0.95	0.82
D	0.99	0.95	0.92	0.94	0.99	0.93	0.97	0.86
E	NA	0.93	0.98	0.92	0.91	Same as B		Same as B
F		0.92	0.98	Same as E				
G		0.97	0.97					
H	0.43	0.94	0.97					
I	0.98	0.92	0.95	0.94	0.92	0.91	0.92	0.79
J	NA	0.98	0.97	0.86	0.98	Same as B		Same as B
L		0.96	0.98	0.96	0.97	0.94	0.95	0.77

The effect of each mix property on the calculated resilient modulus was investigated. The procedure for determining the influence and importance of each parameter includes identifying a trend in resilient modulus variation as a function of the parameter being considered, analyzing the correlation between the resilient modulus and each individual parameter, as well as the correlations between the considered parameters. Five mix parameters were identified as affecting the parameters α and β and therefore the resilient modulus. The parameters were considered in the development of the model: bulk specific gravity (SG), air void (AV) content, asphalt content (AC), voids in mineral aggregates (VMA), and fine to asphalt ratio (F/A), with bulk specific gravity the most influential parameter on α and asphalt content the most prominent for parameter β. The next step was to identify highly influential data points and outliers. During the model building process, three data points were identified as outliers; therefore, they were excluded from the model building process.

4.6.2 Model Development

The proposed model (Equation 4.1) includes two coefficients that depend on the mix properties. Coefficient α represents the resilient modulus at 0°C, while coefficient β represents the sensitivity of the resilient modulus to temperature changes. Using Equation 4.1, the coefficients α and β were determined for each section. One dilemma in developing a model arises from uncertainty about which terms to include in the model. Since five parameters had to be investigated, all possible regressions (2^5=32) were

considered. The final model selected is based on a goodness of fit and a goodness of prediction criteria.

To validate a certain model, data is usually split into two sets—one set for model fitting and another set to validate the prediction capabilities of the developed model. Data splitting requires extensive gathering of data. An alternative to this process involves calculating the PRESS statistic, which is a measure of a model's prediction capabilities, which can be used as a form of validation in the spirit of data splitting. The PRESS statistic is computed as the sum of squares of the PRESS residuals. The procedure involves setting aside the first observation from the data set and using the remaining n-1 observations to estimate the coefficients for a particular candidate model. The first observation is then replaced and the second observation withheld with coefficients estimated again. Each observation is removed one at a time, and thus the candidate model is fitted *n* times. The deleted response is estimated each time, resulting in *n* prediction errors. The model that is finally adopted is fit using the entire data set, making use of all available information. The model with the lower PRESS statistic is the one that performs the best for prediction.

Another prediction parameter, the C_p statistic, was also considered during model selection. The C_p statistic is a compromise between model underfitting and model overfitting. The model with the lower C_p presents the best compromise between overfitting and underfitting. The models were also evaluated for fitting ability in the form of RMSE and the R-squared. In terms of fitting, the model with the higher R-square and lower MSE is the best model. It should be noted that different models might have optimum PRESS statistic, C_p, R-square, or MSE. In the end, the best overall model, a compromise between fitting and predicting capabilities, was selected.

The data used for model development was obtained from 100 mm F/L, L/L, and D/L specimens. The values of α and β, as well as the R-square (obtained by fitting equation 4.1 to the data of the measured resilient modulus) is presented in Table 4.6.

Alpha (α) was found to be related to the bulk density, the asphalt content, as well as to the fine-to-asphalt ratio, while β was found to be related to the bulk density, the natural log of asphalt content, and the voids in mineral aggregates. The relationships for α and β are presented in equations 4.2 and 4.3, respectively.

$$\alpha = 59283.91\ \mathbf{SG} - 1285.19\ \mathbf{AC} - 2109.91\ \mathbf{F/A} - 112749.23 \quad (4.2)$$

$$\beta = 0.11276 - 0.040328\ \mathbf{SG} + 0.032212\ \mathbf{ln(AC)} - 0.001417101\ \mathbf{VMA} \quad (4.3)$$

where,

SG = bulk specific gravity;

AC = asphalt content expressed in percent;

VMA = voids in mineral aggregates expressed in percent;

F/A = fine to asphalt ratio.

Comparison of the measured and the calculated values of α and β, from Table 4-4, is presented in Table 4-11. While building the model, sections E and I (L/L) and Section C (D/L) were eliminated, because statistical analysis showed that these data points are influential and can be considered as outliers.

The average variation between measured and calculated values of α was 6.6%, while the highest variation was 15.5%. The measured variation is well within the variation limit of the IDT test. The average variation for β is 4.6%, with a highest variation of 14.0%. In the statistical analysis for α, MSE was 2652831.94, while PRESS was 73647980.14; the RMSE would therefore be 1629 MPa, while the root mean PRESS would be 1919 MPa. For β, MSE and PRESS were 0.000010506 and 0.000307474, which gives a RMSE and root mean square PRESS of 0.0032413 $^{o}C^{-1}$ and 0.0039209 $^{o}C^{-1}$, respectively.

Table 4-11 Comparison between Calculated and Measured α and β

Mix	Section	Measured α (MPa)	Calculated α (MPa)	Variation (%)	Measured β ($^{o}C^{-1}$)	Calculated β ($^{o}C^{-1}$)	Variation (%)
FL	A	16168	16524	2.2	0.052	0.0531	2.1
	B	17348	17034	1.8	0.0471	0.0496	5.4
	C	19146	18877	1.4	0.0492	0.0515	4.7
	D	19720	18580	5.8	0.0472	0.0538	14.0
	E	19279	18807	2.4	0.0538	0.0544	1.2
	F	19578	20202	3.2	0.0512	0.0493	3.8
	G	18751	18871	0.6	0.0501	0.0513	2.5
	H	17963	19255	7.2	0.0489	0.0492	0.7
	I	23068	21215	8.0	0.0494	0.0504	2.0
	J	14561	15765	8.3	0.0431	0.0461	7.0
	L	13105	14648	11.8	0.0563	0.0561	0.3

Mix	Section	Measured α (MPa)	Calculated α (MPa)	Variation (%)	Measured β ($^oC^{-1}$)	Calculated β ($^oC^{-1}$)	Variation (%)
LL	A	19103	16135	15.5	0.046	0.0483	5.0
	B	21020	22643	7.7	0.0527	0.0493	6.5
	C	20649	20527	0.6	0.0538	0.0510	5.3
	D	20200	20897	3.4	0.0564	0.0540	4.3
	E	15791	20920	32.5	0.051	0.0516	1.1
	I	20523	16258	20.8	0.0492	0.0474	3.6
	J	17522	20227	15.4	0.0481	0.0470	2.2
	L	13841	14773	6.7	0.0592	0.0553	6.6
DL	A	17621	18497	5.0	0.0464	0.0486	4.8
	B	19533	18402	5.8	0.0568	0.0489	13.8
	C	18222	20987	15.2	0.0478	0.0524	9.6
	D	19846	17915	9.7	0.0533	0.0520	2.4
	I	21751	18723	13.9	0.0477	0.0484	1.6
	L	13676	14838	8.5	0.057	0.0544	4.6
Average				**6.6**			**4.6**

4.6.3 Model Evaluation

Finally, the capability of the proposed model to estimate HMA resilient modulus was evaluated. Using Equation 4.4, the average measured resilient modulus of each section was compared to the calculated one at the three test temperatures. The results are presented in Table 4-12, while **Error! Reference source not found.** presents the calculated resilient modulus vs. the measured resilient modulus, as well as any deviation from the equality line. The difference between the measured and predicted resilient moduli varied between 0.1 and 42.8%, with an average of 12.3% and a standard deviation of 9.3%. The greatest difference between measured and calculated resilient moduli is shown in section E L/L. This result was expected since data from section E of L/L was considered an outlier due to the high bulk density. The average variation between the calculated and measured resilient moduli was 7.9%, 11.0%, and 13.2%, while the standard deviation was 8.2%, 8.5%, and 10.6% at 5^{o}C, 25^{o}C, and 40^{o}C, respectively. Considering that the average mix variability ranges between 5.7% and 13.9%, the variation between the measured and calculated resilient moduli is very good. Therefore, the developed model can be considered to predict accurately the resilient modulus of HMA measured by the indirect tension test setup.

Table 4-12 Comparison between Calculated and Measured Resilient Modulus

	5°C			25°C			40°C		
	Measured Mr (MPa)	Calculated Mr (MPa)	Variation	Measured Mr (MPa)	Calculated Mr (MPa)	Variation	Measured Mr (MPa)	Calculated Mr (MPa)	Variation
F/L	12004	12760	5.5%	4760	4411	8.0%	1926	1988	2.5%
	13276	13088	0.1%	5782	4850	14.8%	2517	2303	7.1%
	15165	14911	3.8%	5431	5321	4.1%	2837	2457	15.3%
	15041	13764	5.6%	6540	4691	26.0%	2895	2092	25.5%
	13740	13963	4.3%	6087	4700	20.8%	2083	2077	2.3%
	14249	15791	10.8%	6232	5896	5.4%	2308	2816	22.0%
	13943	14083	4.7%	5982	5044	12.6%	2325	2336	4.1%
	13575	15164	10.9%	6133	5664	8.3%	2427	2706	10.7%
	18315	17344	10.0%	6843	6327	12.1%	3320	2970	15.0%
	11512	12467	8.7%	5282	4956	5.8%	2512	2482	0.8%
	9792	10919	13.0%	3485	3553	3.3%	1390	1531	11.6%
L/L	14868	13770	14.8%	6460	5241	25.3%	2924	2539	20.1%
	15819	17960	11.9%	6051	6704	9.2%	2450	3201	28.8%
	15553	15884	2.3%	5780	5732	0.7%	2360	2669	13.3%
	15060	15716	6.0%	5353	5341	1.3%	1966	2378	22.8%
	11317	16251	42.8%	5239	5791	9.9%	1877	2671	41.5%
	15807	14202	18.8%	6405	5503	22.4%	2823	2702	13.5%
	13807	14041	15.8%	5344	5480	16.7%	2723	2706	13.1%
	10152	11177	10.4%	3418	3697	8.4%	1224	1613	32.1%
D/L	13741	15553	5.6%	5841	5881	6.1%	2703	2836	2.2%
	15145	13845	4.9%	4627	5203	17.0%	2116	2497	22.8%
	14441	16480	11.8%	5676	5781	0.2%	2691	2635	4.0%
	14981	14336	7.8%	5754	5066	15.2%	2314	2321	3.3%
	17211	15692	14.6%	8017	5955	30.4%	3484	2879	22.6%
	10629	10608	6.4%	3141	3575	21.3%	1508	1581	11.7%
Average			**8.0%**			**11.03%**			**13.23%**

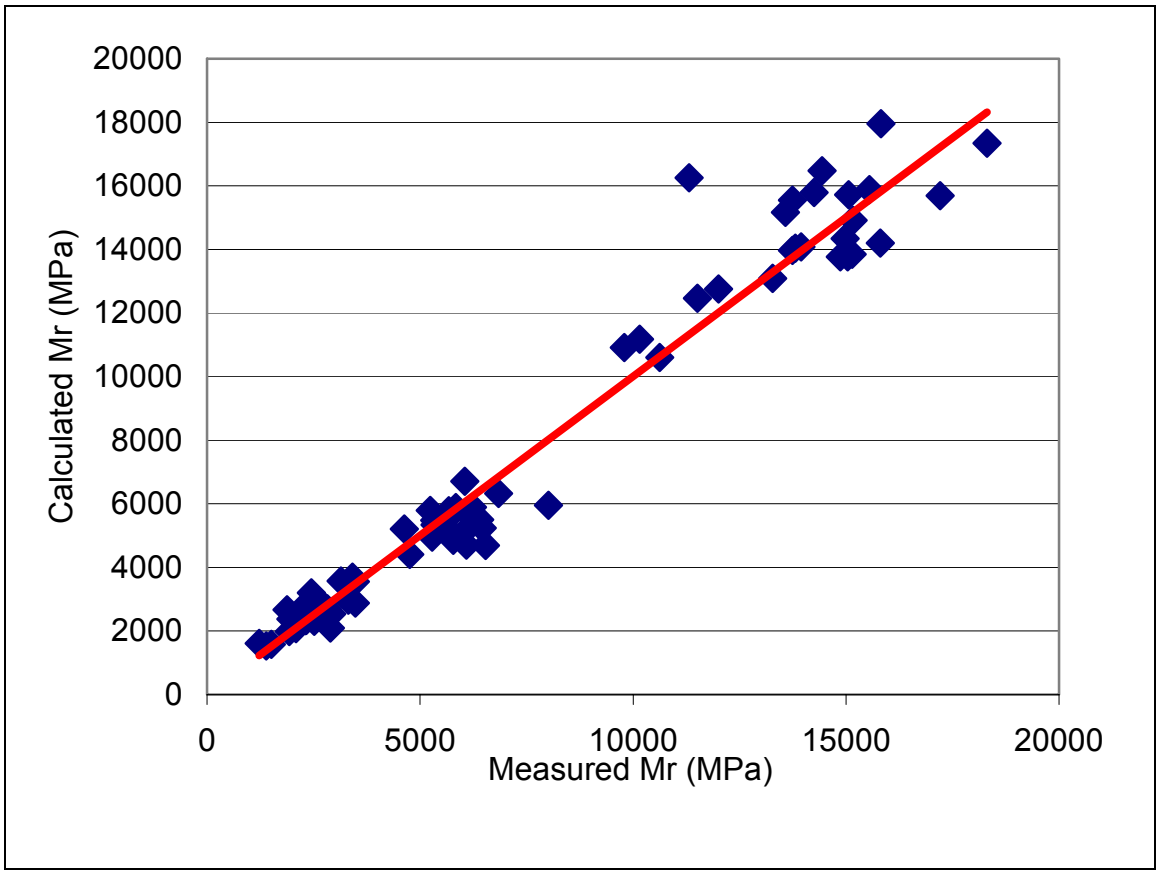

Figure 4-6 Calculated vs. Measured M_r

4.6.4 Resilient Modulus Calculation for F/F Specimens

In Section 4.5.1, it was observed that the resilient modulus of F/F specimens varied from that of F/L specimens. Likewise, the bulk density and percent of air voids in both set of specimens differed. Since the resilient modulus is related to the bulk density, the difference between the resilient moduli of F/F and F/L specimens could be solely due to the differences in bulk density. Therefore, the resilient modulus of F/F specimens was calculated, using the previously developed model, and then compared to the measured one. The results are presented in Table 4-13. The difference between the calculated and measured resilient moduli varies between 1.3% (Section A at 5°C) and 107% section D (40°C). The average variation was 29.3%, with a standard deviation of 26.13%.

Table 4-13 Comparison between calculated and measured F/F resilient modulus

Temperature (^{o}C)	Section	Measured M_r (MPA)	Calculated M_r (MPa)	Difference (%)
5	A	9559	9682	1.29
	B	9154	7414	19.01
	C	8591	10278	19.64
	D	11762	13476	14.57
	E	9862	10401	5.47
	F	NA	NA	NA
	G			
	H	9447	10877	15.14
	I	13507	17032	26.10
	J	NA	NA	NA
	L	5853	4973	15.04
25	A	3883	3181	18.08
	B	3579	2488	30.49
	C	2609	3411	30.74
	D	2356	4537	92.59
	E	3730	3274	12.21
	F	NA	NA	NA
	G			
	H	4100	3791	7.55
	I	4479	6269	39.96
	J	NA	NA	NA
	L	2193	1454	33.72
40	A	2030	1380	32.01
	B	1834	1097	40.20
	C	1207	1491	23.56
	D	968	2006	107.19
	E	NA	NA	NA
	F			
	G			
	H	1899	1719	9.46
	I	1954	2962	51.60
	J	NA	NA	NA
	L			

However, such a high average variation is partly due to the variations that occur in section D at 25°C and 40°C. Quite unexpectedly, the resilient modulus measurements for section D at 25°C and 40°C were very low, which is probably due to the specimens being damaged; therefore, these measurements should be considered non-reliable and should be excluded from the analysis. Doing so would give a maximum variation of 51.6% (section I at 40°C). The average variation would then be 22.3%, with a standard deviation of 13.1%. The average variation between the model-calculated and measured resilient moduli is higher than the average mix variability in the resilient modulus test: 10.3%, 8.9%, and 4.3% at 5°C, 25°C, and 40°C, respectively. However, test results of F/F specimens are based on limited number of data as a result of the limited number of field cores, as well as the inability to test some specimens at 25 and/or 40°C. In conclusion, the difference in the measured resilient moduli between F/L and F/F specimens is partly due to the difference in the volumetric properties, mainly the bulk density. However, the difference in bulk density does not fully explain this difference, which confirms the existence of a compaction shift factor between field cores and laboratory prepared specimens.

4.7 Conclusion

Resilient modulus values were successfully measured using the IDT setup. The mix variability was determined and it was found that the repeatability of the IDT test is high. Shift factors for compaction, and load duration were developed. Field compaction resulted in field cores having lower bulk density and higher air voids than F/L specimens, however, this fact did not entirely explain the difference in the measured resilient modulus. The data analysis method used to calculate the measured resilient modulus (Roque and Buttlar, 1992) was developed to take into account the specimen size effect by introducing correction factors that are function of the specimen diameter to thickness ratio. The method is applicable at low temperature, however as the testing temperature is increased elastic analysis lead to discrepancies between the 100- and 150-mm specimen diameter resilient modulus values. The load duration was found to have an effect on the measured resilient modulus. The effect of load duration increased with increasing temperature. However an interesting finding was the fact that the resilient modulus measured at 0.1 sec load duration was higher than the one measured at 0.03 sec load duration at 5°C, which might be related to the method the IDT test is performed.

Finally a model predicting resilient modulus values from volumetric properties was successfully developed. The resilient modulus values predicted by the model fell well within the range of the test variability.

Chapter 5 Findings, Conclusions, and Recommendations

5.1 Summary

Accurate determination of the material properties is essential for pavement design, maintenance, and rehabilitation. Laboratory testing has the advantage of determining the material properties before the pavement is constructed. Upon completion of the construction, the as built material properties can be determined using FWD testing or by laboratory testing of field cores. The main objective of this research was to develop shift factors between field cores and laboratory prepared specimens. Determining these shift factors allows pavement engineers to determine whether the difference between the laboratory prepared specimens or field cores resilient modulus is due to compaction or construction. Moreover, such a shift factor is important during the design stage when resilient modulus values can be obtained from specimens prepared in the laboratory. Laboratory specimens were prepared using HMA either mixed at the plant during construction or mixed in the laboratory. Also the effect of load pulse duration on the resilient modulus was investigated. The load pulses investigated are 0.1s (as recommended by ASTM D4123) and 0.03s (based on a study on the stress pulse width and truck loading by Loulizi et al., 2002). The tasks that were undertaken in this research can be summarized as follows:

1. Specimen preparation; the specimens were divided into F/F, F/L, L/L, D/L, and D/L tested at 0.03s load pulse duration.
2. Determine the load to be used for resilient modulus testing at each of the testing temperatures for the different mixes. The selected load had to meet the criterion of limiting the strain between 150 and 500 microstrains.
3. Determine the variability in the IDT test. The variability was divided into two parts: (1) variability between the two faces of the IDT specimen, and (2) variability between the specimens of a given mix.
4. Determine the compaction shift factor at each of the testing temperatures between F/F, and F/L specimens.
5. Determine the specimen size shift factor between 100- and 150-mm diameter specimens for F/L/, L/L, and D/L specimens.

6. Determine the load pulse duration shift factor between 0.1s and 0.03s load pulses; this was performed on D/L specimens.
7. Develop a model to correlate the resilient modulus to the temperature and the volumetric properties of the HMA using F/L, L/L, and D/L specimens. This model was then used to calculate the resilient modulus of F/F specimens and compare the results to the measured resilient modulus of F/F specimens.

5.2 Findings

Various findings were encountered during this research. These findings can be summarized as follows:

1. In the tested load range, the resilient modulus was found to be independent of the applied load at 5^{o}C and 25^{o}C. This could not be verified at 40^{o}C due to the limited range of tested loads. The reason for the independence of the resilient modulus to the load intensity is thought to be due to the fact that the tested load range is relatively small compared to the indirect tensile strength of the specimens.
2. Damage to an indirect tension specimen is avoided when the strain is limited between 150 and 500 microstrain.
3. The average specimen variability ranged between 6.7% and 35.5%, while the average mix variability ranged between 5.7% and 13.9%. This indicates that the repeatability of the indirect tension test for resilient modulus calculation is acceptable. Moreover it was found that repeatability is better achieved for specimens produced in the laboratory than for specimens taken from the field.
4. The study showed that there is a compaction shift factor between field cores and laboratory compacted specimens. The shift factor ranged from 1 to 3 with laboratory compacted samples having the higher resilient modulus. An average shift factor ranging between 1.45 and 1.5 seems to represent most mixes at all tested temperatures. The existence of a shift factor is reinforced by the fact that different air void content and specific gravity were measured for F/F and F/L samples.
5. The data analysis procedure used in calculating the resilient modulus accounted for the specimen size effect at 5^{o}C. At 5^{o}C the behavior of HMA is elastic and therefore correcting for the specimen size using an elastic analysis resulted in a

consistent resilient modulus measured for 100- and 150-mm diameter. However, at 25 and 40°C, viscous flow in the specimen resulted in different resilient modulus from 100- and 150-mm diameter specimens, with the former resulting in a higher calculated resilient modulus. The specimen size shift factor increased as the test temperature increased. The average specimen size shift factor was 1.25, and 1.30 at 25, and 40°C, respectively.

6. Analysis of the variability in resilient modulus results showed no difference between 100- and 150-mm diameter specimens which means that 100-mm diameter specimens as accurate as 150-mm diameter specimens in determining the resilient modulus however, the measured values are not the same.
7. The average load duration shift factor varied with temperature, with average load duration shift factors of 0.83, 1.31 and 1.39 at 5°C, 25°C, and 40°C, respectively. These shift factors represent the ratio of the measured resilient modulus at 0.03 sec to the measured resilient modulus at 0.1 sec load duration. An interesting result is the load duration shift factor at 5°C which is smaller than one. The explanation for this fact is that the total accumulated strain using a load duration of 0.1 sec is higher than the one accumulated using a load duration of 0.03 sec. This might lead to lower resilient moduli being measured at a 0.03 sec loading duration. This factor was verified by measuring the resilient modulus at 0.03 sec and 0.1 sec on the same samples which also produced the same shift factor.
8. In characterizing the resilient modulus as a function of temperature, two parameters α and β were identified. α is related to the resilient modulus at 0°C while β represents the mix sensitivity to temperature. These two parameters were related to the mix volumetric properties. α was found to be affected by the mix specific gravity, the asphalt content, and the fine to asphalt ratio; while β was found to be affected by the asphalt content, the specific gravity, and the voids in mineral aggregates. A model was developed to predict the resilient modulus from the mix volumetric properties. The average variation between the model calculated and measured resilient modulus was 7.95%, 11.03%, and 13.23% at 5°C, 25°C, and 40°C, respectively, which is lower than the average mix variation in the indirect tension test for the resilient modulus.

5.3 Conclusions

The resilient moduli of the different HMA placed at the Virginia Smart Road were measured in the laboratory using the IDT setup. The variability in the result was determined and shift factors were developed to account for the effect of compaction, specimen size, and load pulse duration. Finally, a model that relates the resilient modulus to the volumetric properties of the mix was developed. Based on this research, the following conclusions could be drawn:

1. The testing results suggest that as long as the applied load is under 20% of the load to cause failure in the specimen, the resilient modulus of HMA will be independent of the applied load; this is based on results of tests at 25^{o}C.
2. There is a difference between field compaction and laboratory gyratory compaction. The difference results in different resilient moduli between field cores and laboratory produced specimens and cannot fully be explained by the fact that the percent air voids and bulk specific gravity are different for the two sets of specimens.
3. The load duration affects the resilient modulus results. Therefore, resilient modulus results obtained at loading durations similar to the ones experienced in the field should be used for HMA characterization.
4. There is a strong correlation between the resilient modulus of HMA and its volumetric properties. These volumetric properties are the bulk specific gravity, the asphalt content, the fine to asphalt ratio, and the voids in mineral aggregate. A model was developed to predict the HMA resilient modulus from its volumetric properties

5.4 Recommendations

Based on the research's results the following recommendations for testing and future research can be made:

1. It is clear that the load duration has an effect on the measured resilient modulus therefore, it is suggested that a load pulse duration of 0.03 sec be used since it is more representative of the actual traffic loading.
2. The range of the applied load in this research was small compared to the indirect tensile strength of the HMA. In this range, the load had no effect on the

measured resilient modulus. To investigate the effect of load intensity on the measured resilient modulus using Roque and Buttlar's data analysis, the Load intensity range must be increased. Roque and Buttlar showed that a strain of 2000 microstrain may be needed to induce damage to the samples; therefore, the loading can be safely increased to investigate its effect on the resilient modulus.

3. The shift factor between field and laboratory compaction might be partly due to the difference in the sample thickness between F/F and F/L samples. To fully account for the effect of compaction, specimens of the same thickness and same diameter to thickness ratio should be tested.
4. it appears that the viscous flow of HMA in the resilient modulus testing is affected by the thickness to diameter ratio. To quantify this effect, it is suggested that a wider range of specimen diameters and thicknesses be investigated.
5. To quantify the effect of HMA volumetric properties on its resilient modulus for different mixes, it is suggested that a wider range of volumetric and binder properties be used to fine-tune and calibrate the developed model for other HMA.

References

Almudaiheem, J., and Al-Sugair, F., "Effect of Loading Magnitude on Measured Resilient Modulus of Asphalt Concrete Mixes." Transportation Research Record, No.1317, Transportation Research Board, Washington, DC, pp.139-144, 1991.

Baladi, Gilbert Y. Harichandran, Ronald S. Lyles, Richard W. "New relationships between structural properties and asphalt mix parameters." *Transportation Research Record n 1171 1988 p 168-177*

Blakey, F.A., and Beresford, F.D., "Tensile Strain in Concrete" II. C.S.I.R.O. Div. Build. Res. Rep. No. C2. 2-2, 15, 1955.

Brown, E.R., and Foo, Kee Y., "Evaluation of Variability in Resilient Modulus Test Results (ASTM D 4123)", ASTM Journal of Testing & Evaluation, Vol. 19 No 1, p 1-13, 1991.

Cragg R. Pell PS. "Dynamic stiffness of bituminous road materials" *Proceding of the Association of Asphalt Paving Technologists, Tech Session, Oklahoma City, Okla,. v 40 Feb 15-17 1971 p 126-47*

Gemayel, Chaouki A. Mamlouk, Michael S. Characterization of hot-mixed open-graded asphalt mixtures. *Transportation Research Record n 1171 1988 p 184-192*

Heinicke, John J. Vinson, Ted S. "EFFECT OF TEST CONDITION PARAMETERS ON IRMR". *Journal of Transportation Engineering. v 114 n 2 Mar 1988 p 153-172*

Hondros, G., "The Evaluation of Poisson's Ratio and the Modulus of Materials of a Low Tensile Resistance by the Brazilian (Indirect Tensile) Test with Particular Reference to Concrete", Australian Journal of Applied Science, Vol. 10, No. 3, p. 243-268, 1959.

Howeedy, M Fayek, Herrin, Moreland. BEHAVIOR OF COLD MIXES UNDER REPEATED COMPRESSIVE LOADS. *Highw Res Rec. n 404, 1972 p 57-70*

Kim, Y.R., Shah, K.A, and Khosla, N.P, "Influence of Test Parameters in SHRP P07 Procedure on Resilient Moduli of Asphalt Concrete Field Cores", Transportation Research Record 1353, p.82-89, 1992.

Lim, C.T., Tan, S.A., Fwa, T.F., "Specimen Size Effect on The Diametrical Mechanical Testing of Asphalt Mixes", Journal of Testing and Evaluation, JTEVA, Vol. 23, No. 6, pp. 436-441, 1995.

Loulizi, A., Al-Qadi, I.L., Lahour, S., and Freeman, T.E., "Measurement of Vertical Compressive Stress Pulse in Flexible Pavements and Its Representation for Dynamic Loading", Transportation Research Board, Paper No.02-2376, 2002.

Myers, R.H., "Classical and Modern Regression with Applications", second edition

Roque, R., and Ruth, B.E., "Materials Characterization and Response of Flexible Pavements at Low Temperatures." Proceedings of the Association of Asphalt Paving Technoligists, Vol. 56, pp. 130-167, 1987.

Roque, R., and Buttlar, W.G., "Development of a Measurement and Analysis Method to accurately Determine Asphalt concrete Properties Using the Indirect Tensile Mode", Proc., Association of Asphalt Paving Technologists, Vol. 61, 1992.

Schmidt, R J. "PRACTICAL METHOD FOR MEASURING THE RESILIENT MODULUS OF ASPHALT-TREATED MIXES." *Highway Research Record n 404, 1972 p 22-29*

15. Von Quintus, Harold L. Harrigan, Edward. Lytton, Robert L. How SHRP reliably predicts pavement performance *Pacific Rim TransTech Conference. Publ by ASCE, New York, NY, USA. 1993. p 298-307*

Wright, P.J.F., "Comments on an indirect tensile test for concrete" Mag. Conc. Res. 20: 87-96, 1955.

Appendix A

Mixture Designs and Gradations

Figure A.1 Mixture designs for SM12.5D, section A.

Design / Lab		
Aggregate		**%**
#78 Quartzite	Salem Stone Co., Sylvatus, VA	15
#8 Quartzite	Salem Stone Co., Sylvatus, VA	30
#9 Quartzite	Salem Stone Co., Sylvatus, VA	10
#10 Limestone	Sisson and Ryan Quarry, Shawsville, VA	20
Sand	Castle Sand Co., New Castle VA	10
Fine RAP	Adams Construction Co., Blacksburg, VA	15
Binder		**%**
PG 70-22	Associated Asphalt, Inc., Roanoke, VA	5.6

Lab / Lab		
Aggregate		**%**
#78 Quartzite	Salem Stone Co., Sylvatus, VA	5
#8 Quartzite	Salem Stone Co., Sylvatus, VA	30
#9 Quartzite	Salem Stone Co., Sylvatus, VA	20
#10 Limestone	Sisson and Ryan Quarry, Shawsville, VA	20
Sand	Castle Sand Co., New Castle VA	10
Fine RAP		15
Binder		**%**
PG 70-22	Associated Asphalt, Inc., Roanoke, VA	5.9

Figure A. 2 Gradation of SM-12.5D, field-field mixture, section A.

Sieve opening (mm)	Sieve #	% Passing	Control Point LL	Control Point UL	Restricted Zone LL	Restricted Zone UL	Decision
19	3/4	100.0	-	100	-	-	-
12.5	1/2	99.6	90	100	-	-	P
9.5	3/8	98.5	-	90	-	-	F
4.75	#4	84.2	-	-	-	-	-
2.36	#8	47.7	28	58	39.1	39.1	P
1.18	#16	37.3	-	-	25.6	31.6	P
0.6	#30	27.0	-	-	19.1	23.1	P
0.3	#50	14.7	-	-	15.5	15.5	P
0.15	#100	10.2	-	-	-	-	-
0.075	#200	5.6	2	10	-	-	P

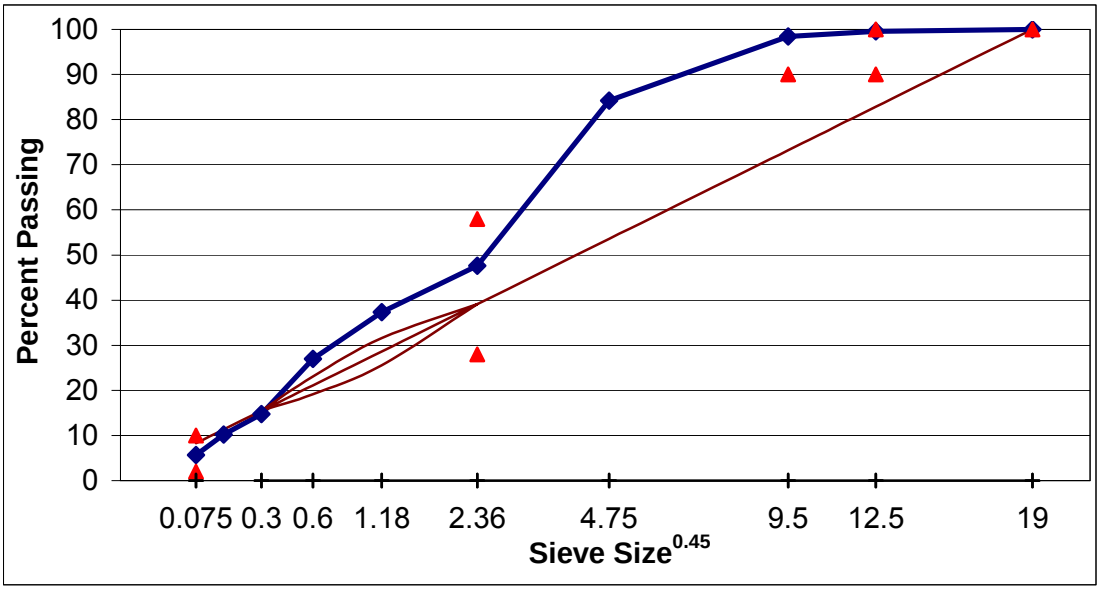

Figure A. 3 Gradation of SM-12.5D, field-lab mixture, section A.

Sieve opening (mm)	Sieve #	% Passing	Control Point LL	Control Point UL	Restricted Zone LL	Restricted Zone UL	Decision
19	3/4	100.0	-	100	-	-	P
12.5	1/2	99.6	90	100	-	-	P
9.5	3/8	98.5	-	90	-	-	F
4.75	#4	84.2	-	-	-	-	-
2.36	#8	47.7	28	58	39.1	39.1	P
1.18	#16	37.3	-	-	25.6	31.6	P
0.6	#30	27.0	-	-	19.1	23.1	P
0.3	#50	14.7	-	-	15.5	15.5	P
0.15	#100	10.2	-	-	-	-	-
0.075	#200	5.6	2	10	-	-	P

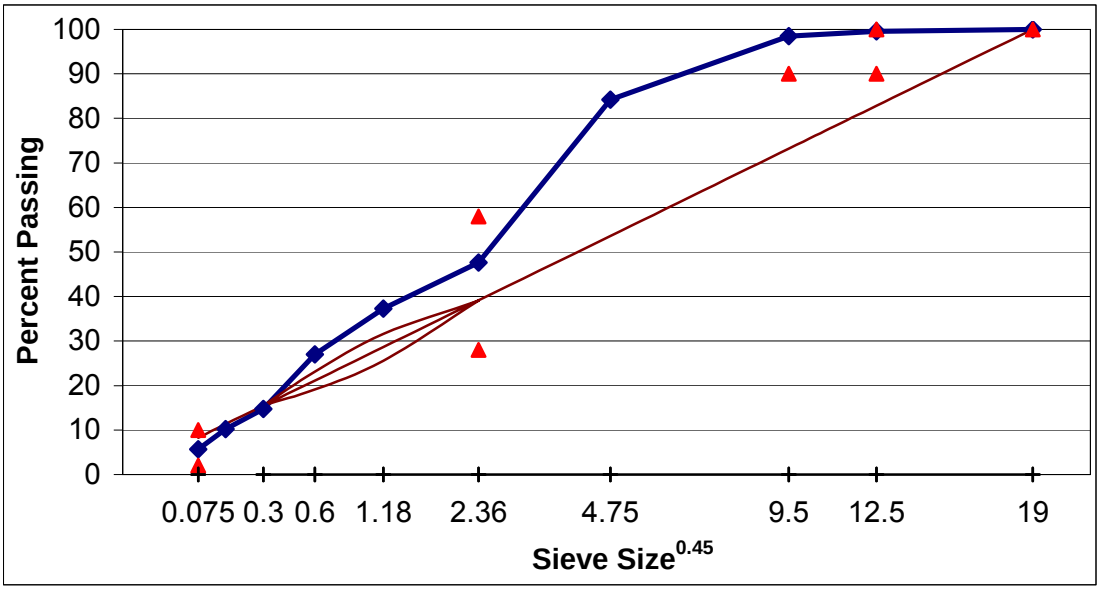

Figure A. 4 Gradation of SM-12.5D, lab-lab mixture, section A.

Sieve opening (mm)	Sieve #	% Passing	Control Point LL	Control Point UL	Restricted Zone LL	Restricted Zone UL	Decision
19	3/4	100.0		100			P
12.5	1/2	99.5	90	100			P
9.5	3/8	98.9	-	90			F
4.75	#4	91.3	-	-			
2.36	#8	58.3	28	58	39.1	39.1	F
1.18	#16	38.8	-	-	25.6	31.6	P
0.6	#30	28.7	-	-	19.1	23.1	P
0.3	#50	20.1	-	-	15.5	15.5	P
0.15	#100	15.6	-	-			
0.075	#200	12.3	2	10			F

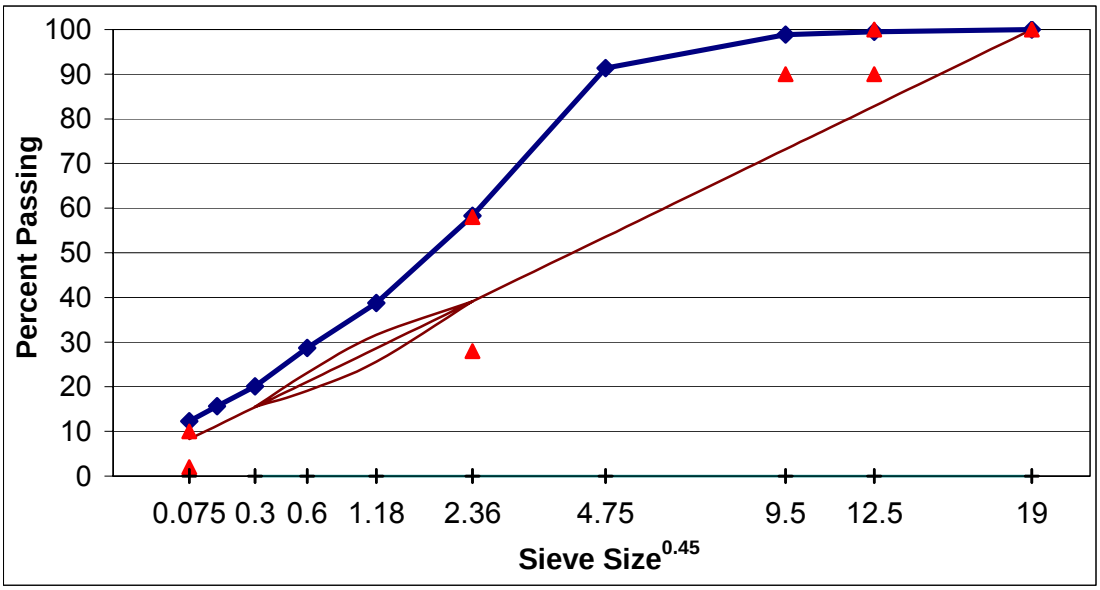

Figure A. 5 Gradation of SM-12.5D, design-lab mixture, section A.

Sieve opening (mm)	Sieve #	% Passing	Control Point LL	Control Point UL	Restricted Zone LL	Restricted Zone UL	Decision
19	3/4	100.0		100			P
12.5	1/2	98.4	90	100			P
9.5	3/8	89.9	-	90			P
4.75	#4	50.1	-	-			
2.36	#8	27.7	28	58	39.1	39.1	F
1.18	#16	20.2	-	-	25.6	31.6	P
0.6	#30	15.3	-	-	19.1	23.1	P
0.3	#50	9.7	-	-	15.5	15.5	P
0.15	#100	7.3	-	-			
0.075	#200	6.0	2	10			P

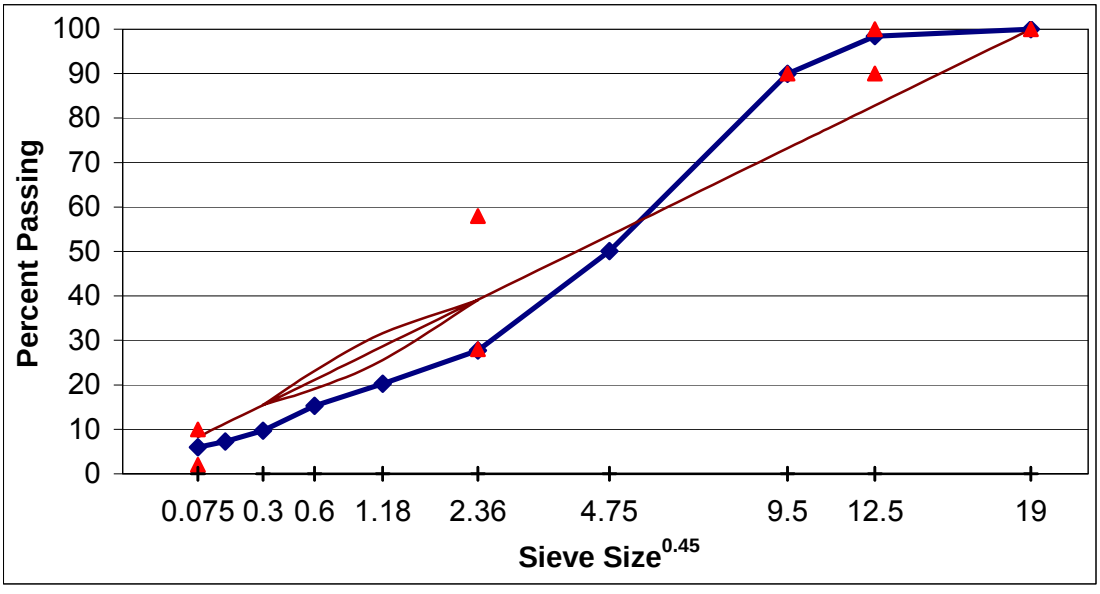

. Figure A. 6 Mixture designs for SM9.5D, section B.

Design / Lab		
Aggregate		**%**
#8 Quartzite	Salem Stone Co., Sylvatus, VA	60
#10 Limestone	ACCO Stone Co., Blacksburg, VA	20
Concrete Sand	Wythe Stone Co., Wytheville, VA	10
Fine RAP	Adams Construction Co., Blacksburg, VA	10
Binder		**%**
PG 70-22	Associated Asphalt, Inc., Roanoke, VA	5.6

Lab / Lab		
Aggregate		**%**
#8 Quartzite	Salem Stone Co., Sylvatus, VA	36
#10 Limestone	ACCO Stone Co., Blacksburg, VA	20
Concrete Sand	Wythe Stone Co., Wytheville, VA	10
#10 Quartzite	Salem Stone Co., Sylvatus, VA	23
ite passing #200	Salem Stone Co., Sylvatus, VA	1
Fine RAP	Adams Construction Co., Blacksburg, VA	10
Binder		**%**
PG 70-22	Associated Asphalt, Inc., Roanoke, VA	4.7

Figure A. 7 Gradation of SM-9.5D, field-field mixture, section B.

Sieve opening (mm)	Sieve #	% Passing	Control Point LL	Control Point UL	Restricted Zone LL	Restricted Zone UL	Decision
12.5	1/2	98.5	-	100			F
9.5	3/8	90.3	90	100			P
4.75	#4	51.9	-	90			P
2.36	#8	35.4	32	67	47.2	47.2	P
1.18	#16	26.7	-	-	31.6	37.6	P
0.6	#30	18.1	-	-	23.5	27.5	P
0.3	#50	11.9	-	-	18.7	18.7	P
0.15	#100	9.4	-	-			
0.075	#200	7.8	2	10			P

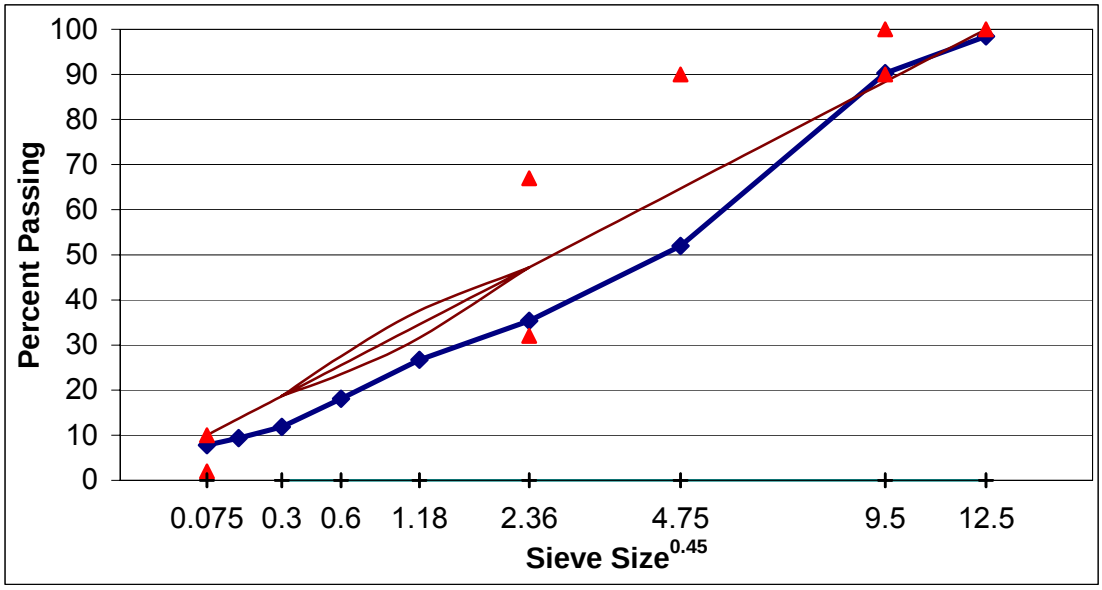

Figure A. 8 Gradation of SM-9.5D, field-lab mixture, section B.

Sieve opening (mm)	Sieve #	% Passing	Control Point LL	Control Point UL	Restricted Zone LL	Restricted Zone UL	Decision
12.5	1/2	98.5	-	100			F
9.5	3/8	90.3	90	100			P
4.75	#4	51.9	-	90			P
2.36	#8	35.4	32	67	47.2	47.2	P
1.18	#16	26.7	-	-	31.6	37.6	P
0.6	#30	18.1	-	-	23.5	27.5	P
0.3	#50	11.9	-	-	18.7	18.7	P
0.15	#100	9.4	-	-			
0.075	#200	7.8	2	10			P

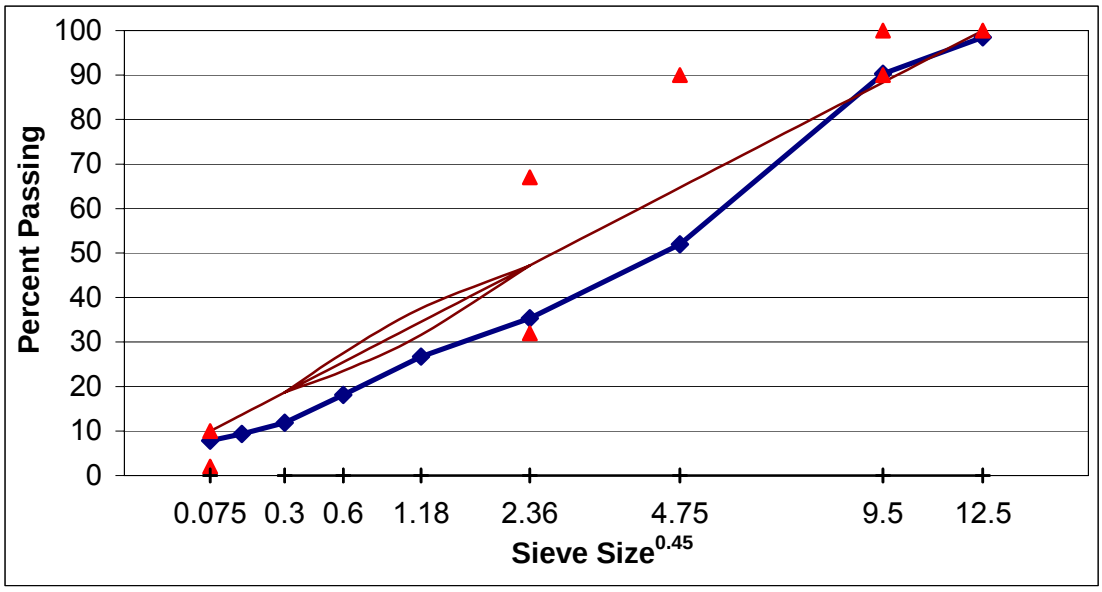

Figure A. 9 Gradation of SM-9.5D, lab-lab mixture, section B.

Sieve opening (mm)	Sieve #	% Passing	Control Point LL	Control Point UL	Restricted Zone LL	Restricted Zone UL	Decision
12.5	1/2	98.5	-	100			F
9.5	3/8	91.5	90	100			P
4.75	#4	58.8	-	90			P
2.36	#8	42.5	32	67	47.2	47.2	P
1.18	#16	30.8	-	-	31.6	37.6	P
0.6	#30	22.9	-	-	23.5	27.5	P
0.3	#50	15.1	-	-	18.7	18.7	P
0.15	#100	11.1	-	-			
0.075	#200	8.7	2	10			P

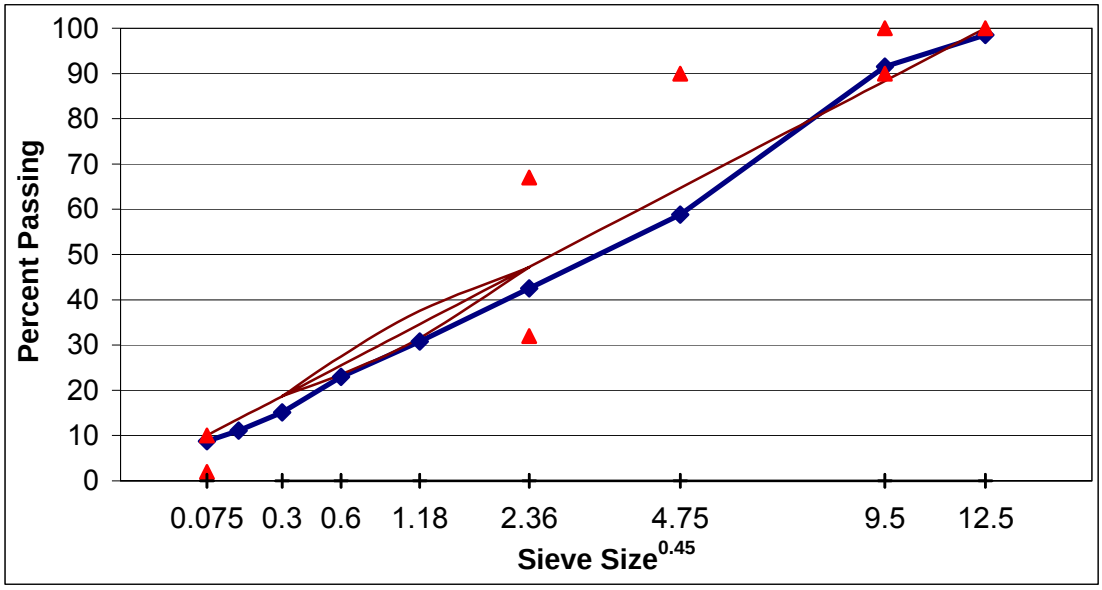

Figure A. 10 Gradation of SM-9.5D, design-lab mixture, section B.

Sieve opening (mm)	Sieve #	% Passing	Control Point LL	Control Point UL	Restricted Zone LL	Restricted Zone UL	Decision
12.5	1/2	99.7	-	100			F
9.5	3/8	86.1	90	100			F
4.75	#4	33.7	-	90			P
2.36	#8	22.9	32	67	47.2	47.2	F
1.18	#16	18.2	-	-	31.6	37.6	P
0.6	#30	14.0	-	-	23.5	27.5	P
0.3	#50	8.8	-	-	18.7	18.7	P
0.15	#100	6.6	-	-			
0.075	#200	5.5	2	10			P

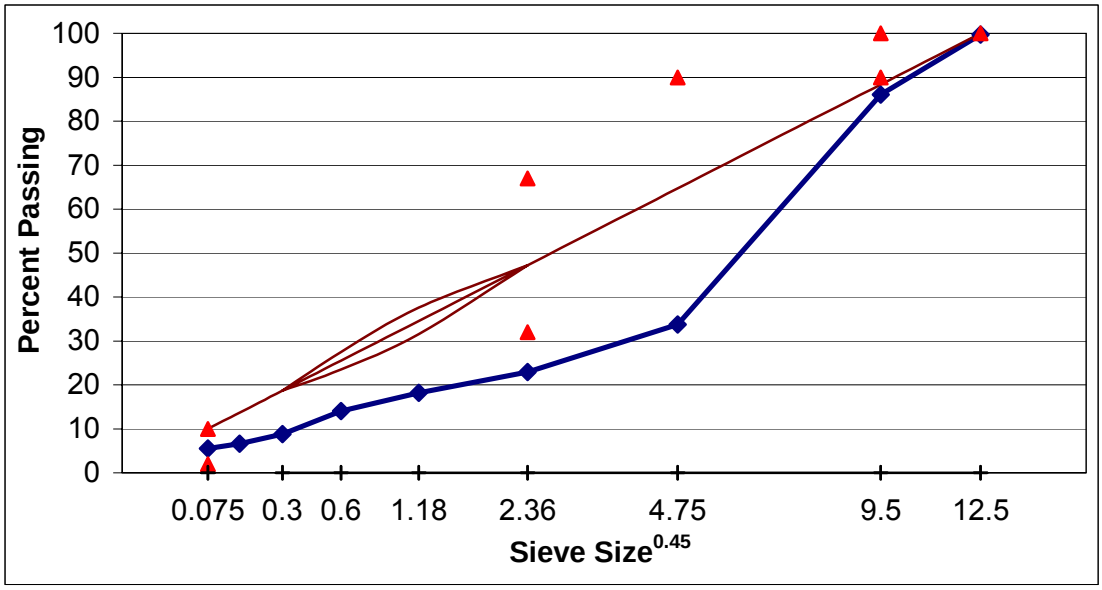

Figure A. 11 Mixture designs for SM9.5E, section C.

Design / Lab		
Aggregate		**%**
#8 Quartzite	Salem Stone Co., Sylvatus, VA	54
#10 Quartzite	Salem Stone Co., Sylvatus, VA	21
Concrete Sand	Wythe Stone Co., Wytheville, VA	10
Fine RAP	Adams Construction Co., Blacksburg, VA	15
Binder		**%**
PG 76-22	Koch Materials Co., Pennsauken, NJ	5.8

Lab / Lab		
Aggregate		**%**
#8 Quartzite	Salem Stone Co., Sylvatus, VA	52
#10 Quartzite	Salem Stone Co., Sylvatus, VA	23
Concrete Sand	Wythe Stone Co., Wytheville, VA	10
Fine RAP	Adams Construction Co., Blacksburg, VA	15
Binder		**%**
PG 76-22	Koch Materials Co., Pennsauken, NJ	5.8

Figure A. 12 Gradation of SM-9.5E, field-field mixture, section C.

Sieve opening (mm)	Sieve #	% Passing	Control Point LL	Control Point UL	Restricted Zone LL	Restricted Zone UL	Decision
12.5	1/2	99.4	-	100			F
9.5	3/8	95.0	90	100			P
4.75	#4	61.7	-	90			P
2.36	#8	40.3	32	67	47.2	47.2	P
1.18	#16	29.2	-	-	31.6	37.6	P
0.6	#30	22.6	-	-	23.5	27.5	P
0.3	#50	15.3	-	-	18.7	18.7	P
0.15	#100	10.7	-	-			
0.075	#200	8.2	2	10			P

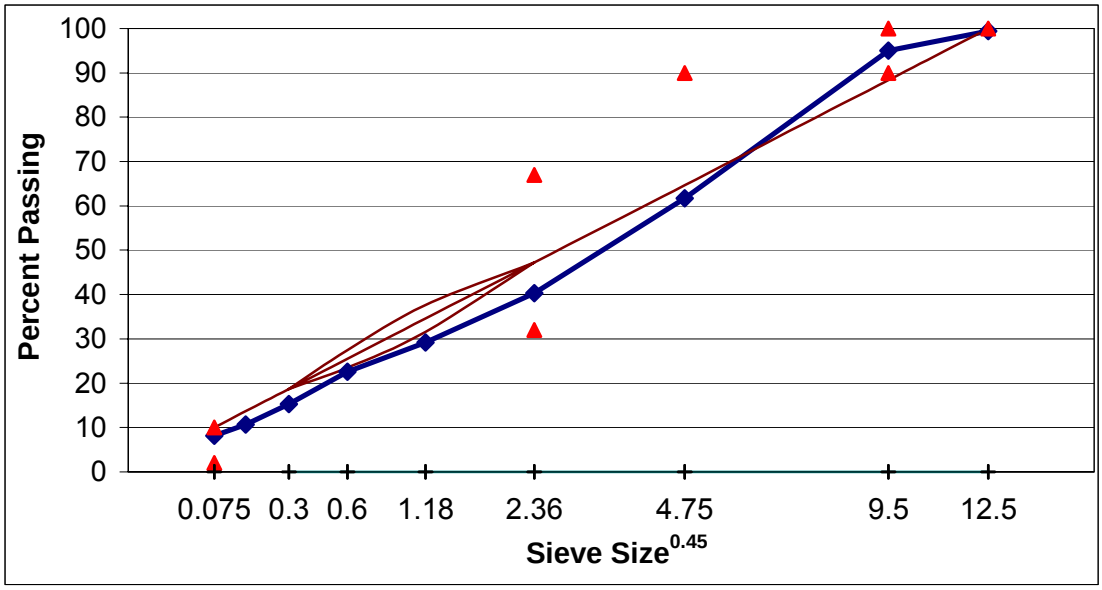

Figure A. 13 Gradation of SM-9.5E, field-lab mixture, section C.

Sieve opening (mm)	Sieve #	% Passing	Control Point LL	Control Point UL	Restricted Zone LL	Restricted Zone UL	Decision
12.5	1/2	98.0	-	100			F
9.5	3/8	90.9	90	100			P
4.75	#4	55.3	-	90			P
2.36	#8	34.3	32	67	47.2	47.2	P
1.18	#16	27.0	-	-	31.6	37.6	P
0.6	#30	19.7	-	-	23.5	27.5	P
0.3	#50	14.1	-	-	18.7	18.7	P
0.15	#100	11.1	-	-			
0.075	#200	8.0	2	10			P

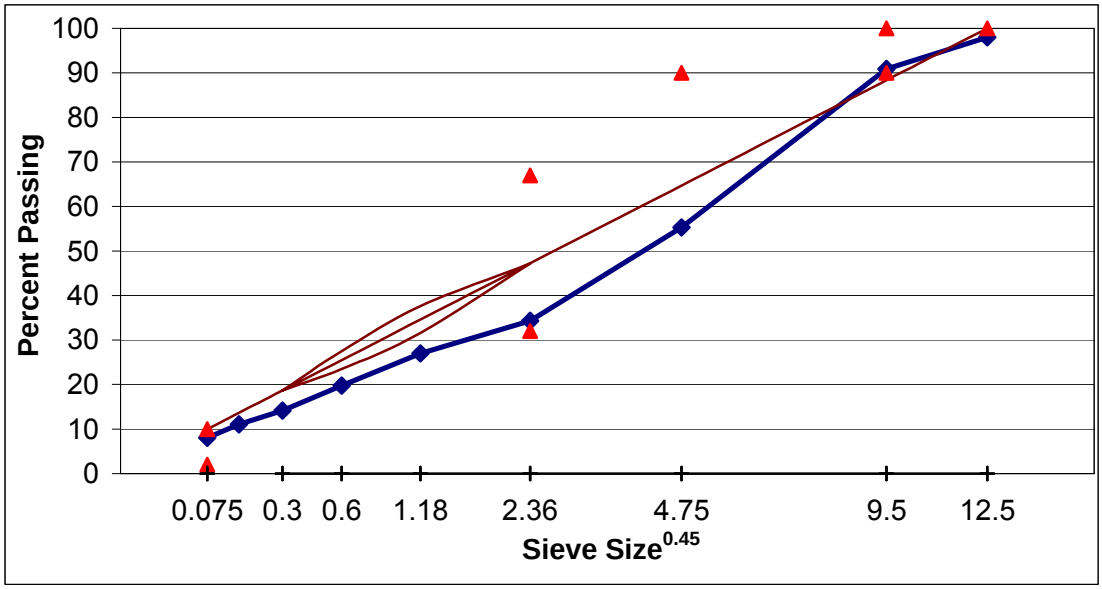

Figure A. 14 Gradation of SM-9.5E, lab-lab mixture, section C.

Sieve opening (mm)	Sieve #	% Passing	Control Point LL	Control Point UL	Restricted Zone LL	Restricted Zone UL	Decision
12.5	1/2	99.7	-	100			F
9.5	3/8	90.2	90	100			P
4.75	#4	44.6	-	90			P
2.36	#8	35.2	32	67	47.2	47.2	P
1.18	#16	27.3	-	-	31.6	37.6	P
0.6	#30	21.0	-	-	23.5	27.5	P
0.3	#50	13.8	-	-	18.7	18.7	P
0.15	#100	10.1	-	-			
0.075	#200	7.6	2	10			P

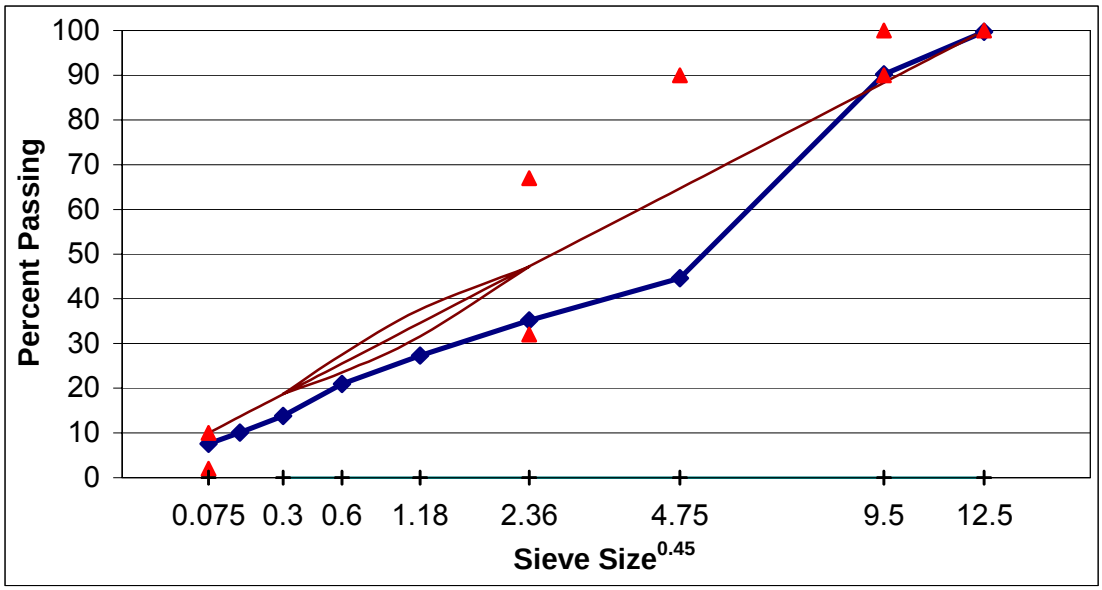

Figure A. 15 Gradation of SM-9.5E, design-lab mixture, section C.

Sieve opening (mm)	Sieve #	% Passing	Control Point LL	Control Point UL	Restricted Zone LL	Restricted Zone UL	Decision
12.5	1/2	99.4	-	100			F
9.5	3/8	86.5	90	100			F
4.75	#4	44.9	-	90			P
2.36	#8	32.8	32	67	47.2	47.2	P
1.18	#16	25.2	-	-	31.6	37.6	P
0.6	#30	19.3	-	-	23.5	27.5	P
0.3	#50	12.5	-	-	18.7	18.7	P
0.15	#100	8.9	-	-			
0.075	#200	6.6	2	10			P

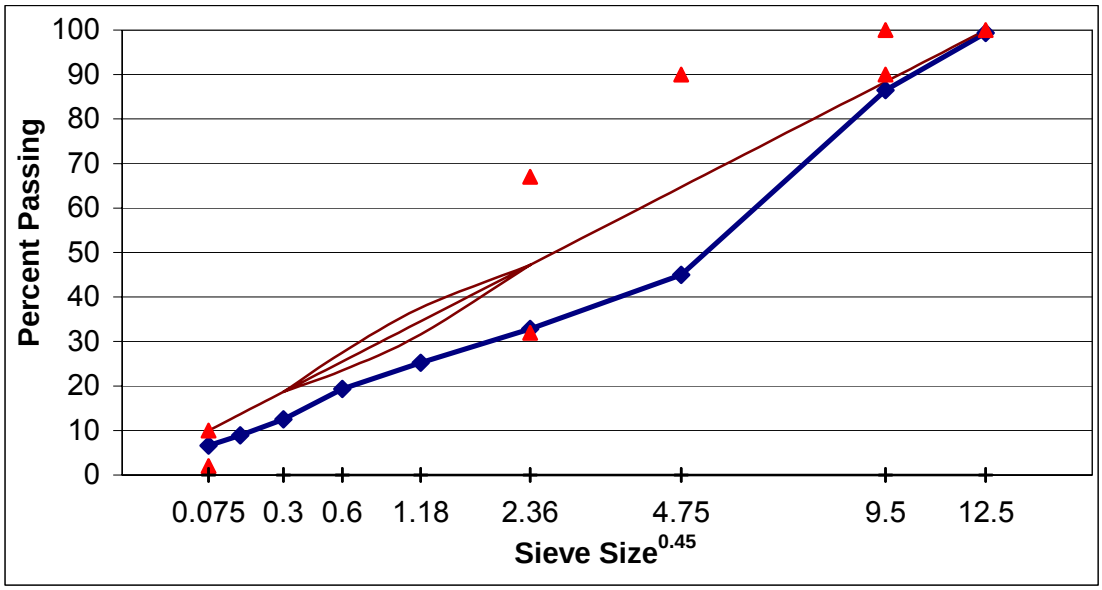

Figure A. 16 Mixture designs for SM-9.5A, section D.

Design / Lab		
Aggregate		**%**
#8 Quartzite	Salem Stone Co., Sylvatus, VA	50
#10 Quartzite	Salem Stone Co., Sylvatus, VA	30
Concrete Sand	Wythe Stone Co., Wytheville, VA	10
Fine RAP	Adams Construction Co., Blacksburg, VA	10
Binder		**%**
PG 64-22	Associated Asphalt, Inc., Roanoke, VA	5.6

Lab / Lab		
Aggregate		**JMF %**
#8 Quartzite	Salem Stone Co., Sylvatus, VA	50
#10 Quartzite	Salem Stone Co., Sylvatus, VA	30
Concrete Sand	Wythe Stone Co., Wytheville, VA	10
Fine RAP	Adams Construction Co., Blacksburg, VA	10
Binder		**%**
PG 64-22	Associated Asphalt, Inc., Roanoke, VA	5.6?

Figure A. 17 Gradation of SM-9.5A, field-field mixture, section D.

Sieve opening (mm)	Sieve #	% Passing	Control Point LL	Control Point UL	Restricted Zone LL	Restricted Zone UL	Decision
12.5	1/2	99.3	-	100			F
9.5	3/8	92.4	90	100			P
4.75	#4	54.9	-	90			P
2.36	#8	34.8	32	67	47.2	47.2	P
1.18	#16	25.7	-	-	31.6	37.6	P
0.6	#30	20.4	-	-	23.5	27.5	P
0.3	#50	15.3	-	-	18.7	18.7	P
0.15	#100	11.8	-	-			
0.075	#200	9.2	2	10			P

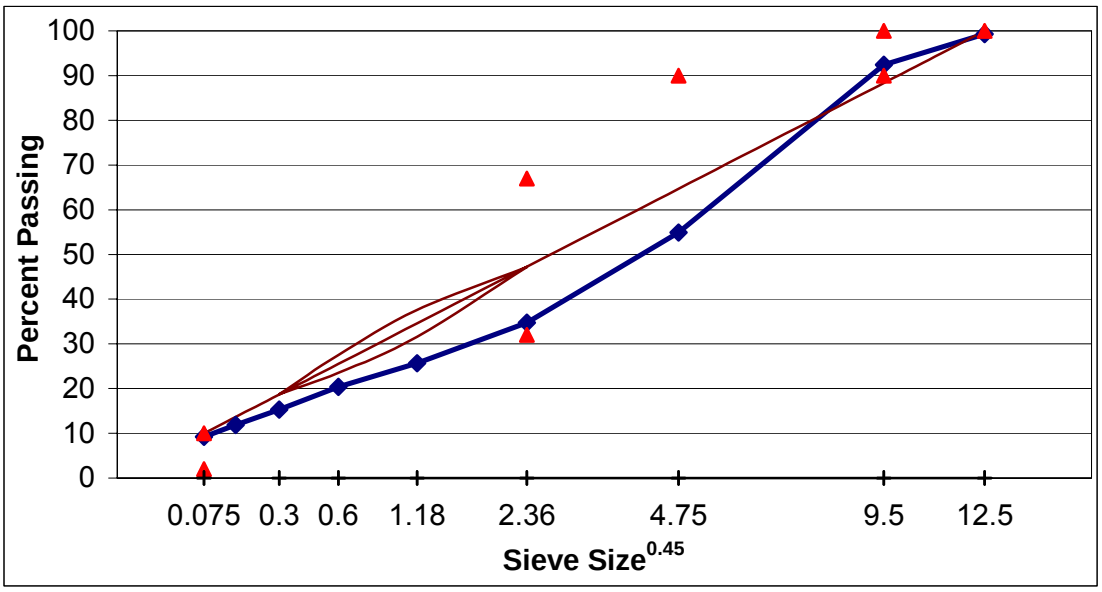

Figure A. 18 Gradation of SM-9.5A, field-lab mixture, section D.

Sieve opening (mm)	Sieve #	% Passing	Control Point LL	Control Point UL	Restricted Zone LL	Restricted Zone UL	Decision
12.5	1/2	99.3	-	100			F
9.5	3/8	92.4	90	100			P
4.75	#4	54.9	-	90			P
2.36	#8	34.8	32	67	47.2	47.2	P
1.18	#16	25.7	-	-	31.6	37.6	P
0.6	#30	20.4	-	-	23.5	27.5	P
0.3	#50	15.3	-	-	18.7	18.7	P
0.15	#100	11.8	-	-			
0.075	#200	9.2	2	10			P

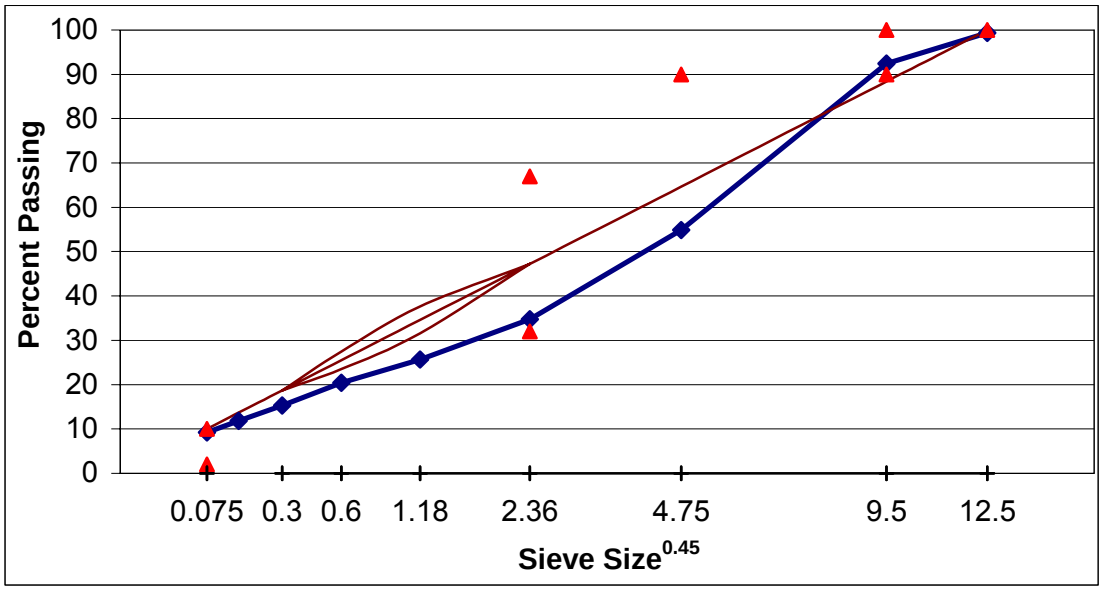

Figure A.19 Gradation of SM-9.5A, lab-lab mixture, section D.

Sieve opening (mm)	Sieve #	% Passing	Control Point LL	Control Point UL	Restricted Zone LL	Restricted Zone UL	Decision
12.5	1/2	100.0	-	100			P
9.5	3/8	89.3	90	100			F
4.75	#4	50.8	-	90			P
2.36	#8	37.0	32	67	47.2	47.2	P
1.18	#16	27.7	-	-	31.6	37.6	P
0.6	#30	20.4	-	-	23.5	27.5	P
0.3	#50	12.3	-	-	18.7	18.7	P
0.15	#100	8.0	-	-			
0.075	#200	5.7	2	10			P

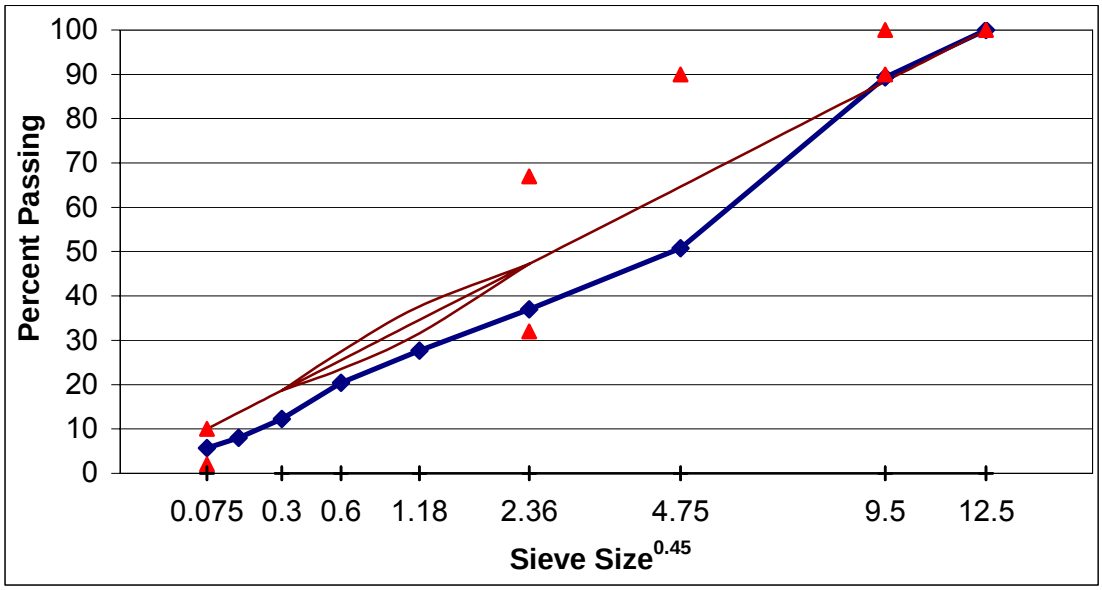

Figure A. 20 Gradation of SM-9.5A, design-lab mixture, section D.

Sieve opening (mm)	Sieve #	% Passing	Control Point LL	Control Point UL	Restricted Zone LL	Restricted Zone UL	Decision
12.5	1/2	99.2	-	100			F
9.5	3/8	92.3	90	100			P
4.75	#4	58.3	-	90			P
2.36	#8	41.7	32	67	47.2	47.2	P
1.18	#16	28.7	-	-	31.6	37.6	P
0.6	#30	20.3	-	-	23.5	27.5	P
0.3	#50	12.4	-	-	18.7	18.7	P
0.15	#100	8.6	-	-			
0.075	#200	6.3	2	10			P

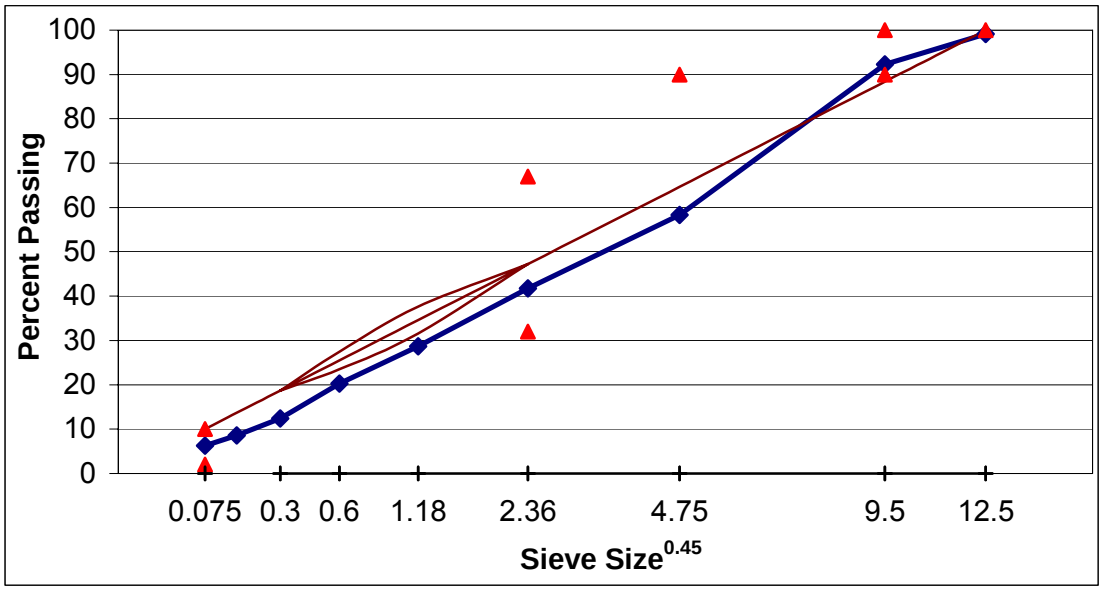

Figure A. 21 Mixture designs for SM9.5D, setions E, F, G, and H.

Design / Lab		
Aggregate		**%**
#8 Quartzite	Salem Stone Co., Sylvatus, VA	60
#10 Limestone	ACCO Stone Co., Blacksburg, VA	20
Concrete Sand	Wythe Stone Co., Wytheville, VA	10
Fine RAP	Adams Construction Co., Blacksburg, VA	10
Binder		**%**
PG 70-22	Associated Asphalt, Inc., Roanoke, VA	5.4

Lab / Lab		
Aggregate		**%**
#8 Quartzite	Salem Stone Co., Sylvatus, VA	48
#10 Quartzite	Salem Stone Co., Sylvatus, VA	12
#10 Limestone	ACCO Stone Co., Blacksburg, VA	20
Concrete Sand	Wythe Stone Co., Wytheville, VA	10
Fine RAP	Adams Construction Co., Blacksburg, VA	10
Binder		**%**
PG 70-22	Associated Asphalt, Inc., Roanoke, VA	5.8

Figure A. 22 Gradation of SM-9.5D, field-field mixture, section E.

Sieve opening (mm)	Sieve #	% Passing	Control Point LL	Control Point UL	Restricted Zone LL	Restricted Zone UL	Decision
12.5	1/2	97.6	-	100			F
9.5	3/8	92.9	90	100			P
4.75	#4	63.3	-	90			P
2.36	#8	42.6	32	67	47.2	47.2	P
1.18	#16	31.5	-	-	31.6	37.6	P
0.6	#30	20.5	-	-	23.5	27.5	P
0.3	#50	13.3	-	-	18.7	18.7	P
0.15	#100	10.4	-	-			
0.075	#200	7.6	2	10			P

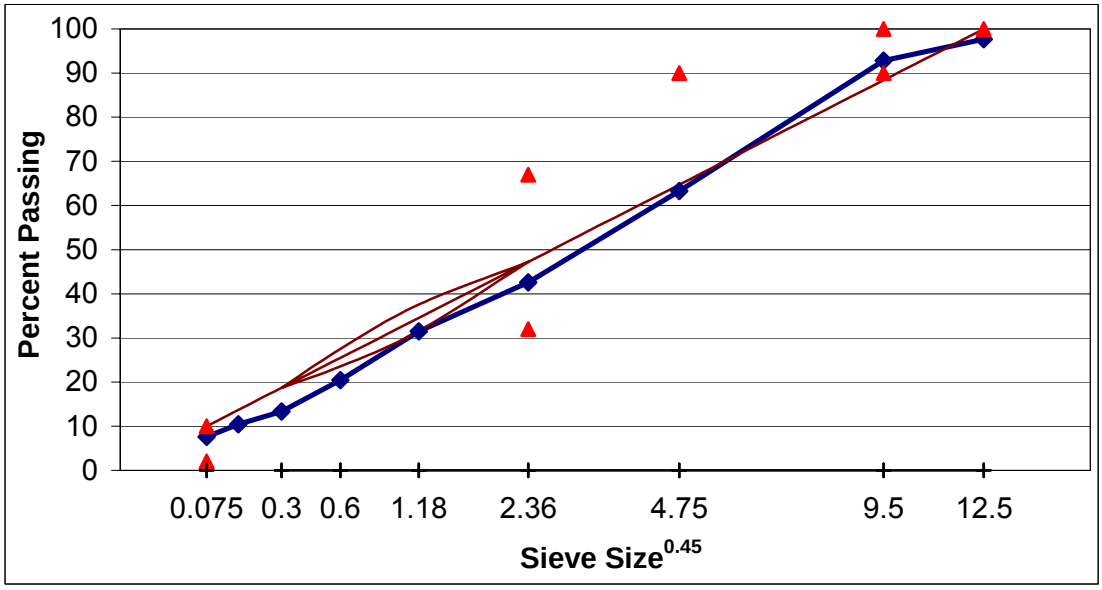

Figure A. 23 Gradation of SM-9.5D, field-lab mixture, section E.

Sieve opening (mm)	Sieve #	% Passing	Control Point LL	Control Point UL	Restricted Zone LL	Restricted Zone UL	Decision
12.5	1/2	97.6	-	100			F
9.5	3/8	92.9	90	100			P
4.75	#4	63.3	-	90			P
2.36	#8	42.6	32	67	47.2	47.2	P
1.18	#16	31.5	-	-	31.6	37.6	P
0.6	#30	20.5	-	-	23.5	27.5	P
0.3	#50	13.3	-	-	18.7	18.7	P
0.15	#100	10.4	-	-			
0.075	#200	7.6	2	10			P

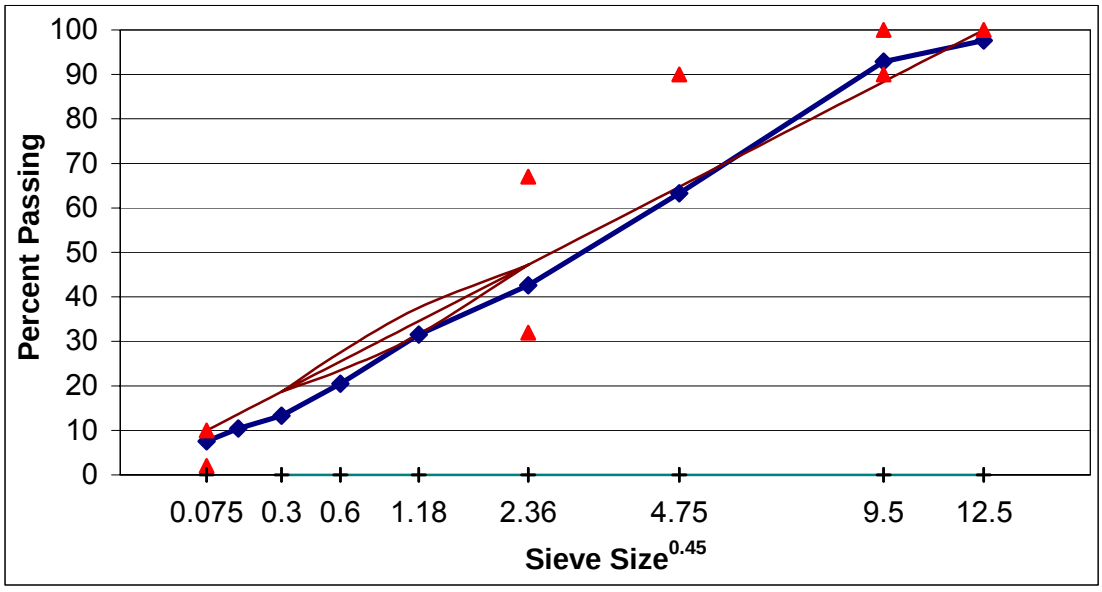

Figure A. 24 Gradation of SM-9.5D, lab-lab mixture, section E.

Sieve opening (mm)	Sieve #	% Passing	Control Point LL	Control Point UL	Restricted Zone LL	Restricted Zone UL	Decision
12.5	1/2	99.3	-	100			F
9.5	3/8	93.0	90	100			P
4.75	#4	61.4	-	90			P
2.36	#8	42.4	32	67	47.2	47.2	P
1.18	#16	31.0	-	-	31.6	37.6	P
0.6	#30	23.0	-	-	23.5	27.5	P
0.3	#50	15.2	-	-	18.7	18.7	P
0.15	#100	11.1	-	-			
0.075	#200	8.5	2	10			P

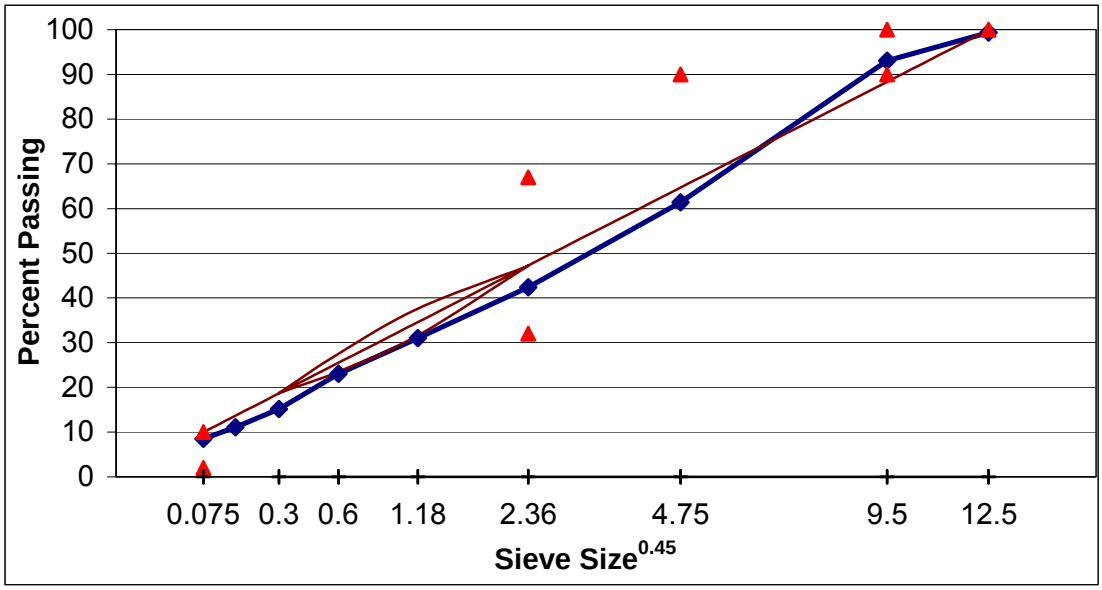

Figure A. 25 Gradation of SM-9.5D, field-field mixture, section F.

Sieve opening (mm)	Sieve #	% Passing	Control Point LL	Control Point UL	Restricted Zone LL	Restricted Zone UL	Decision
12.5	1/2	97.6	-	100			F
9.5	3/8	92.9	90	100			P
4.75	#4	63.3	-	90			P
2.36	#8	42.6	32	67	47.2	47.2	P
1.18	#16	31.5	-	-	31.6	37.6	P
0.6	#30	20.5	-	-	23.5	27.5	P
0.3	#50	13.3	-	-	18.7	18.7	P
0.15	#100	10.4	-	-			
0.075	#200	7.6	2	10			P

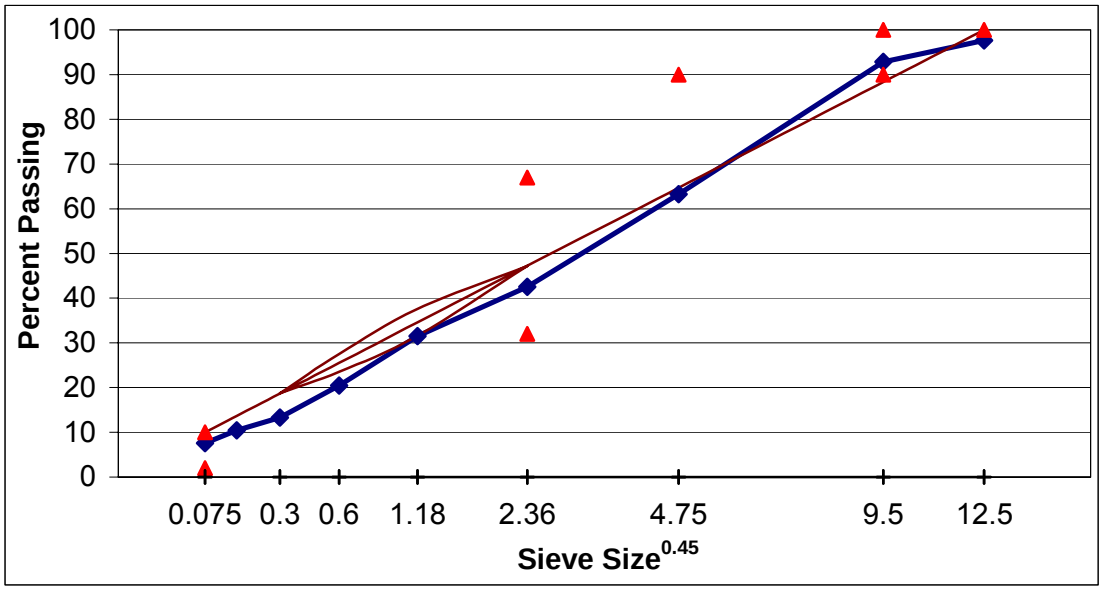

Figure A. 26 Gradation of SM-9.5D, field-lab mixture, section F.

Sieve opening (mm)	Sieve #	% Passing	Control Point LL	Control Point UL	Restricted Zone LL	Restricted Zone UL	Decision
12.5	1/2	99.4	-	100			F
9.5	3/8	93.4	90	100			P
4.75	#4	56.7	-	90			P
2.36	#8	38.6	32	67	47.2	47.2	P
1.18	#16	25.7	-	-	31.6	37.6	P
0.6	#30	18.4	-	-	23.5	27.5	P
0.3	#50	12.1	-	-	18.7	18.7	P
0.15	#100	8.7	-	-			
0.075	#200	6.9	2	10			P

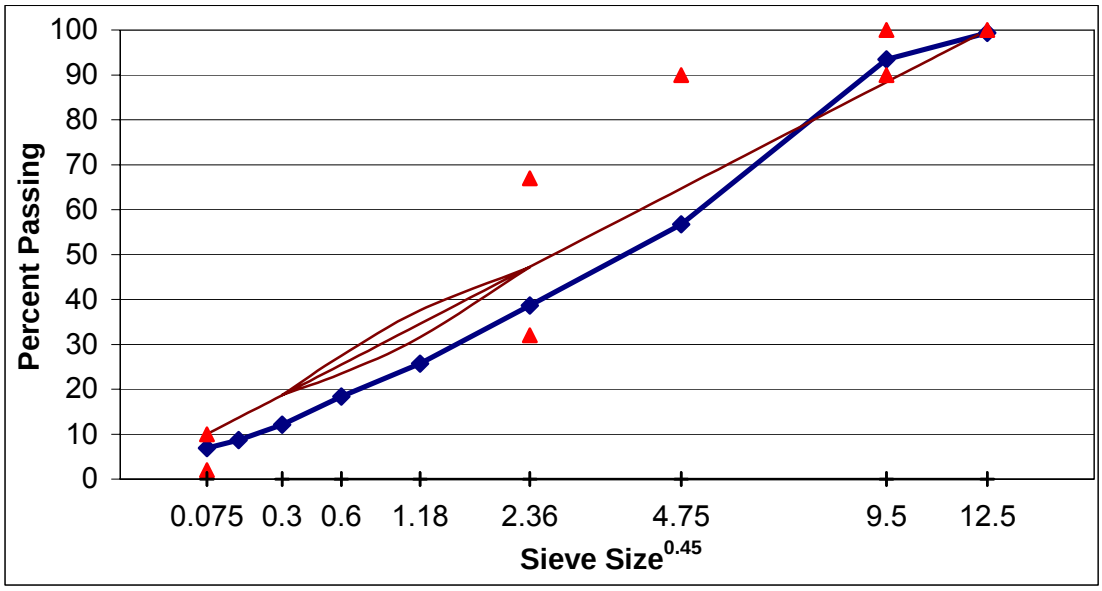

Figure A. 27 Gradation of SM-9.5D, field-field mixture, section G.

Sieve opening (mm)	Sieve #	% Passing	Control Point LL	Control Point UL	Restricted Zone LL	Restricted Zone UL	Decision
12.5	1/2	97.6	-	100			F
9.5	3/8	92.9	90	100			P
4.75	#4	63.3	-	90			P
2.36	#8	42.6	32	67	47.2	47.2	P
1.18	#16	31.5	-	-	31.6	37.6	P
0.6	#30	20.5	-	-	23.5	27.5	P
0.3	#50	13.3	-	-	18.7	18.7	P
0.15	#100	10.4	-	-			
0.075	#200	7.6	2	10			P

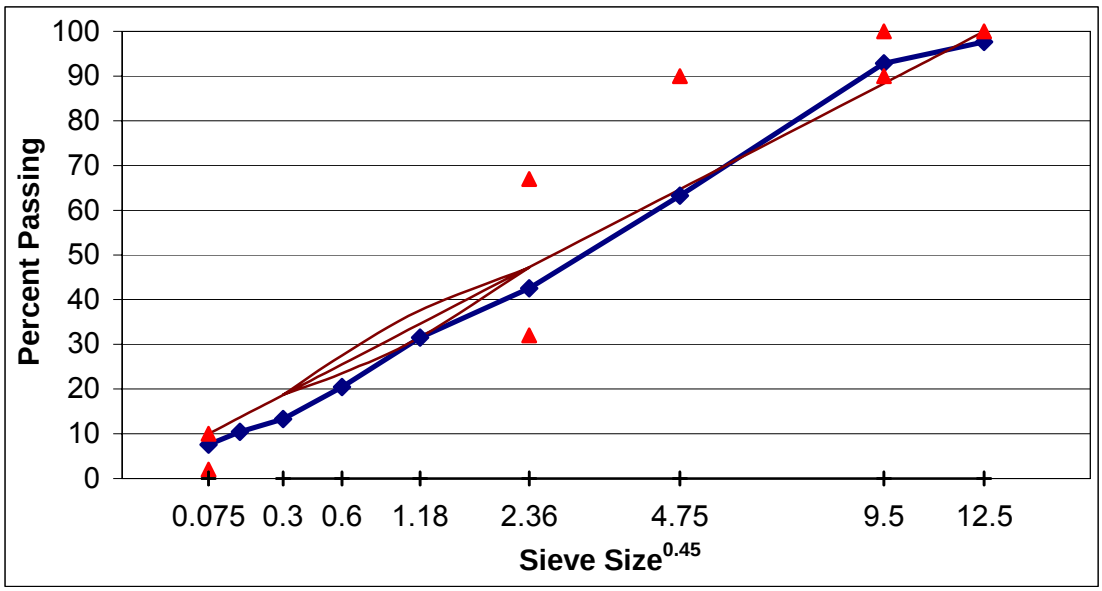

Figure A. 28 Gradation of SM-9.5D, field-lab mixture, section G.

Sieve opening (mm)	Sieve #	% Passing	Control Point LL	Control Point UL	Restricted Zone LL	Restricted Zone UL	Decision
12.5	1/2	98.4	-	100			F
9.5	3/8	95.1	90	100			P
4.75	#4	62.3	-	90			P
2.36	#8	42.2	32	67	47.2	47.2	P
1.18	#16	28.9	-	-	31.6	37.6	P
0.6	#30	20.9	-	-	23.5	27.5	P
0.3	#50	13.8	-	-	18.7	18.7	P
0.15	#100	10.3	-	-			
0.075	#200	8.3	2	10			P

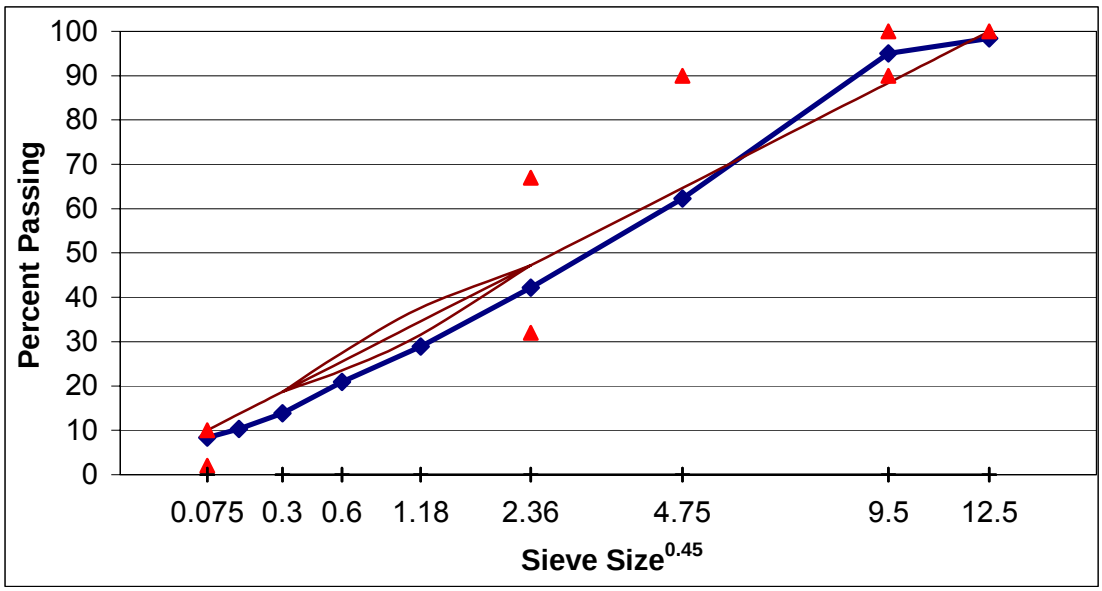

Figure A. 29 Gradation of SM-9.5D, field-field mixture, section H.

Sieve opening (mm)	Sieve #	% Passing	Control Point LL	Control Point UL	Restricted Zone LL	Restricted Zone UL	Decision
12.5	1/2	98.3	-	100			F
9.5	3/8	94.3	90	100			P
4.75	#4	63.8	-	90			P
2.36	#8	43.1	32	67	47.2	47.2	P
1.18	#16	29.3	-	-	31.6	37.6	P
0.6	#30	20.9	-	-	23.5	27.5	P
0.3	#50	13.5	-	-	18.7	18.7	P
0.15	#100	9.6	-	-			
0.075	#200	7.6	2	10			P

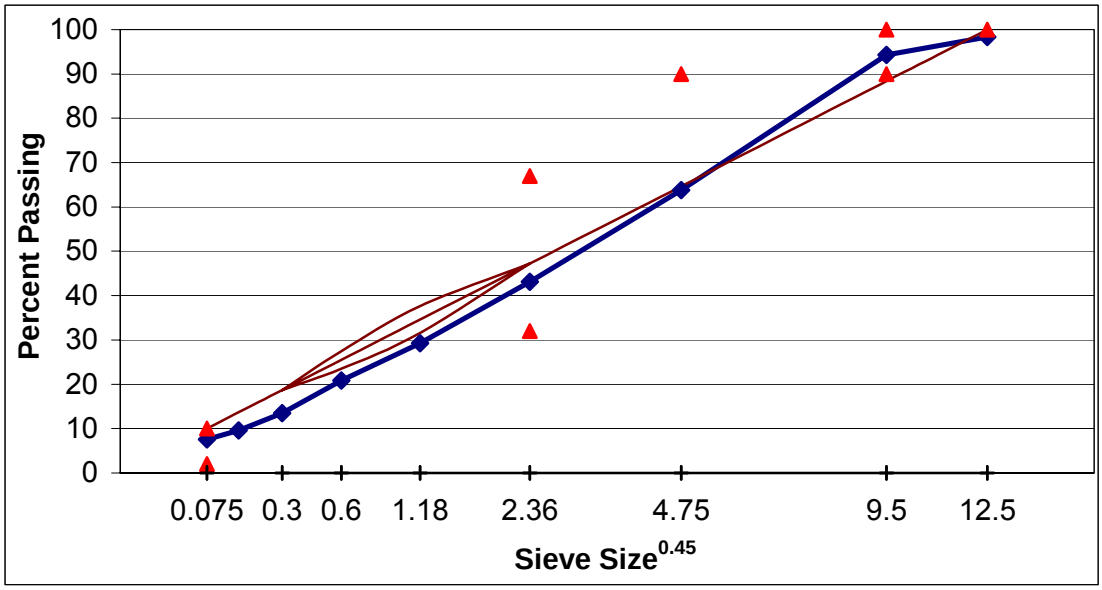

Figure A. 30 Gradation of SM-9.5D, field-lab mixture, section H.

Sieve opening (mm)	Sieve #	% Passing	Control Point LL	Control Point UL	Restricted Zone LL	Restricted Zone UL	Decision
12.5	1/2	98.3	-	100			F
9.5	3/8	94.3	90	100			P
4.75	#4	63.8	-	90			P
2.36	#8	43.1	32	67	47.2	47.2	P
1.18	#16	29.3	-	-	31.6	37.6	P
0.6	#30	20.9	-	-	23.5	27.5	P
0.3	#50	13.5	-	-	18.7	18.7	P
0.15	#100	9.6	-	-			
0.075	#200	7.6	2	10			P

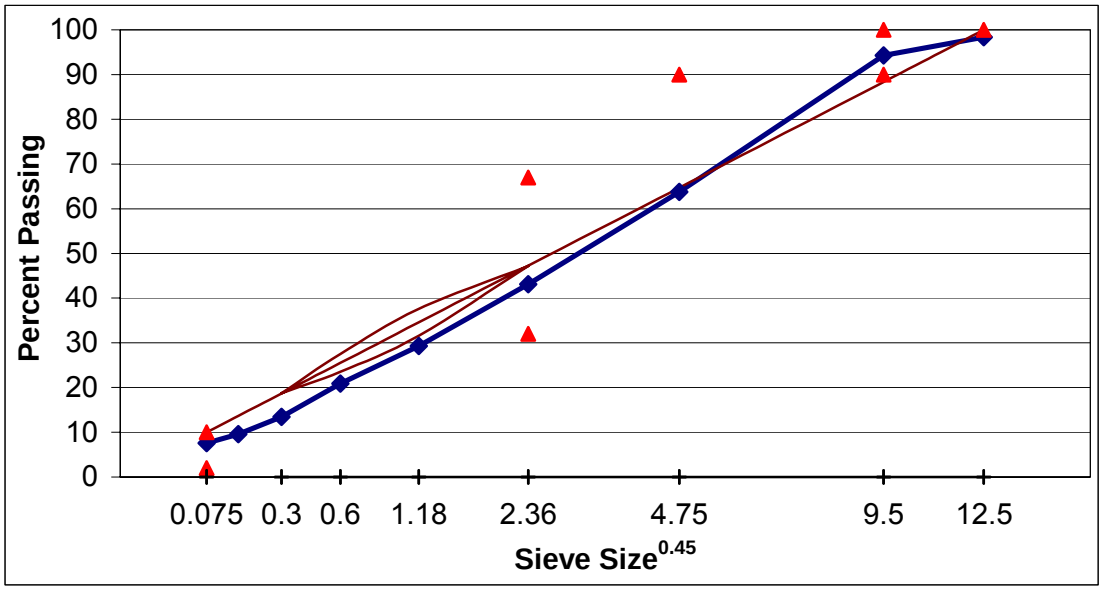

Figure A. 31 Mixture design for SM-9.5A, section I.

Design / Lab		
Aggregate		**%**
#8 Quartzite	Salem Stone Co., Sylvatus, VA	50
#10 Quartzite	Salem Stone Co., Sylvatus, VA	30
Concrete Sand	Wythe Stone Co., Wytheville, VA	10
Fine RAP	Adams Construction Co., Blacksburg, VA	10
Binder		**%**
PG 64-22	Associated Asphalt, Inc., Roanoke, VA	4.8

Lab / Lab		
Aggregate		**%**
#8 Quartzite	Salem Stone Co., Sylvatus, VA	50
#10 Quartzite	Salem Stone Co., Sylvatus, VA	30
Concrete Sand	Wythe Stone Co., Wytheville, VA	10
Fine RAP	Adams Construction Co., Blacksburg, VA	10
Binder		**%**
PG 64-22	Associated Asphalt, Inc., Roanoke, VA	5.04

Figure A. 32 Gradation of SM-9.5A, field-field mixture, section I.

Sieve opening (mm)	Sieve #	% Passing	Control Point LL	Control Point UL	Restricted Zone LL	Restricted Zone UL	Decision
12.5	1/2	100.0	-	100			P
9.5	3/8	95.0	90	100			P
4.75	#4	51.8	-	90			P
2.36	#8	35.0	32	67	47.2	47.2	P
1.18	#16	27.8	-	-	31.6	37.6	P
0.6	#30	20.6	-	-	23.5	27.5	P
0.3	#50	13.9	-	-	18.7	18.7	P
0.15	#100	10.6	-	-			
0.075	#200	7.3	2	10			P

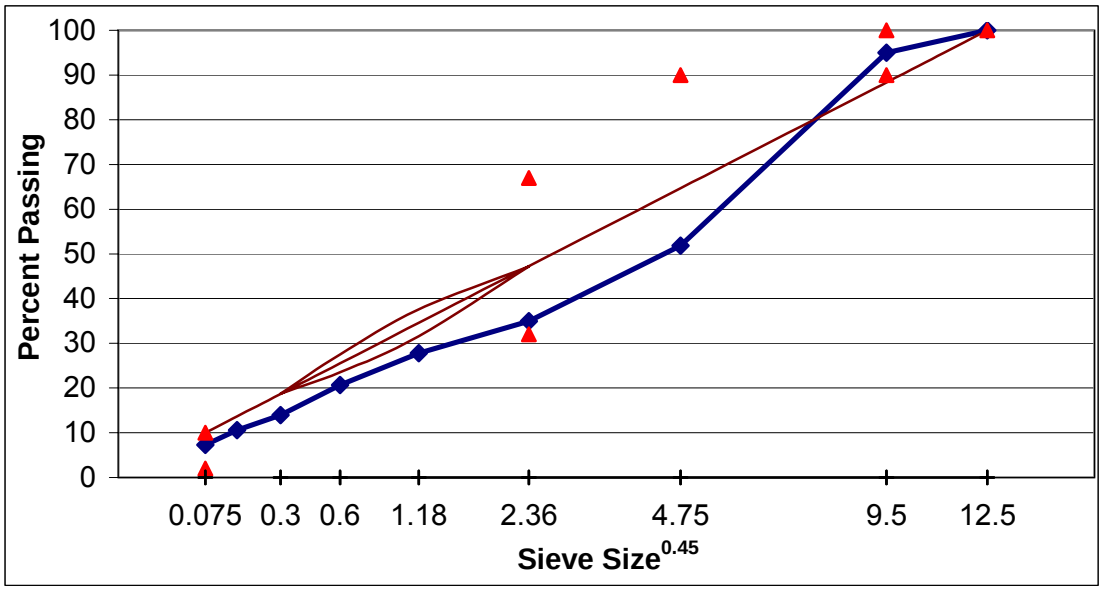

Figure A. 33 Gradation of SM-9.5A, field-lab mixture, section I.

Sieve opening (mm)	Sieve #	% Passing	Control Point LL	Control Point UL	Restricted Zone LL	Restricted Zone UL	Decision
12.5	1/2	100.0	-	100			P
9.5	3/8	95.0	90	100			P
4.75	#4	51.8	-	90			P
2.36	#8	35.0	32	67	47.2	47.2	P
1.18	#16	27.8	-	-	31.6	37.6	P
0.6	#30	20.6	-	-	23.5	27.5	P
0.3	#50	13.9	-	-	18.7	18.7	P
0.15	#100	10.6	-	-			
0.075	#200	7.3	2	10			P

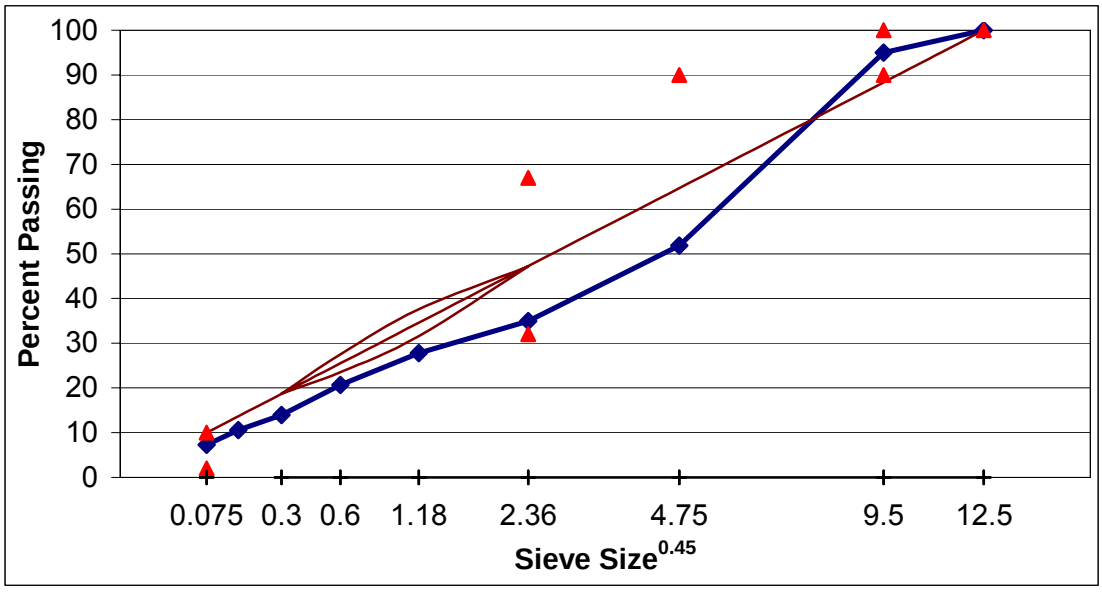

Figure A. 34 Gradation of SM-9.5A, lab-lab mixture, section I.

Sieve opening (mm)	Sieve #	% Passing	Control Point LL	Control Point UL	Restricted Zone LL	Restricted Zone UL	Decision
12.5	1/2	99.4	-	100			F
9.5	3/8	92.7	90	100			P
4.75	#4	54.2	-	90			P
2.36	#8	37.6	32	67	47.2	47.2	P
1.18	#16	28.4	-	-	31.6	37.6	P
0.6	#30	21.2	-	-	23.5	27.5	P
0.3	#50	13.6	-	-	18.7	18.7	P
0.15	#100	9.6	-	-			
0.075	#200	7.0	2	10			P

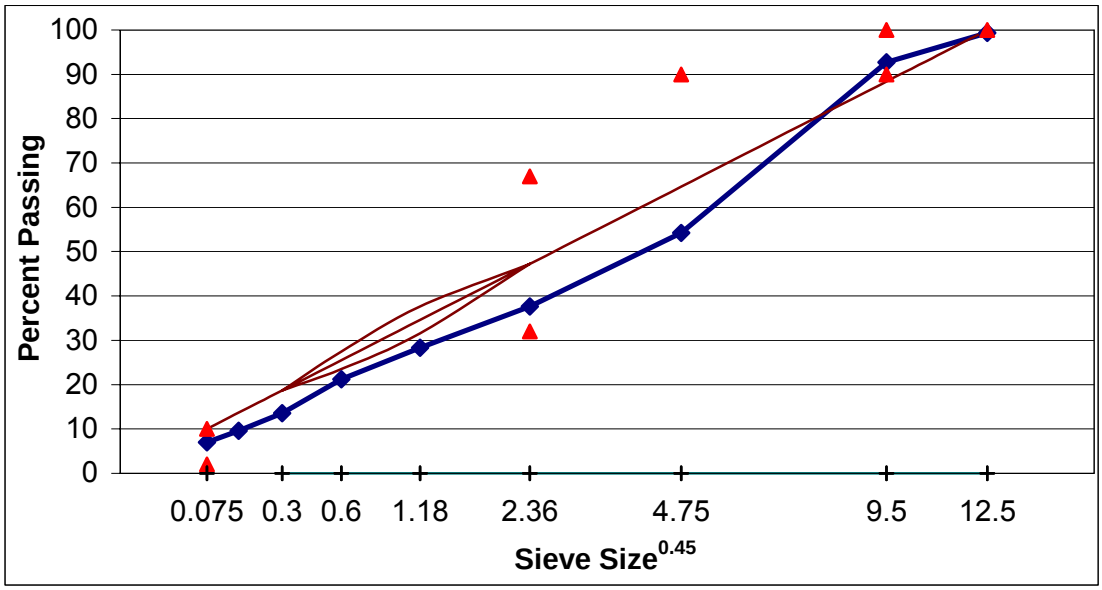

Figure A. 35 Gradation of SM-9.5A, design-lab mixture, section I.

Sieve opening (mm)	Sieve #	% Passing	Control Point LL	Control Point UL	Restricted Zone LL	Restricted Zone UL	Decision
12.5	1/2	98.9	-	100			F
9.5	3/8	88.6	90	100			F
4.75	#4	56.7	-	90			P
2.36	#8	43.5	32	67	47.2	47.2	P
1.18	#16	31.0	-	-	31.6	37.6	P
0.6	#30	22.1	-	-	23.5	27.5	P
0.3	#50	13.9	-	-	18.7	18.7	P
0.15	#100	10.1	-	-			
0.075	#200	7.6	2	10			P

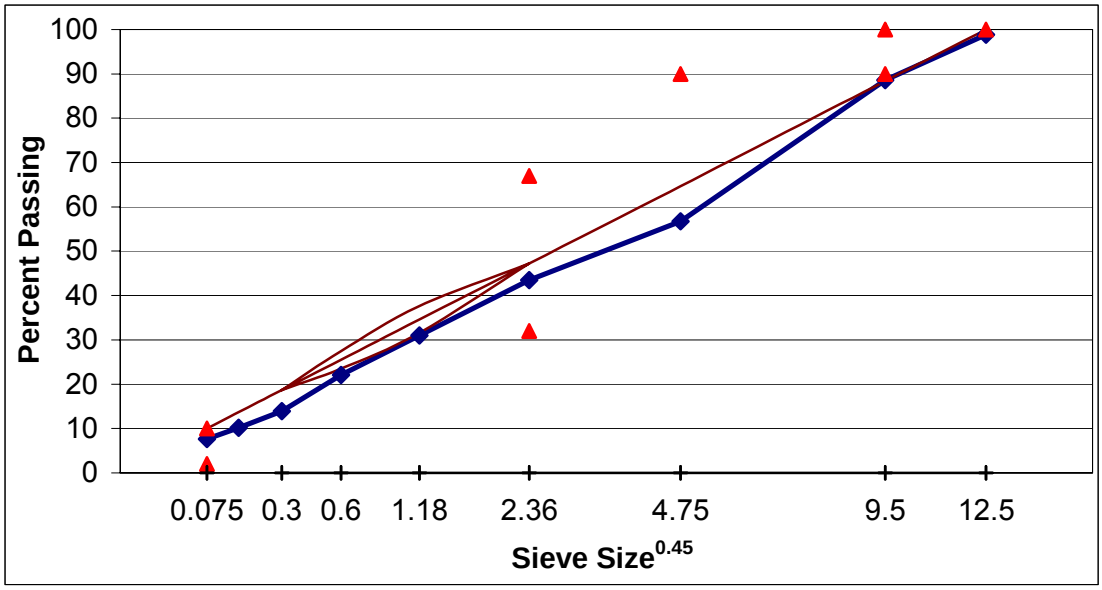

Figure A. 36 Mixture design for SM-9.5D, section J.

Lab / Lab		
Aggregate		**%**
#8 Quartzite	Salem Stone Co., Sylvatus, VA	48
#10 Quartzite	Salem Stone Co., Sylvatus, VA	12
#10 Limestone	ACCO Stone Co., Blacksburg, VA	20
Concrete Sand	Wythe Stone Co., Wytheville, VA	10
Fine RAP	Adams Construction Co., Blacksburg, VA	10
Binder		**%**
PG 70-22	Associated Asphalt, Inc., Roanoke, VA	4.9

Figure A. 37 Gradation of SM-9.5D, field-field mixture, section J.

Sieve opening (mm)	Sieve #	% Passing	Control Point LL	Control Point UL	Restricted Zone LL	Restricted Zone UL	Decision
12.5	1/2	99.2	-	100			F
9.5	3/8	91.6	90	100			P
4.75	#4	50.5	-	-			
2.36	#8	34.6	32	67	47.2	47.2	P
1.18	#16	26.2	-	-	31.6	37.6	P
0.6	#30	17.9	-	-	23.5	27.5	P
0.3	#50	11.8	-	-	18.7	18.7	P
0.15	#100	9.1	-	-			
0.075	#200	6.3	2	10			P

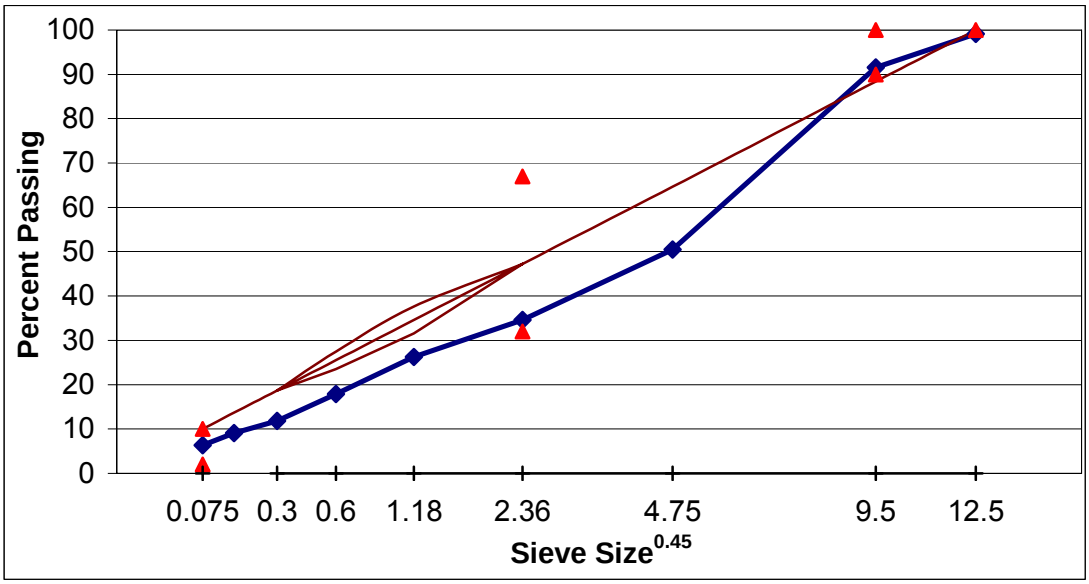

Figure A. 38 Gradation of SM-9.5D, field-lab mixture, section J.

Sieve opening (mm)	Sieve #	% Passing	Control Point LL	Control Point UL	Restricted Zone LL	Restricted Zone UL	Decision
12.5	1/2	99.2	-	100			F
9.5	3/8	91.6	90	100			P
4.75	#4	50.5	-	-			
2.36	#8	34.6	32	67	47.2	47.2	P
1.18	#16	26.2	-	-	31.6	37.6	P
0.6	#30	17.9	-	-	23.5	27.5	P
0.3	#50	11.8	-	-	18.7	18.7	P
0.15	#100	9.1	-	-			
0.075	#200	6.3	2	10			P

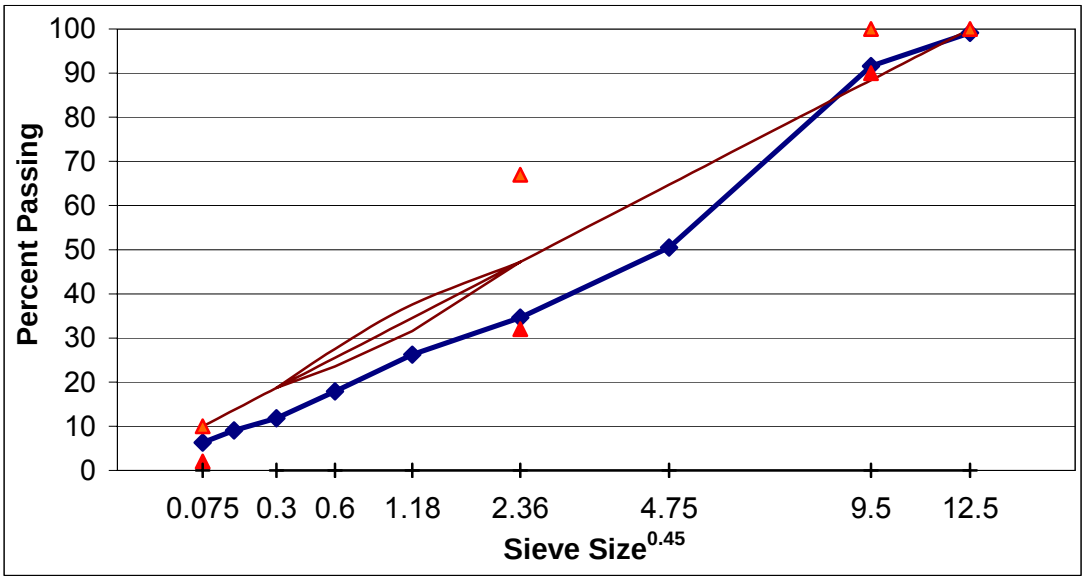

Figure A. 39 Gradation of SM-9.5D, lab-lab mixture, section J.

Sieve opening (mm)	Sieve #	% Passing	Control Point LL	Control Point UL	Restricted Zone LL	Restricted Zone UL	Decision
12.5	1/2	100.0	-	100			P
9.5	3/8	93.9	90	100			P
4.75	#4	52.9	-	-			
2.36	#8	31.6	32	67	47.2	47.2	F
1.18	#16	22.8	-	-	31.6	37.6	P
0.6	#30	17.4	-	-	23.5	27.5	P
0.3	#50	11.2	-	-	18.7	18.7	P
0.15	#100	8.4	-	-			
0.075	#200	6.7	2	10			P

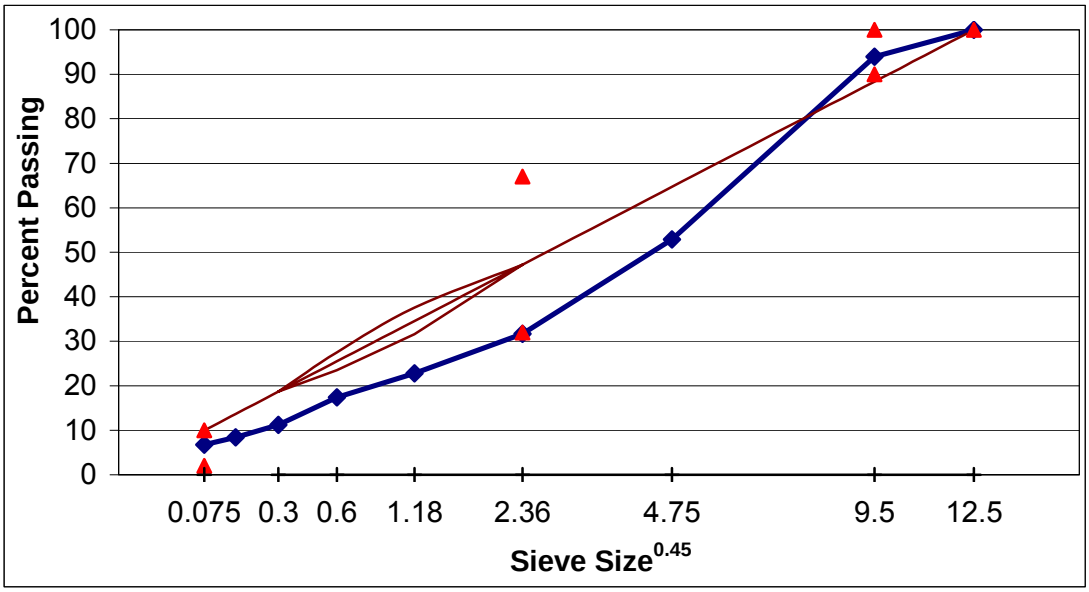

Figure A. 40 Mixture designs for SM-12.5A, section L.

Design / Lab		
Aggregate		**%**
#68 Quartzite	Salem Stone Co., Sylvatus, VA	26
#8 Quartzite	Salem Stone Co., Sylvatus, VA	55
#10 Quartzite	Salem Stone Co., Sylvatus, VA	10
Lime Filler	James River Lime, Buchanan, VA	9
Binder		**%**
PG 76-22	Koch Materials Co., Pennsauken, NJ	7.2
Fiber		**%**
Cellulose	Hi-Tech Asphalt Solutions, Mechanicsville, VA	0.3

Lab / Lab		
Aggregate		**%**
#68 Quartzite	Salem Stone Co., Sylvatus, VA	8
#8 Quartzite	Salem Stone Co., Sylvatus, VA	71
#10 Quartzite	Salem Stone Co., Sylvatus, VA	12
Lime Filler	James River Lime, Buchanan, VA	9
Binder		**%**
PG 76-22	Koch Materials Co., Pennsauken, NJ	6.8
Fiber		**%**
Cellulose	Hi-Tech Asphalt Solutions, Mechanicsville, VA	0.3

Note: Aggregate and binder percentages are by weight of mixture. Fiber percentages are by weight of binder.

Figure A. 41 Gradation of SM-12.5A, field-field mixture, section L.

Sieve opening (mm)	Sieve #	% Passing	Control Point LL	Control Point UL	Restricted Zone LL	Restricted Zone UL	Decision
19	3/4	100.0		100			P
12.5	1/2	99.4	90	100			P
9.5	3/8	87.7	-	90			P
4.75	#4	36.8	-	-			
2.36	#8	25.0	28	58	39.1	39.1	F
1.18	#16	21.4	-	-	25.6	31.6	P
0.6	#30	18.9	-	-	19.1	23.1	P
0.3	#50	16.1	-	-	15.5	15.5	P
0.15	#100	13.9	-	-			
0.075	#200	11.2	2	10			F

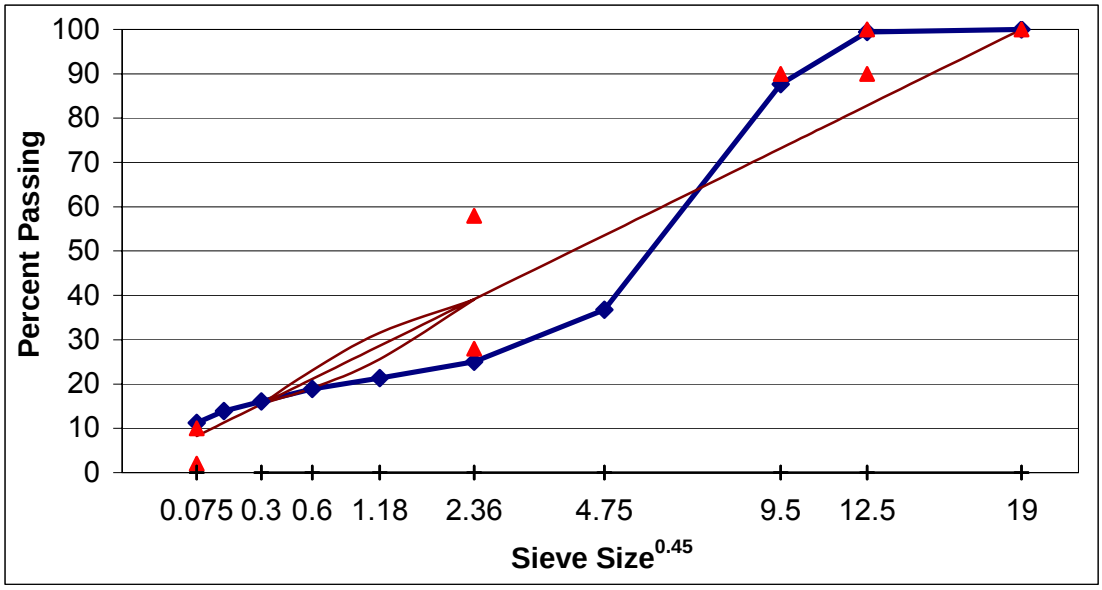

Figure A. 42 Gradation of SM-12.5A, field-lab mixture, section L.

Sieve opening (mm)	Sieve #	% Passing	Control Point LL	Control Point UL	Restricted Zone LL	Restricted Zone UL	Decision
19	3/4	100.0		100			P
12.5	1/2	99.4	90	100			P
9.5	3/8	87.7	-	90			P
4.75	#4	36.8	-	-			
2.36	#8	25.0	28	58	39.1	39.1	F
1.18	#16	21.4	-	-	25.6	31.6	P
0.6	#30	18.9	-	-	19.1	23.1	P
0.3	#50	16.1	-	-	15.5	15.5	P
0.15	#100	13.9	-	-			
0.075	#200	11.2	2	10			F

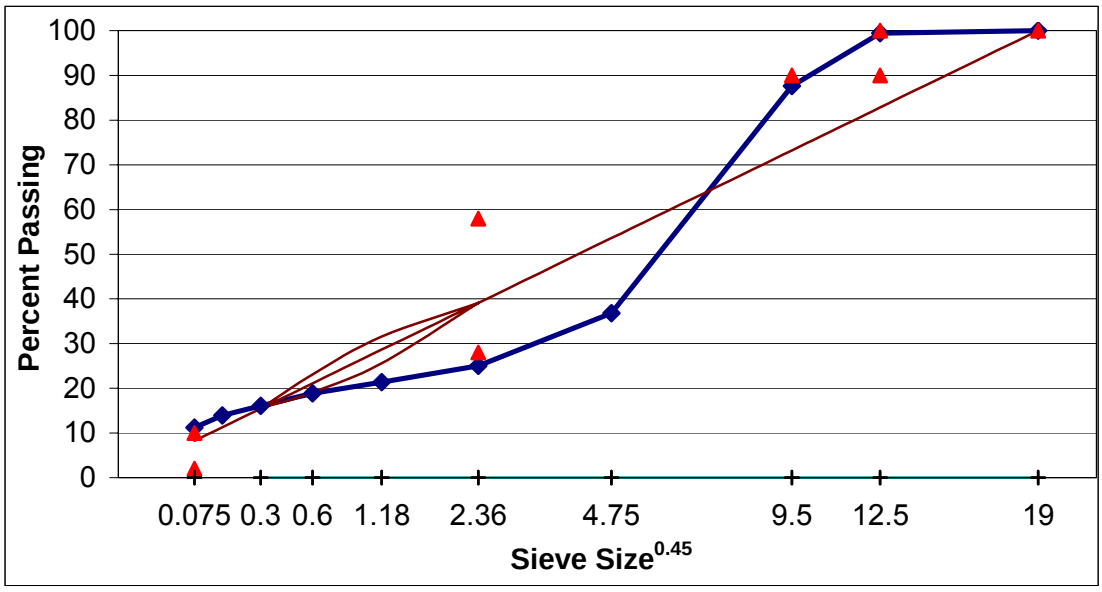

Figure A. 43 Gradation of SM-12.5A, lab-lab mixture, section L.

Sieve opening (mm)	Sieve #	% Passing	Control Point LL	Control Point UL	Restricted Zone LL	Restricted Zone UL	Decision
19	3/4	100.0		100			P
12.5	1/2	92.8	90	100			P
9.5	3/8	76.3	-	90			P
4.75	#4	28.1	-	-			
2.36	#8	21.8	28	58	39.1	39.1	F
1.18	#16	17.9	-	-	25.6	31.6	P
0.6	#30	15.3	-	-	19.1	23.1	P
0.3	#50	14.0	-	-	15.5	15.5	P
0.15	#100	13.1	-	-			
0.075	#200	11.7	2	10			F

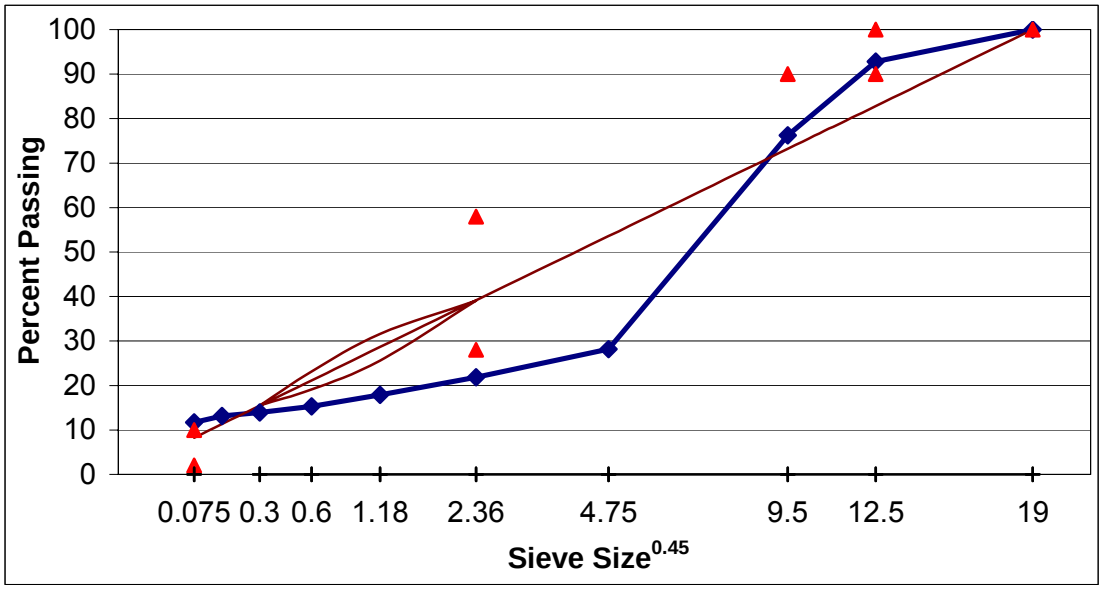

Figure A. 44 Gradation of SM-12.5A, design-lab mixture, section L.

Sieve opening (mm)	Sieve #	% Passing	Control Point LL	Control Point UL	Restricted Zone LL	Restricted Zone UL	Decision
19	3/4	100.0		100			P
12.5	1/2	92.6	90	100			P
9.5	3/8	72.1	-	90			P
4.75	#4	27.8	-	-			
2.36	#8	19.5	28	58	39.1	39.1	F
1.18	#16	16.7	-	-	25.6	31.6	P
0.6	#30	14.8	-	-	19.1	23.1	P
0.3	#50	13.7	-	-	15.5	15.5	P
0.15	#100	12.9	-	-			
0.075	#200	11.7	2	10			F

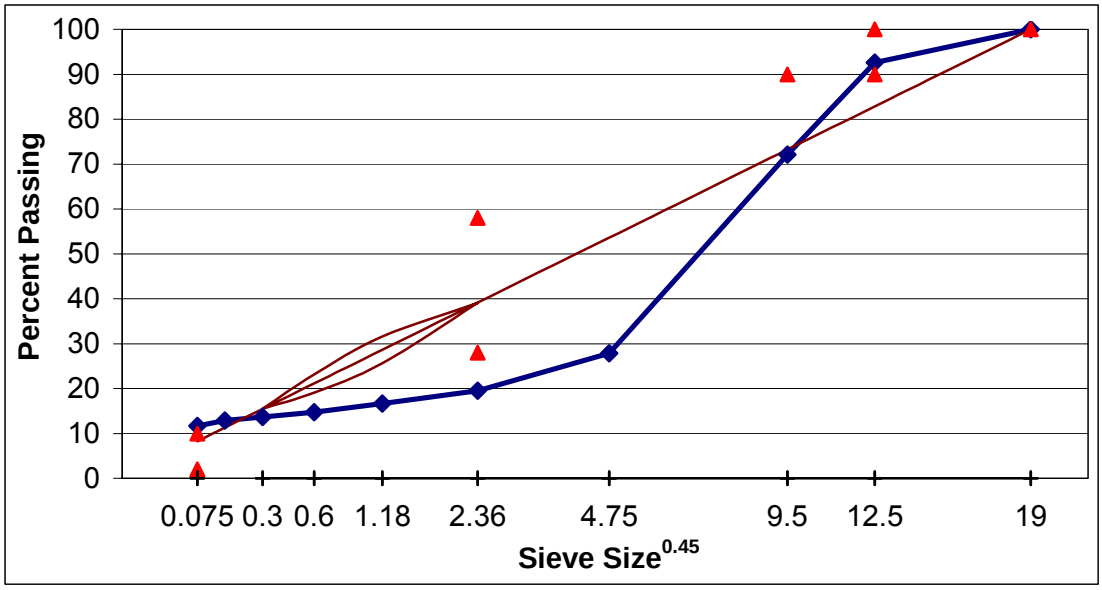

Appendix B

Mixture Specifications and Volumetric Properties

Table B. 1 Volumetric properties for SM-12.5D mixtures, section A.

Property	Field / Field	Field / Lab	Lab / Lab	Design / Lab
% Asphalt	5.86	5.86	5.93	5.55
G_{mm}	2.422	2.422	2.510	2.497
G_{mb}	2.282	2.345	2.380	2.376
G_b	1.03	1.03	1.03	1.03
G_{se}	2.644	2.644	2.760	2.725
G_{sb}	2.618	2.618	2.734	2.699
CF	0.026	0.026	0.026	0.026
Bulk Density	142.4	146.3	148.5	148.3
Density at N_{ini}	-	134.2	134.0	133.1
% passing #200	5.64	5.64	12.28	5.96

Table B. 2 VDOT specifications for SM-12.5D mixtures, section A.

Property	Specification Min.	Specification Max.	Field / Field		Field / Lab		Lab / Lab		Design / Lab	
VTM (%)	2.5	5.5	5.8	Fail	3.2	Pass	5.2	Pass	4.8	Pass
VMA (%)	12	-	18.0	Pass	15.7	Pass	18.1	Pass	16.8	Pass
VFA (%)	62	80	67.8	Pass	79.8	Pass	71.4	Pass	71.4	Pass
% Density at N_{ini}	-	89	-	-	88.8	Pass	85.6	Pass	85.5	Pass
F/A ratio	0.6	1.3	1.0	Pass	1.0	Pass	2.2	Fail	1.1	Pass

Table B. 3 Volumetric properties for SM-9.5D mixtures, section B.

Property	Field / Field	Field / Lab	Lab / Lab	Design / Lab
% Asphalt	4.71	4.71	5.36	5.33
G_{mm}	2.450	2.450	2.513	2.494
G_{mb}	2.239	2.362	2.468	2.370
G_b	1.03	1.03	1.03	1.03
G_{se}	2.629	2.629	2.736	2.711
G_{sb}	2.574	2.574	2.681	2.656
CF	0.055	0.055	0.055	0.055
Bulk Density	139.7	147.4	154.0	147.9
Density at N_{ini}	-	135.1	141.7	133.1
% passing #200	7.81	7.81	8.72	5.52

Table B. 4 VDOT specifications for SM-9.5D mixtures, section B.

Property	Specification		Field / Field		Field / Lab		Lab / Lab		Design / Lab	
	Min.	Max.								
VTM (%)	2.5	5.5	8.6	Fail	3.6	Pass	1.8	Fail	5.0	Pass
VMA (%)	12	-	17.1	Pass	12.5	Pass	12.9	Pass	15.5	Pass
VFA (%)	62	80	49.7	Fail	71.6	Pass	86.0	Fail	68.0	Pass
% Density at N_{ini}	-	89	-	-	88.4	Pass	90.4	Fail	85.6	Pass
F/A ratio	0.6	1.3	2.0	Fail	2.0	Fail	1.9	Fail	1.2	Pass

Table B. 5 Volumetric properties for SM-9.5E mixtures, section C.

Property	Field / Field	Field / Lab	Lab / Lab	Design / Lab
% Asphalt	5.80	5.80	6.02	6.16
G_{mm}	2.455	2.455	2.477	2.463
G_{mb}	2.309	2.399	2.426	2.431
G_b	1.03	1.03	1.03	1.03
G_{se}	2.684	2.684	2.721	2.711
G_{sb}	2.654	2.654	2.691	2.681
CF	0.03	0.03	0.03	0.03
Bulk Density	144.1	149.7	151.4	151.7
Density at N_{ini}	-	137.5	139.0	137.4
% passing #200	8.18	8.03	7.56	6.60

Table B. 6 VDOT specifications for SM-12.5E mixtures, section C.

Property	Specification		Field / Field		Field / Lab		Lab / Lab		Design / Lab	
	Min.	Max.								
VTM (%)	2.5	5.5	6.0	Fail	2.3	Fail	2.0	Fail	1.3	Fail
VMA (%)	12	-	18.1	Pass	14.9	Pass	15.3	Pass	14.9	Pass
VFA (%)	62	80	67.0	Pass	84.6	Fail	86.6	Fail	91.4	Fail
% Density at N_{ini}	-	89	-	-	89.7	Fail	89.9	Fail	89.4	Fail
F/A ratio	0.6	1.3	1.5	Fail	1.5	Fail	1.3	Pass	1.1	Pass

Table B. 7 Volumetric properties for SM-9.5A mixtures, section D.

Property	Field / Field	Field / Lab	Lab / Lab	Design / Lab
% Asphalt	6.29	6.29	6.76	6.25
G_{mm}	2.440	2.440	2.455	2.468
G_{mb}	2.393	2.408	2.434	2.379
G_b	1.03	1.03	1.03	1.03
G_{se}	2.687	2.687	2.729	2.722
G_{sb}	2.653	2.653	2.695	2.688
CF	0.034	0.034	0.034	0.034
Bulk Density	149.4	150.3	151.9	148.4
Density at N_{ini}	-	138.9	140.4	135.8
% passing #200	9.20	9.20	5.72	6.26

Table B. 8 VDOT specifications for SM-9.5D mixtures, section D.

Property	Specification		Field / Field		Field / Lab		Lab / Lab		Design / Lab	
	Min.	Max.								
VTM (%)	2.5	5.5	1.9	Fail	1.3	Fail	0.9	Fail	3.6	Pass
VMA (%)	12	-	15.5	Pass	14.9	Pass	15.8	Pass	17.0	Pass
VFA (%)	62	80	87.6	Fail	91.2	Fail	94.4	Fail	78.7	Pass
% Density at N_{ini}	-	89	-	-	91.2	Fail	91.6	Fail	88.1	Pass
F/A ratio	0.6	1.3	1.6	Fail	1.6	Fail	0.9	Pass	1.1	Pass

Table B. 9 Volumetric properties for SM-9.5D mixtures, section E.

Property	Field / Field	Field / Lab	Lab / Lab
% Asphalt	5.85	5.85	6.00
G_{mm}	2.434	2.434	2.489
G_{mb}	2.317	2.400	2.442
G_b	1.03	1.03	1.03
G_{se}	2.659	2.659	2.737
G_{sb}	2.604	2.604	2.682
CF	0.055	0.055	0.055
Bulk Density	144.6	149.8	152.4
Density at N_{ini}	-	137.3	140.2
% passing #200	7.57	7.57	8.47

Table B. 10 VDOT specifications for SM-9.5D mixtures, section E.

Property	Specification		Field / Field		Field / Lab		Lab / Lab	
	Min.	Max.						
VTM (%)	2.5	5.5	4.8	Pass	1.4	Fail	1.9	Fail
VMA (%)	12	-	16.2	Pass	13.2	Pass	14.4	Pass
VFA (%)	62	80	70.5	Pass	89.6	Fail	86.8	Fail
% Density at N_{ini}	-	89	-	-	90.4	Fail	90.2	Fail
F/A ratio	0.6	1.3	1.5	Fail	1.5	Fail	1.6	Fail

Table B. 11 Volumetric properties for SM-9.5D mixtures, section F.

Property	Field / Field	Field / Lab
% Asphalt	5.85	5.42
G_{mm}	2.434	2.502
G_{mb}	2.317	2.412
G_b	1.03	1.03
G_{se}	2.659	2.725
G_{sb}	2.604	2.670
CF	0.055	0.055
Bulk Density	144.6	150.5
Density at N_{ini}	-	137.5
% passing #200	7.57	6.88

Table B. 12 VDOT specifications for SM-9.5D mixtures, section F.

Property	Specification		Field / Field		Field / Lab	
	Min.	Max.				
VTM (%)	2.5	5.5	4.8	Pass	3.6	Pass
VMA (%)	12	-	16.2	Pass	14.5	Pass
VFA (%)	62	80	70.5	Pass	75.4	Pass
% Density at N_{ini}	-	89	-	-	88.1	Pass
F/A ratio	0.6	1.3	1.5	Fail	1.5	Fail

Table B. 13 Volumetric properties for SM-9.5D mixtures, section G.

Property	Field / Field	Field / Lab
% Asphalt	5.85	6.29
G_{mm}	2.434	2.499
G_{mb}	2.317	2.410
G_b	1.03	1.03
G_{se}	2.659	2.763
G_{sb}	2.604	2.708
CF	0.055	0.055
Bulk Density	144.6	150.4
Density at N_{ini}	-	137.6
% passing #200	7.57	8.35

Table B. 14 VDOT specifications for SM-9.5D mixtures, section G.

Property	Specification		Field / Field		Field / Lab	
	Min.	Max.				
VTM (%)	2.5	5.5	4.8	Pass	3.6	Pass
VMA (%)	12	-	16.2	Pass	16.6	Pass
VFA (%)	62	80	70.5	Pass	78.6	Pass
% Density at N_{ini}	-	89	-	-	88.2	Pass
F/A ratio	0.6	1.3	1.5	Fail	1.5	Fail

Table B. 15 Volumetric properties for SM-9.5D mixtures, section H.

Property	Field / Field	Field / Lab
% Asphalt	5.85	5.63
G_{mm}	2.434	2.507
G_{mb}	2.317	2.403
G_b	1.03	1.03
G_{se}	2.659	2.741
G_{sb}	2.604	2.686
CF	0.055	0.055
Bulk Density	144.6	149.9
Density at N_{ini}	-	137.4
% passing #200	7.57	7.57

Table B. 16 VDOT specifications for SM-9.5D mixtures, section H.

Property	Specification		Field / Field		Field / Lab	
	Min.	Max.				
VTM (%)	2.5	5.5	4.8	Pass	4.1	Pass
VMA (%)	12	-	16.2	Pass	15.6	Pass
VFA (%)	62	80	70.5	Pass	73.4	Pass
% Density at N_{ini}	-	89	-	-	87.8	Pass
F/A ratio	0.6	1.3	1.5	Fail	1.5	Fail

Table B. 17 Volumetric properties for SM-9.5A mixtures, section I.

Property	Field / Field	Field / Lab	Lab / Lab	Design / Lab
% Asphalt	5.42	5.42	5.31	5.37
G_{mm}	2.467	2.467	2.489	2.498
G_{mb}	2.440	2.429	2.340	2.390
G_b	1.03	1.03	1.03	1.03
G_{se}	2.681	2.681	2.704	2.718
G_{sb}	2.647	2.647	2.670	2.684
CF	0.034	0.034	0.034	0.034
Bulk Density	152.3	151.6	146.0	149.1
Density at N_{ini}	-	138.1	133.4	137.0
% passing #200	7.27	7.27	6.97	7.64

Table B. 18 VDOT specifications for SM-9.5A mixtures, section I.

Property	Specification		Field / Field		Field / Lab		Lab / Lab		Design / Lab	
	Min.	Max.								
VTM (%)	2.5	5.5	1.1	Fail	1.5	Fail	6.0	Fail	4.3	Pass
VMA (%)	12	-	12.8	Pass	13.2	Pass	17.0	Pass	15.7	Pass
VFA (%)	62	80	91.6	Fail	88.5	Fail	64.8	Pass	72.5	Pass
% Density at N_{ini}	-	89	-	-	89.8	Fail	85.9	Pass	87.9	Pass
F/A ratio	0.6	1.3	1.5	Fail	1.5	Fail	1.4	Fail	1.6	Fail

Table B. 19 Volumetric properties for SM-9.5D mixtures, section J.

Property	Field / Field	Field / Lab	Lab / Lab
% Asphalt	4.90	4.90	5.06
G_{mm}	2.518	2.518	2.524
G_{mb}	2.252	2.328	2.408
G_b	1.03	1.03	1.03
G_{se}	2.721	2.721	2.736
G_{sb}	2.666	2.666	2.681
CF	0.055	0.055	0.055
Bulk Density	140.5	145.3	150.2
Density at N_{ini}	-	133.0	137.6
% passing #200	6.31	6.31	6.72

Table B. 20 VDOT specifications for SM-9.5D mixtures, section J.

Property	Specification		Field / Field		Field / Lab		Lab / Lab	
	Min.	Max.						
VTM (%)	2.5	5.5	10.6	Fail	7.5	Fail	4.6	Pass
VMA (%)	12	-	19.7	Pass	16.9	Pass	14.7	Pass
VFA (%)	62	80	46.3	Fail	55.5	Fail	68.6	Pass
% Density at N_{ini}	-	89	-	-	84.6	Pass	87.3	Pass
F/A ratio	0.6	1.3	1.5	Fail	1.5	Fail	1.6	Fail

Table B. 21 Volumetric properties for SM-12.5A mixtures, section L.

Property	Field / Field	Field / Lab	Lab / Lab	Design / Lab
% Asphalt	6.80	6.80	6.44	6.33
G_{mm}	2.402	2.402	2.402	2.415
G_{mb}	2.226	2.359	2.359	2.359
G_b	1.03	1.03	1.03	1.03
G_{se}	2.661	2.661	2.644	2.657
G_{sb}	2.631	2.631	2.614	2.627
CF	0.03	0.03	0.03	0.03
Bulk Density	138.9	147.2	147.2	147.2
Density at N_{ini}	-	134.5	134.1	132.0
% passing #200	11.25	11.25	11.71	11.67

Table B. 22 VDOT specifications for SM-12.5A mixtures, section L.

Property	Specification		Field / Field		Field / Lab		Lab / Lab		Design / Lab	
	Min.	Max.								
VTM (%)	2.5	5.5	7.3	Fail	1.8	Fail	1.8	Fail	2.3	Fail
VMA (%)	12		21.1	Pass	16.4	Pass	15.6	Pass	15.9	Pass
VFA (%)	62	80	65.3	Pass	89.0	Fail	88.5	Fail	85.3	Fail
% Density at N_{ini}	-	89	-	-	89.7	Fail	89.5	Fail	87.6	Pass
F/A ratio	0.6	1.3	1.8	Fail	1.8	Fail	1.9	Fail	2.0	Fail

Appendix C

Indirect Tensile Strength

F/L 100-mm Diameter Specimens

Sample	Thickness	Load, N	strength*E-3, kN/mm2	Average	Std Dev	Average (Mr, creep)	Std Dev (Mr, Creep)
A1-4in-FL	63.57	18245	1.827	1.966	0.106	1.926	0.123
A2-4in-FL	broken	-	-				
A3-4in-FL	62.76	18606	1.887				
A4-4in-FL	61.42	19891	2.062			2.027	0.049
A5-4in-FL	63.31	20521	2.063				
A6-4in-FL	62.67	19613	1.992				
B1-4in-FL	63.31	21590	2.171	2.083	0.117	2.060	0.135
B2-4in-FL	62.95	20748	2.098				
B3-4in-FL	63.41	19012	1.909				
B4-4in-FL	64.14	22471	2.230			2.107	0.119
B5-4in-FL	62.21	20512	2.099				
B6-4in-FL	61.56	19272	1.993				
C1-4in-FL	63.21	23552	2.372	2.467	0.131	2.355	0.015
C2-4in-FL	64.52	26867	2.651				
C3-4in-FL	64.42	23785	2.351				
C4-4in-FL	63.81	25795	2.574			2.579	0.070
C5-4in-FL	62.21	22892	2.343				
C6-4in-FL	62.87	24809	2.512				
D1-4in-FL	62.04	19511	2.002	2.209	0.159	2.076	0.095
D2-4in-FL	62.54	23003	2.342				
D3-4in-FL	64.37	20658	2.043				
D4-4in-FL	62.57	23271	2.368			2.342	0.026
D5-4in-FL	62.42	21414	2.184				
D6-4in-FL	63.68	23176	2.317				

Sample	Thickness	Load, N	strength*E-3, kN/mm2	Average	Std Dev	Average (Mr, creep)	Std Dev (Mr, Creep)
E1-4in-FL	62.53	19687	2.004	2.131	0.123	2.029	0.080
E2-4in-FL	63.34	22071	2.218				
E3-4in-FL	62.53	19287	1.964				
E4-4in-FL	63.15	22235	2.242			2.234	0.014
E5-4in-FL	63.10	20993	2.118				
E6-4in-FL	63.32	22286	2.241				
F1-4in-FL	63.86	21566	2.150	2.275	0.174	2.128	0.098
F2-4in-FL	63.64	24627	2.464				
F3-4in-FL	62.45	19825	2.021				
F4-4in-FL	64.64	24579	2.421			2.421	0.044
F5-4in-FL	62.70	21805	2.214				
F6-4in-FL	62.62	23385	2.377				
G1-4in-FL	62.23	20873	2.135	2.195	0.130	2.089	0.076
G2-4in-FL	63.04	23212	2.344				
G3-4in-FL	64.06	21441	2.131				
G4-4in-FL	64.30	23370	2.314			2.302	0.050
G5-4in-FL	64.32	20216	2.001				
G6-4in-FL	63.44	22387	2.247				
H1-4in-FL	62.48	18624	1.898	2.161	0.175	2.021	0.130
H2-4in-FL	66.25	24000	2.306				
H3-4in-FL	62.64	21229	2.157				
H4-4in-FL	63.15	22528	2.271			2.301	0.027
H5-4in-FL	60.93	19231	2.009				
H6-4in-FL	63.20	23077	2.325				

Sample	Thickness	Load, N	strength*E-3, kN/mm2	Average	Std Dev	Average (Mr, creep)	Std Dev (Mr, Creep)
I1-4in-FL	63.52	23098	2.315	2.537	0.145	2.431	0.130
I2-4in-FL	63.60	26936	2.696				
I3-4in-FL	63.60	24048	2.407				
I4-4in-FL	64.13	26180	2.599			2.642	0.049
I5-4in-FL	64.50	26055	2.572				
I6-4in-FL	64.27	26566	2.631				
J1-4in-FL	63.84	18418	1.837	1.884	0.073	1.834	0.068
J2-4in-FL	63.24	18830	1.896				
J3-4in-FL	64.74	17946	1.765				
J4-4in-FL	63.31	19386	1.949			1.934	0.034
J5-4in-FL	64.74	19332	1.901				
J6-4in-FL	64.41	19813	1.958				
L1-4in-FL	65.29	17241	1.681	1.906	0.162	1.779	0.094
L2-4in-FL	62.75	19852	2.014				
L3-4in-FL	62.64	18379	1.868				
L4-4in-FL	64.91	19905	1.952			2.032	0.091
L5-4in-FL	61.71	17322	1.787				
L6-4in-FL	61.50	20586	2.131				

L/L 100-mm Diameter Specimens

Sample	Thickness	Load, N	strength*E-3, kN/mm2	Average	Std Dev	Average (Mr, creep)	Std Dev (Mr, Creep)
A1-4in-LL	63.20	23445	2.362	2.571	0.131	2.494	0.133
A2-4in-LL	65.20	28041	2.738				
A3-4in-LL	63.47	24854	2.493				
A4-4in-LL	64.67	26801	2.638			2.648	0.086
A5-4in-LL	64.85	26769	2.628				
A6-4in-LL	64.33	25944	2.567				
B1-4in-LL	63.16	26150	2.636	2.488	0.127	2.552	0.163
B2-4in-LL	63.20	23749	2.392				
B3-4in-LL	62.48	23212	2.365				
B4-4in-LL	64.77	24517	2.410			2.423	0.039
B5-4in-LL	66.45	27718	2.656				
B6-4in-LL	61.90	23976	2.466				
C1-4in-LL	63.22	29239	2.944	2.961	0.055	2.989	0.040
C2-4in-LL	61.80	29140	3.002				
C3-4in-LL	62.38	29600	3.021				
C4-4in-LL	58.73	26855	2.911			2.933	0.061
C5-4in-LL	63.34	29869	3.002				
C6-4in-LL	61.07	27691	2.887				
D1-4in-LL	65.19	22289	2.177	2.199	0.118	2.280	0.090
D2-4in-LL	64.50	20500	2.023				
D3-4in-LL	64.77	23582	2.318				
D4-4in-LL	64.93	22020	2.159			2.117	0.082
D5-4in-LL	63.87	23531	2.345				
D6-4in-LL	62.43	21282	2.170				

Sample	Thickness	Load, N	strength*E-3, kN/mm2	Average	Std Dev	Average (Mr, creep)	Std Dev (Mr, Creep)
E1-4in-LL	61.30	20873	2.168	2.214	0.082	2.262	0.084
E2-4in-LL	65.30	21611	2.107				
E3-4in-LL	64.37	23122	2.287				
E4-4in-LL	61.93	21456	2.206			2.167	0.053
E5-4in-LL	60.57	22175	2.331				
E6-4in-LL	59.93	20592	2.187				
I1-4in-LL	65.20	23006	2.246	2.303	0.079	2.323	0.091
I2-4in-LL	64.63	230068	2.272				
I3-4in-LL	64.26	23206	2.299				
I4-4in-LL	63.80	22172	2.212			2.283	0.078
I5-4in-LL	64.63	24597	2.423				
I6-4in-LL	64.77	24069	2.366				
J1-4in-LL	62.56	20760	2.113	1.995	0.122	1.990	0.131
J2-4in-LL	62.17	20473	2.096				
J3-4in-LL	64.42	18750	1.853				
J4-4in-LL	64.77	18672	1.835			1.999	0.143
J5-4in-LL	64.37	20267	2.004				
J6-4in-LL	63.83	20715	2.066				
L1-4in-LL	63.78	15898	1.587	1.653	0.088	1.664	0.094
L2-4in-LL	63.77	15494	1.547				
L3-4in-LL	64.58	16602	1.637				
L4-4in-LL	62.83	16110	1.632			1.642	0.101
L5-4in-LL	64.52	17928	1.769				
L6-4in-LL	64.37	17672	1.748				

D/L 100-mm Diameter Specimens

Sample	Thickness	Load, N	strength*E-3, kN/mm2	Average	Std Dev	Average (Mr, creep)	Std Dev (Mr, Creep)
A1-4in-DL	63.00	19213	1.941	1.979	0.053	1.988	0.075
A2-4in-DL	63.07	19228	1.941				
A3-4in-DL	63.72	19508	1.949				
A4-4in-DL	63.23	19463	1.960			1.969	0.034
A5-4in-DL	63.36	20649	2.075				
A6-4in-DL	62.43	19684	2.007				
B1-4in-DL	62.61	15485	1.575	1.659	0.076	1.681	0.094
B2-4in-DL	64.00	15927	1.584				
B3-4in-DL	63.96	17630	1.755				
B4-4in-DL	63.10	16949	1.710			1.637	0.065
B5-4in-DL	65.42	17606	1.713				
B6-4in-DL	63.90	16241	1.618				
C1-4in-DL	63.27	26267	2.643	2.563	0.101	2.642	0.024
C2-4in-DL	63.27	25505	2.566				
C3-4in-DL	63.64	26640	2.665				
C4-4in-DL	63.30	24606	2.475			2.484	0.078
C5-4in-DL	63.76	26210	2.617				
C6-4in-DL	63.77	24146	2.411				

Sample	Thickness	Load, N	strength*E-3, kN/mm2	Average	Std Dev	Average (Mr, creep)	Std Dev (Mr, Creep)
D1-4in-DL	64.46	24338	2.404	2.375	0.088	2.424	0.092
D2-4in-DL	63.47	22973	2.304				
D3-4in-DL	63.58	25204	2.524				
D4-4in-DL	64.70	23185	2.281			2.327	0.060
D5-4in-DL	64.30	23669	2.343				
D6-4in-DL	64.93	24427	2.395				
I1-4in-DL	63.57	33700	3.375	3.180	0.119	3.253	0.123
I2-4in-DL	63.30	30439	3.061				
I3-4in-DL	63.38	31165	3.130				
I4-4in-DL	63.70	31867	3.185			3.107	0.068
I5-4in-DL	62.20	31789	3.254				
I6-4in-DL	62.00	29946	3.075				
L1-4in-DL	66.08	20368	1.962	1.897	0.057	1.932	0.061
L2-4in-DL	65.50	18854	1.833				
L3-4in-DL	62.79	18367	1.862				
L4-4in-DL	62.33	18430	1.882			1.862	0.026
L5-4in-DL	61.93	19198	1.973				
L6-4in-DL	65.23	19180	1.872				

Vitae

Samer Katicha was born on May the 11, 1976 in Beirut, Lebanon. He received his high school diplomat from the “College Notre Dame de Jamhour” in 1994. After that he joined the American University of Beirut where he received his bachelor in engineering (BE) in 1999. After graduation, Samer served as an engineer in the military, as part of a required one year military service. In August 2000, he decided to go back to school by entering the graduate program at the Charles E Via Department of Civil and Environmental Engineering at Virginia Tech which earned him a Masters degree in 2003 under the supervision of Dr. Imad Al-Qadi. During the same period samer worked as a Graduate Research Assistant with the Roadway Infrastructure Group (RIG) at the Virginia Tech Transportation Institute. Currently, Samer is pursuing a Ph. D. degree under the supervision of Dr. Imad Al-Qadi.